Protein Transformation by Mesophases: Studies with Sodium Dodecyl Sulfate and Electric Field

A Thesis Submitted for the Degree of

DOCTOR OF PHILOSOPHY

By

NOORUL HUDA

School of Chemistry
University Of Hyderabad
Hyderabad 500046
INDIA

JUNE 2023

Dedicated to

My Mother

CONTENTS

School of Chemistry
University of Hyderabad
Hyderabad –500 046

STATEMENT

I hereby declare that the matter embodied in this thesis is the result of investigations carried out by me in the School of Chemistry, University of Hyderabad, Hyderabad, under the supervision of **Prof. Abani K. Bhuyan**.

In keeping with the general practice of reporting scientific observations, due acknowledgments have been made whenever the work described is based on the finding of other investigators. Any omission which might have occurred by oversight or error is regretted.

Hyderabad
JUNE 2023

Noorul Huda
(17CHPH07)

DECLARATION

I, **Noorul Huda**, hereby declare that this thesis entitled **"Protein Transformation by Mesophases: Studies with Sodium Dodecyl Sulfate and Electric Field"** submitted by me under the guidance and supervision of **Prof. Abani K. Bhuyan**, is a bonafide research work which is also free from plagiarism. I also declare that it has not been submitted previously in part or in full to this university or any other university or institution for the award of any degree or diploma. I hereby agree that my thesis can be deposited in Shodhganga/INFLIBNET.

A report on plagiarism statistics from the University Librarian is enclosed.

Date: 26/06/2023

Name: Noorul Huda

Reg. No.: 17CHPH07

Signature of the student

Signature of the Supervisor

ABANI K. BHUYAN, Ph.D.
Professor
University of Hyderabad
School of Chemistry
Hyderabad - 500 046.

Prof. Abani K. Bhuyan
School of Chemistry
University of Hyderabad
Hyderabad – 500 046, India

Phone: +91 40 23134810 (O)
Fax: +91-40-23012460
Email: akbsc@uohyd.ac.in

CERTIFICATE

This is to certify that the thesis entitled **"Protein Transformation by Mesophases: Studies with Sodium Dodecyl Sulfate and Electric Field"** submitted by **Mr. Noorul Huda** bearing registration number **17CHPH07** in partial fulfillment of the requirements for the award of Doctor of Philosophy (Ph. D.) is a bonafide work carried out by her under my supervision and guidance in School of Chemistry, University of Hyderabad. This thesis is free from plagiarism and has not been submitted previously in part or in full to this or any other University or Institution for the award of any degree or diploma. Further, the student has five publications before submission of the thesis for adjudication and has produced shreds of evidence for the same in the form of reprints.

Parts of this thesis have been published as the following articles:

1. **N. Huda**, M. Hossain, A. K. Bhuyan, *Biopolymers.* **2019**, *110*, 23255 (***Chapter 3***).
2. **N. Huda**, A. K. Bhuyan, *J. Phys. Chem. B.* **2023***, 127,* 20, 4386–4395 (***Chapter 4***).
3. **N. Huda**, A. K. Bhuyan, *Cryst. GrowthDes.***2023** (accepted for publication). (***Chapter 5***).

He has also made presentations in the following conferences and attended workshops:

1. **Poster:** "**Conformational Analysis of Protein in Electric Field**" in ***Chemfest 2020*** (In-house symposium) at University of Hyderabad
2. **Oral and Poster:** "**Effect of Electric Field on Protein Conformation**" in ***Chemfest 2022*** (In-house symposium) at University of Hyderabad.
3. **Poster:** "**Obligate amorphous aggregate in electric field-promoted protein crystallization**" in ***Chemfest 2023*** (In-house symposium) at University of Hyderabad. (**Best Poster presentation**).

Further the student has passed the following courses towards the fulfilment of coursework requirement for Ph. D.

Sl. No.	Course No.	Title of the Course	No. of Credits	Result
1.	CY801	Research Proposal	4	Pass
2.	CY805	Instrumental Methods-A	4	Pass
3.	CY806	Instrumental Methods-B	4	Pass

Abani K. Bhuyan
26/06/2023

Prof. Abani K. Bhuyan

(Thesis Supervisor)

ABANI K. BHUYAN, Ph.D.
Professor
University of Hyderabad
School of Chemistry
Hyderabad - 500 046.

Dean

School of Chemistry

University of Hyderabad

Dean
SCHOOL OF CHEMISTRY
University of Hyderabad
Hyderabad-500 046

ACKNOWLEDGEMENTS

I would like to express my deepest gratitude and heartfelt appreciation to the following individuals and groups, without whom the completion of this thesis would not have been possible:

I am immensely grateful to my supervisor, Prof. Abani K. Bhuyan, for his unwavering support, valuable insights, and guidance throughout this research endeavour. His expertise, dedication, and encouragement played a pivotal role in shaping the direction of my study.

I would like to extend my heartfelt gratitude to the members of my doctoral committee, Prof. Akhila Kumar Sahoo and Dr. Murali Banovath. Their insightful suggestions, constructive criticism, and intellectual engagement have immensely enriched the quality of this work.

I want to thank present and former deans, School of Chemistry, University of Hyderabad, and all the faculty members of the School of chemistry for their help and support on various occasions.

I want to acknowledge CSIR and UGC for financial support during my Ph.D. research tenure.

My heartfelt appreciation extends to Mr. Durgesh and Mr. Mahender (NMR, School of Chemistry), Mr. Sunil (SEM, School of Chemistry), Mr. Rajesh (TEM, School of Chemistry) Mr. Anand (IR, School of Chemistry) and Mr. Abraham for his help in official work (School Office). Their constant support, from administrative assistance to technical expertise, has been crucial throughout my academic journey. I am grateful for their tireless efforts behind the scenes, which have made the pursuit of knowledge a seamless and enriching experience.

I would also like to thank my lab seniors, Dr. P. Sashi and Dr. D. Santi Swarupini for their constructive comments and helpful discussions. I am very grateful to all my colleagues, Mujahid, Kirthi, and Ramesh for their help and creating a pleasant research environment, making it a memorable and enjoyable journey. I would specially like to thank Mujahid for being there in my highs and lows and always having open ears for my personal and professional problems. I extend my gratitude to all the project students who have worked with me, Rajesh, Trupti and Hizana.

I am thankful to my dear friends, Isha, Ishfaq, Mujahid, Asif and Dr. Bilal Ahmed for their unwavering support, understanding, and encouragement that have been a constant source of motivation. My special thanks to Isha for believing in my abilities, shared laughter, and moments of respite from academic rigors that have played a pivotal role in keeping me inspired and focused. Your presence has made this journey all the more meaningful, and I am grateful for the enduring bond we share. Especially, I would like to thank Dr. Ankit K. Srivastav who always had an open ear for my worries and guided me through my Ph.D. studies.

I would like to express my heartfelt appreciation to my childhood friends Sachin and Minhaj, who have been with me through thick and thin. Your unwavering friendship, support, and laughter have been a constant source of joy and encouragement throughout my life, including during the completion of this thesis. Thank you for always believing in me and for being by my side, both in childhood and now as I embark on this new chapter of my academic journey.

I would like to take a moment to honour and express my deepest gratitude to my mother Shahnaz. Though she is no longer physically with me, her presence, love, and unwavering belief in my abilities continue to inspire and motivate me every day. Her profound impact on my life, her support, and the values she instilled in me have shaped the person I am today. I am forever grateful for her sacrifices, her guidance, and the countless life lessons she taught me. While she may not be here to witness the completion of this thesis, I know that the memories we shared will forever guide me on this journey. This achievement is dedicated to her memory and the profound influence she had on my life. Thank you, Mom, for being my guiding light and for shaping me into the person I am today.

I would like to express my deepest gratitude to my family, my father Mr. Mohammad Abdullah and my sister Azra for their unwavering love, support, and sacrifices that have been the foundation upon which my achievements rest. Your beliefs in my abilities, constant encouragement, and sacrifices have fuelled my determination to succeed. I am forever grateful for your unyielding faith in me.

Finally, I thank almighty for making this happen.

Noorul Huda

June 2023

List of abbreviations and symbols

SLS	Sodium lauryl sulfate
SDBS	Sodium dodecylbenzenesulfonate
SDS	Sodium dodecyl sulfate
CATB	Cetyltrimethylammonium bromide
PEG	Polyethylene glycol
CMC	Critical micellar concentration
NMR	Nuclear magnetic resonance
ANS	8-anilinonaphthalene sulfonate
PFG	Pulsed field gradient
FWHM	Full width at half maxima
R_H	Hydrodynamic radii
CD	Circular dichroism
UV	Ultraviolet
ThT	4-[3,6-dimethyl benzothiazol-2-yl]-N,N-dimethylaniline
FESEM	Field emission scanning electron microscopy
DNA	Deoxyribonucleic acid
EF	Electric field
MD	Molecular dynamics
BSA	Bovine serum albumin
DC	Direct current
AC	Alternating current
IR	Infrared
SEM	Scanning electron microscopy
Tyr	Tyrosine
Trp	Tryptophan
Asp	Aspartic acid
Glu	Glutamic acid
QN	Quasi-native
HEWL	Hen egg white lysozyme

BPTI	Bovine pancreatic trypsin inhibitor
ATR-IR	Attenuated Total Reflectance Infrared spectroscopy
TEM	Transmission electron microscopy
α-LA	α-lactalbumin
β-LG	β-lactoglobulin
Mb	Myoglobin
Abs	Absorbance
SAED	Selected area electron diffraction
SDS-PAGE	Sodium dodecyl sulfate-polyacrylamide gel electrophoresis
TSN	Two-state nucleation
MSN	Multistep nucleation

CHAPTER 1

INTRODUCTION

1.1 Overview

A constant uneasiness rings at the background of all our studies related to protein structure, dynamics, and folding. This discomfort emanates from the dark side of proteins that lead to degenerative diseases, including Alzheimer's, Parkinson's, diabetes, and plausibly many yet to know. These diseases are not caused by some micro-organism but rather by something conceptually simpler, i.e., incorrect protein folding.[1,2] Proteins being at the heart for lives on the planet, their structure and conformation have a major and complex role in how they are destined to operate.[3] A slight perturbation in their structure or conformation can impair their functioning and may result in devastating consequences.

The alpha helix is often considered to be the most prominent structural feature in the protein functioning in its native conformation.[4] When an extensive conformational change occurs from alpha helix to beta sheet, it exposes hydrophobic amino acid residues and promotes protein aggregation.[5] This conformational change is considered to be a characteristic of amyloid aggregation.[6,7] This change in protein conformation, resulting in changes in the content of secondary, tertiary and quaternary structure without affecting the primary structure is referred to as denaturation.

While many chemical denaturants are known and studied, this thesis is intended to study the effect of two denaturants – a chemical agent, anionic surfactant sodium dodecyl sulfate (SDS), and a physical agent in the form of a weak electric field. The conformational changes brought about by these physical denaturants often pass through dense states of proteins, which

act as mesophases. The mesophases or mesomorphic phases facilitate the unfolded protein to undergo aggregation, fibrillation, and in some cases crystallization.[8]

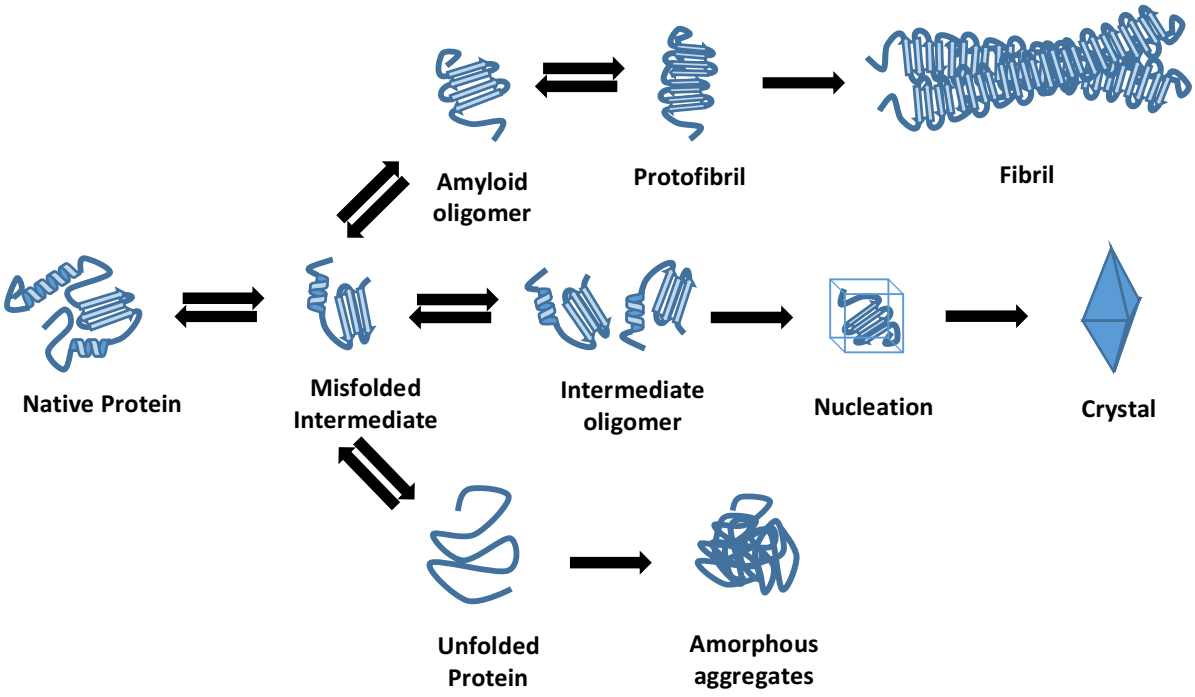

Figure 1. Schematic diagram of some possible pathways followed by protein unfolding.[9]

1.2. Mesophases

Mesophase refers to the intermediate phase of matter that exhibit properties between those of a solid and a liquid. It is also known as mesomorphic state.[10] Mesophases are often observed in certain types of materials, most commonly in liquid crystals. In a mesophase, the molecules or particles are arranged in an ordered or semi-ordered fashion similar to a crystal structure, but they also retain some degree of mobility similar to a liquid. This unique combination of ordered and mobile characteristics gives rise to distinct physical properties.[11] One of the most well-known examples of mesophases is liquid crystals that can flow like a liquid and exhibit some degree of order as in a solid. They have a characteristic molecular arrangement where the molecules are aligned in a specific direction, giving rise to optical properties such as

birefringence.[12] Liquid crystals are widely used in various display technologies, such as LCD (liquid crystal display) screens.

1.2.1. *Mesophases and liquid crystals*

The history of mesophases, particularly in the context of liquid crystals, is an interesting and significant aspect of scientific development. In the late 18th century, Swedish botanist and physicist Carl Wilhelm Scheele observed liquid crystalline behavior in a substance called "cholesterin" (also known as cholesterol) extracted from gallstones. In 1888, Austrian botanist Friedrich Reinitzer observed the presence of two distinct melting points in cholesteryl benzoate, indicating a change in physical state.[13] This observation marked the first recognition of liquid crystalline behaviour.

In the early 20th century, the Dutch physicist and chemist Hendrik Antoon Lorentz proposed a molecular theory for materials that are half liquid and half solid.[14] He suggested that the behaviour of liquid crystals could be explained by anisotropic (directionally dependent) molecular alignment. The German physicist Otto Lehmann also made significant contributions to the field. In 1904, he coined the term "liquid crystal" to describe the intermediate state between a liquid and a crystalline solid.[15] Lehmann extensively studied liquid crystals and characterized different mesophases. In the 1940s and 1950s, the American physicist and chemist George W. Gray made ground breaking contributions to the understanding of liquid crystals.[16] He classified liquid crystals into three main types: nematic, smectic, and cholesteric based on their different molecular arrangements and behaviours.[17] Gray's classification laid the foundation for further research and exploration of mesophases.

In recent decades, research on liquid crystals has continued to expand uncovering new mesophases, understanding their properties, and exploring their applications in various fields. The discovery and characterization of more complex mesophases, such as the blue phases and

discotic phases, have opened up new avenues for research and technological advancements. It's important to note that the field of liquid crystals is interdisciplinary, involving contributions from physics, chemistry, materials science, and engineering. The understanding and utilization of mesophases in liquid crystals have had a profound impact on various technological applications, particularly in display technologies, optical devices, and sensors.[18–20] The field remains an active area of scientific exploration and technological development to this day.

1.2.2. *Classification of mesophases*

The classification of mesophases is based on the molecular arrangements and ordering of the constituent molecules. Some general factors that contribute for classification of mesophases are, molecular shape and symmetry, molecular interactions, molecular flexibility, chirality, layering, stacking and molecular orientation.[11,12] Based on these factors, mesophases can be classified as follows:

1. Nematic (N) Phase

   The nematic phase is the simplest and most common mesophase observed in liquid crystals. In this phase, the molecules have no long-range positional order but exhibit directional alignment.[21] The molecules align parallel to each other along a common preferred direction called the director ($\vec{n}$), as shown in Figure 2(a).

2. Cholesteric (Ch) Phase

   The cholesteric phase, also known as the chiral nematic phase, exhibits a helical molecular arrangement. The term "cholesteric" for this mesophase type comes from the first known liquid crystals based on derivatives of cholesterol. The molecules form layers with a helical twist along the director axis. The molecules are twisted along a hypothetical axis to form

a helical arrangement, as shown in Figure 2(b). The pitch (p) of the helix determines the wavelength of light selectively reflected by the liquid crystal, resulting in iridescent colours.[22,23]

3. Smectic (Sm) Phases

Smectic phases are characterized by the presence of molecular layers or sheets. The layers have long-range positional ordering, while the molecules within each layer have short-range positional ordering.[23] Smectic phases are further divided into several sub-phases based on the arrangement and behaviour of the layers, which are represented in Figure 2(c):

i. Smectic A (SmA): In this phase, the molecules are aligned parallel to each other within the layers, forming a liquid-like state. The layers, however, have long-range positional order, resulting in a distinct layered structure.

ii. Smectic B (SmB): SmB phase is characterized by tilted molecules within the layers, forming a tilted or tilted-layer structure. The tilt direction can vary, leading to different subphases such as SmB, SmB*, and SmB-I.

iii. Smectic C (SmC): SmC phase is similar to SmA but with an additional feature, the molecules are tilted with respect to the layer normal, resulting in a tilted structure. SmC phase exhibits ferroelectric properties, meaning that the molecular alignment can be switched by an external electric field.

iv. Smectic F (SmF): SmF phase is characterized by a helical arrangement of the layers, forming a chiral smectic structure. This phase is also ferroelectric and exhibits a spontaneous polarization.

4. Discotic (D) Phase:

Discotic phases or columnar phases are a class of mesophases observed in certain materials, particularly discotic liquid crystals. Unlike conventional liquid crystals, which consist of rod-shaped molecules, discotic liquid crystals are composed of disc-shaped molecules.[24] In discotic phases, the disc-shaped molecules arrange themselves in columns or stacks that extend through the material. The individual columns are usually held together by weak intermolecular interactions; such as van der Waals forces or π-π stacking. The columns can be oriented perpendicular to the plane of the material, parallel to the plane, or have an inclined orientation as shown in Figure 2(d).

Discotic phases are further divided into several sub-phases based on the arrangement and behaviour of the layers:

i. Discotic Nematic (N_D): The Nem phase serves as a transitional phase situated between the isotropic liquid phase and the discotic columnar phase. In this phase, the disc-shaped molecules have orientation order but lack positional order along the columns.

ii. Discotic Columnar Hexagonal (Col_h): In this phase, the columns exhibit a hexagonal lattice arrangement, forming a two-dimensional network in the plane perpendicular to the columns. This phase exhibits long-range positional order in two dimensions.

iii. Discotic Columnar Rectangular (Col_r): In the Col_r phase, the columns form a rectangular lattice, resulting in a more elongated columnar structure compared to the Col_h phase.

It's important to note that the classification of mesophases is an active area of research, and new phases and sub-phases continue to be discovered and characterized, further expanding our understanding of liquid crystal behaviour.[24]

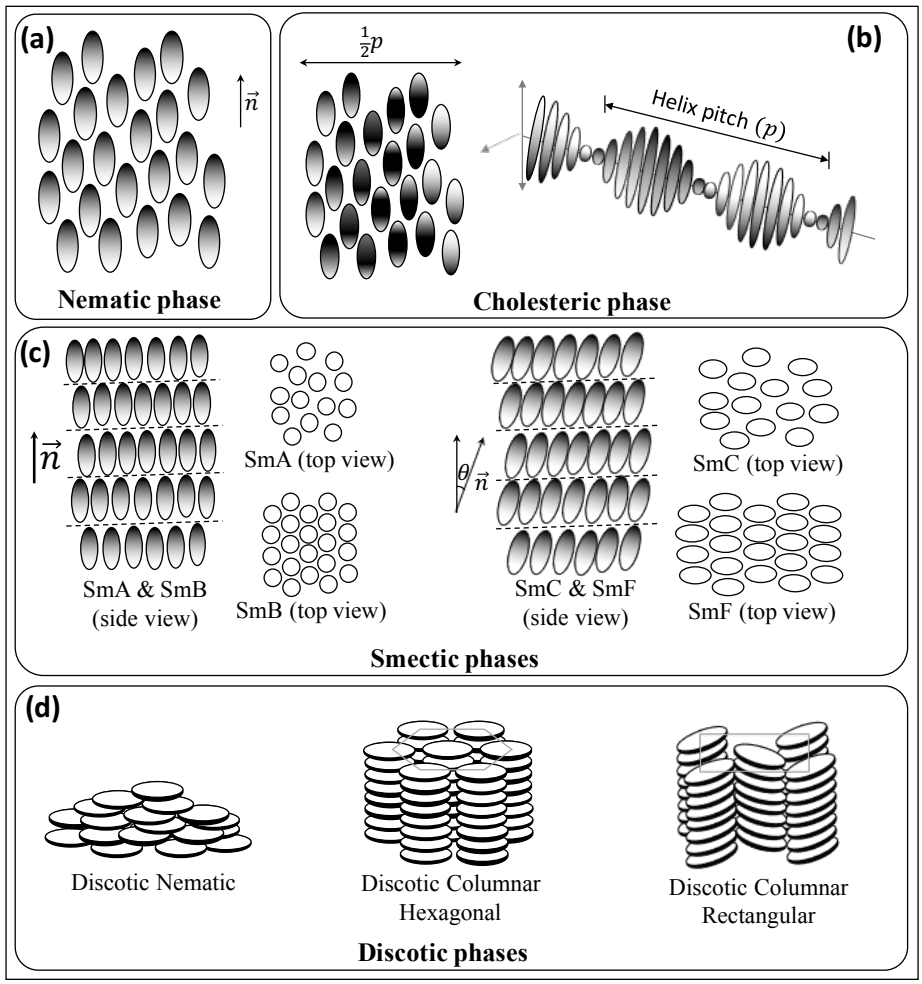

Figure 2. Schematic diagram of various types of mesophases as labelled.[25]

1.2.3. *Mesophases in biological systems*

In biological systems, the concept of mesophases is not commonly used in the same sense as in liquid crystals. However, there are specific instances where ordered structures or phase behaviour similar to mesophases can be observed. Some of these instances are mentioned below:

1. Cellular Membranes

   Biological membranes such as cell membranes and organelle membranes can exhibit liquid crystalline behaviour. Lipids, which are a major component of membranes, can undergo phase transitions between different ordered states, including gel phase and liquid

crystalline phase. The ordered arrangement of lipids within membranes is essential for maintaining membrane integrity, fluidity, and the organization of membrane proteins.[26]

2. Protein Aggregates and Amyloids

   These can exhibit ordered structures with specific arrangements and are associated with various diseases. Amyloid fibrils, for example, are composed of misfolded proteins that assemble into a characteristic cross-β structure. These structures often possess a high degree of order and can exhibit mesophase-like properties.[27]

3. Liquid-Liquid Phase Separation (LLPS)

   LLPS is a phenomenon observed in biological systems where intracellular components undergo de-mixing to form liquid-like phases. Biomolecular condensates, which are dynamic and membrane-less organelles formed through LLPS, can exhibit liquid droplet-like behaviour with distinct phases.[28] The formation and dissolution of biomolecular condensates are tightly regulated and play important roles in cellular processes such as signal transduction and gene regulation.

4. Microscopic Structures

   Biological systems often exhibit hierarchical organization and ordered structures at different length scales. For example, collagen fibres in connective tissues,[29] microtubules in the cytoskeleton,[30] and DNA supercoiling[31] can display ordered arrangements that resemble mesophases on a microscopic level.

It is important to note that the concept of mesophases in liquid crystals and the behaviour observed in biological systems are not directly equivalent. However, by examining the ordered

structures, phase transitions, and hierarchical organizations present in biological systems one can draw analogies to mesophases in liquid crystals.

1.3. Surfactants

Surfactants are compounds that are commonly used in various industries and products, including cleaning agents, personal care products, and pharmaceuticals. The term "surfactant" is short for "surface-active agent," which refers to their ability to lower the surface tension of liquids, making them more effective at removing dirt, oil, and other substances. Surfactants have a unique chemical structure that allows them to interact with both water-soluble and oil-soluble substances, making them effective at emulsifying and dispersing them in water.[32–34] This property makes them useful in a wide range of applications, including foaming agents, wetting agents, and solubilizers. Examples of surfactants include soaps, detergents, and emulsifiers. They are typically classified based on their ionic charge, with anionic, cationic, non-ionic, and amphoteric surfactants being the four main types. The choice of surfactant depends on the specific application, as each type has different properties and performance characteristics.[35]

1.3.1. *Types of surfactants*

Surfactants can be classified into several types based on their chemical structure and the nature of their hydrophilic and hydrophobic groups.[32,33] Here are some common types of surfactants.

1. Anionic Surfactants: These surfactants have a negatively charged hydrophilic group, such as a sulfate ($-OSO_3^-$) or carboxylate ($-COO^-$). Anionic surfactants are commonly found in

cleansers like soaps, detergents, and shampoos. Examples include sodium lauryl sulfate (SLS) and sodium dodecylbenzenesulfonate (SDBS).

2. Cationic Surfactants: Cationic surfactants have a positively charged hydrophilic group such as an amine or a quaternary ammonium salt. They are often used as disinfectants, fabric softeners, and in hair conditioners. Examples include cetyltrimethylammonium bromide (CTAB) and benzalkonium chloride.

3. Nonionic Surfactants: They have no charge on their hydrophilic group. They are commonly used in personal care products, pharmaceuticals, and industrial applications. Nonionic surfactants are known for their mildness and compatibility with various systems. Examples include polyethylene glycol (PEG), polysorbate 80, and alkyl ethoxylates.

4. Amphoteric Surfactants: These have both positively and negatively charged groups, allowing them to function as both anionic and cationic surfactants depending on the pH of the solution. They are used in products like shampoos, facial cleansers, and baby care products. Examples include cocamidopropyl betaine and sodium cocoamphoacetate.

5. Zwitterionic Surfactants: Zwitterionic surfactants have both positive and negative charges within the same molecule. They are similar to amphoteric surfactants but typically have a balanced charge at neutral pH. Zwitterionic surfactants are known for their mildness and are used in personal care products and pharmaceuticals. Examples include betaines and sulfobetaines.

6. Silicone Surfactants: They contain silicone-based hydrophobic groups and are used in personal care and cosmetic products. They provide a unique combination of properties, including high spread ability and conditioning effects.

It is to be noted that surfactants can have diverse applications and can be customized for specific purposes. Different types of surfactants have varying characteristics, such as foaming ability, solubility, and compatibility, making them suitable for various formulations in industrial products.[34,35]

1.3.2. *Micellization*

Micellization is a process in which surfactant molecules spontaneously arrange themselves in a solution to form micelles.[36,37] Surfactants are molecules that have both hydrophilic (water-loving) and hydrophobic (water-repelling) regions. When surfactant molecules are introduced into a polar solvent, they tend to aggregate to minimize their exposure to the liquid environment. In a typical micellization process the hydrophobic tails of surfactant molecules group together forming the core of the micelle, while the hydrophilic heads remain on the surface facing the surrounding solvent. This arrangement allows the micelle to achieve a lower free energy state compared to the dispersed individual surfactant molecules.[36–38]

Micelles have a distinct structure, with a hydrophobic core and a hydrophilic shell. They can vary in size and shape depending on the nature of the surfactant, molar concentrations of the monomers, and the solution conditions. The critical micelle concentration (CMC) is the concentration at which micelles start to form in a solution.[37–39] Below the CMC, the surfactant molecules are predominantly dispersed as individual monomers.

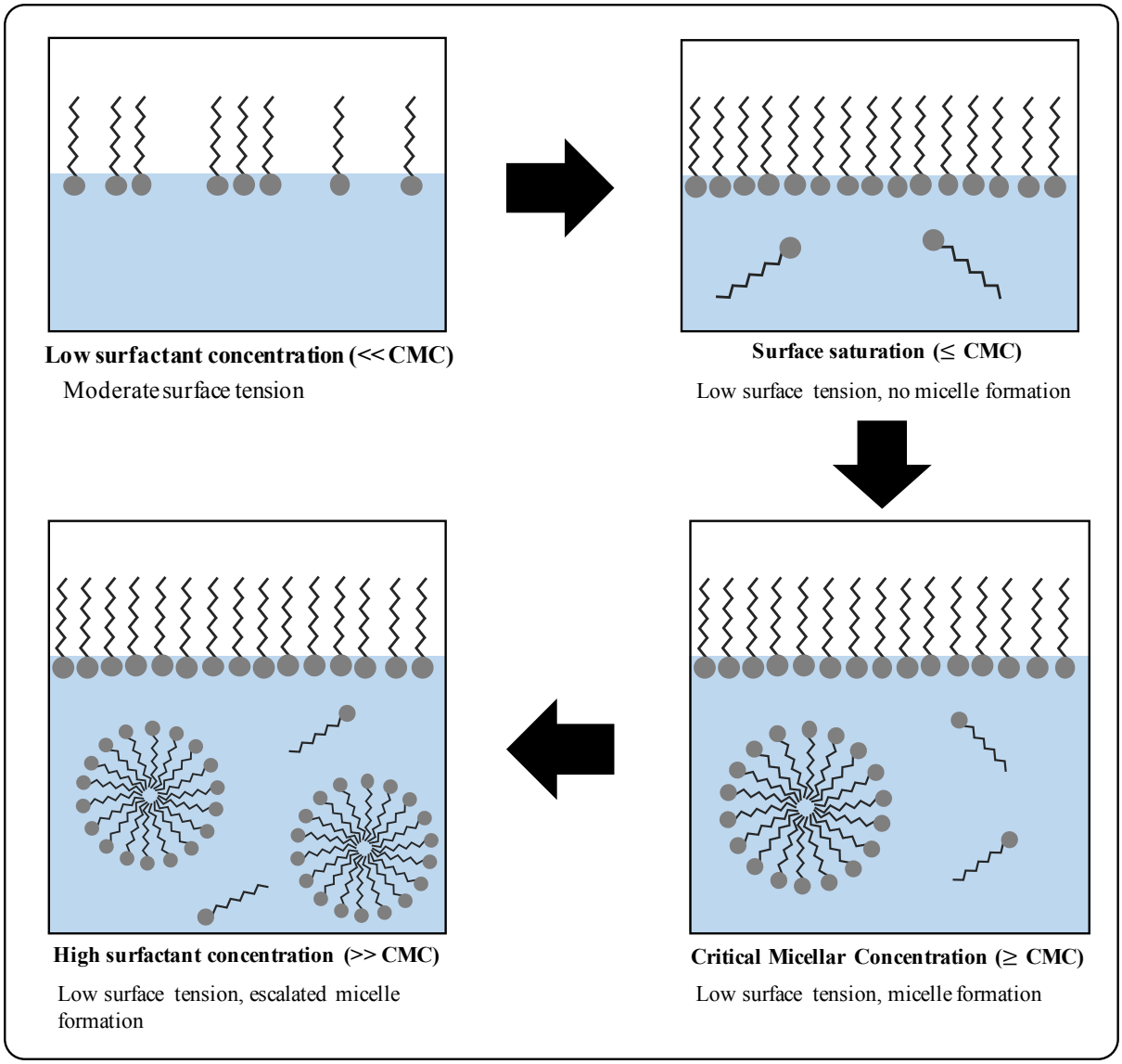

Figure 3. Schematic diagram for micellization.

Micellization is an important phenomenon in various fields, including chemistry, biology, and industry. It plays a crucial role in many processes such as detergency, emulsification, solubilization, and drug delivery. Micelles can solubilize hydrophobic substances in their core, making them useful for delivering poorly soluble drugs or enhancing the solubility of various compounds. They can also stabilize emulsions by forming a protective layer around oil droplets in water.[38,39] Overall, micellization is a self-assembly process of surfactant molecules in a solvent, leading to the formation of micelles with unique structures and properties.

1.3.3. *Thermodynamic models of micellization*

The mass-action model and the phase-separation or phase-equilibrium model are two models based on thermodynamic theories of micellization that are typically used to explain how surfactant monomers spontaneously self-organize into micelles. According to the former, monomers and micelles are two separate phases, and the surfactant is a two-phase system above the critical micelle concentration (CMC), which symbolizes the point of maximal solubility.[40,41] The latter defines a micelle as an association of bound gegenions and surface active ions created by mass-action principles. Although there are many similarities between the two models, the phase-equilibrium model makes the link between the conventional Gibbs energy of micellization and CMC under constant pressure and temperature look unclear. The micellar reference state in the phase-separation model is poorly defined because the activity coefficient of the micellar composition appears zero here, whereas the mass-action model allows the solution state for the reference state of both monomers and micelles, as well as any other relevant components when considered present in the system.[42] The phase-equilibrium model is sometimes referred to as a pseudo-phase model as a result of these issues, which include conflict with Gibbs phase rule. In spite of this, the phase-equilibrium model is quite helpful in practice for offering straightforward mathematical evaluations of surfactant solution characteristics.

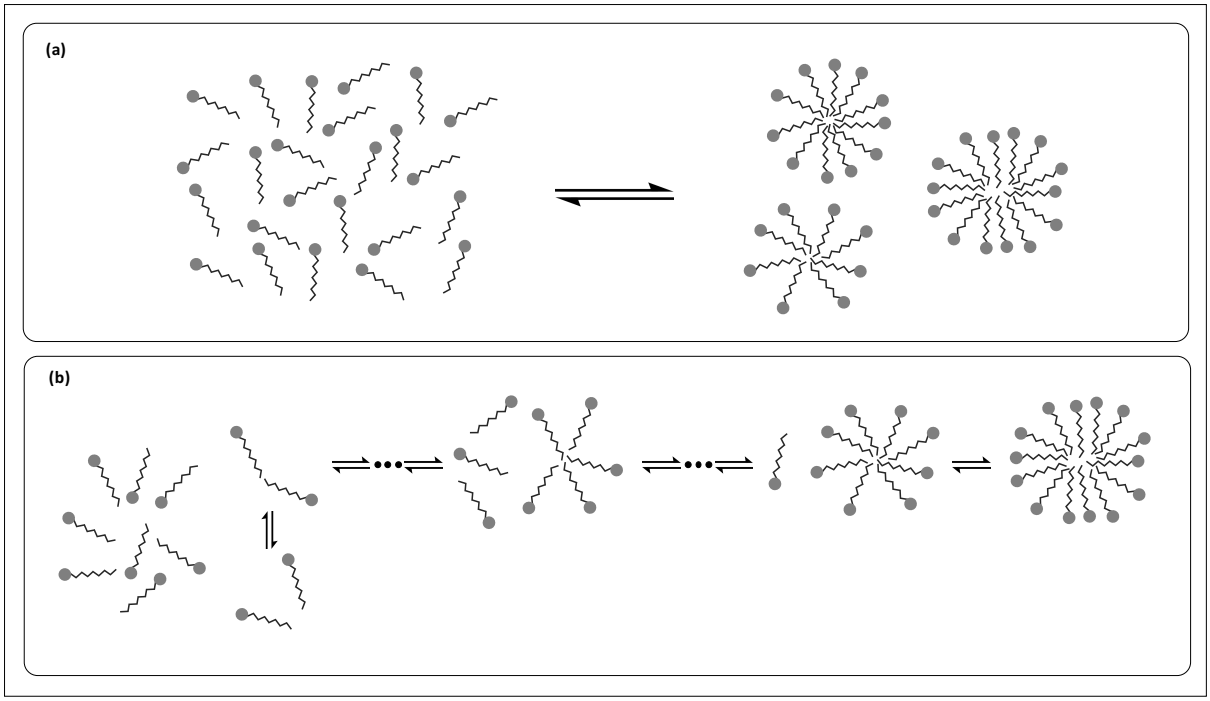

Figure 4. Schematic diagram representing (a) phase-separation model and (b) mass-action model of micellization.

1.3.4. *Micelles as mesophases*

Micelles can be considered a type of mesophase in certain systems. In the context of mesophases, micelles can be classified as a type of liquid crystalline phase. They are considered to be a form of the isotropic liquid phase, characterized by the absence of any long-range organization in the arrangement of micelles.[43–45] However, within the micelles themselves, there is an organized arrangement of the hydrophobic tails.[44] The size and shape of micelles can vary depending on factors such as surfactant structure, concentration, temperature, and the presence of other molecules.[38,39] Micelles can have spherical, cylindrical, or lamellar shapes, depending on the characteristics of the surfactant molecules and the solvent.[46] Micelles play important roles in various biological and industrial processes. In biological systems, they are involved in solubilizing and transporting hydrophobic molecules such as lipids and fat-soluble vitamins.[46] In industrial applications, micelles are utilized in detergents, emulsifiers, and drug

delivery systems.[44] Thus one can consider micelles as a mesophase due to their self-assembled, organized structure, even though they belong to the isotropic liquid phase category within the broader context of liquid crystals.

1.4. Protein–surfactant interaction

The interactions between surfactants and proteins can have important implications for protein structure, stability, solubility, and function.[47] Depending upon the type of surfactant used, following types of interactions are possible.

1. Solubilization and stabilization: Surfactants can solubilize hydrophobic proteins or protein regions by forming micelles or bilayers around them, thereby enhancing their solubility in aqueous solutions.[47–49] This solubilization can stabilize proteins, preventing aggregation or denaturation caused by exposure to hydrophobic environments.
2. Denaturation: Certain surfactants, particularly those with strong hydrophobic properties, can disrupt protein structure and lead to denaturation.[47,49] This can occur when surfactant molecules interact with the hydrophobic regions of proteins, causing unfolding or misfolding of the protein structure.
3. Protein unfolding and refolding: Surfactants can induce protein unfolding by disrupting the native interactions that stabilize the folded protein structure.[47] Conversely, some surfactants, known as denaturants or chaotropic agents, can promote protein refolding when used in appropriate conditions by disrupting non-native interactions that hinder the folding process.[50]
4. Binding and conformational changes: Surfactants can interact with proteins through various types of interactions, such as hydrophobic interactions, electrostatic interactions, or specific binding interactions,[47,48] inducing conformational changes in the protein structure that leads to alterations in protein function or activity.

5. Detergent properties: Surfactants are commonly used as detergents to solubilize and isolate proteins from biological samples.[47,48] The choice of surfactant is crucial as different surfactants can have varying effects on protein structure and function. Some surfactants, such as non-ionic detergents like Triton X-100[51] or Tween, are milder and better suited for preserving protein structure compared to ionic detergents like SDS which are more denaturing.[52]
6. Other applications: These include protein purification,[44] membrane protein extraction[48], protein crystallization,[53] and protein stability studies.[54] They can be used to disrupt membranes, solubilize membrane proteins,[53] or modulate protein-protein interactions.[55]

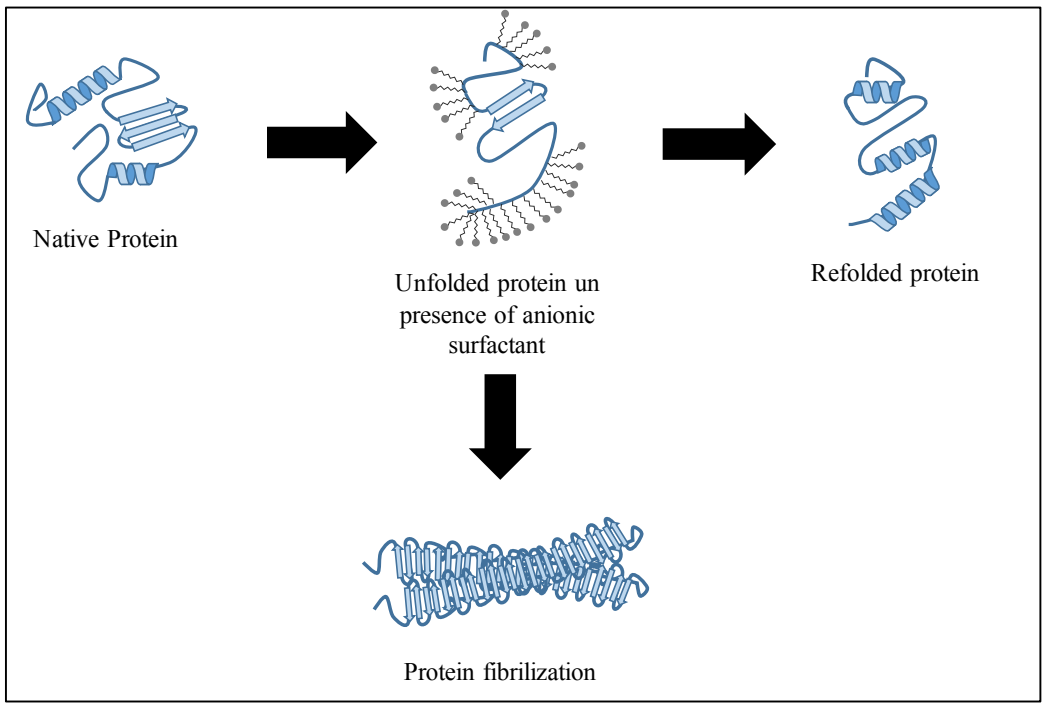

Figure 4. Schematic diagram of protein–surfactant interaction.

The specific effects of surfactants on proteins depend on factors such as the surfactant type, concentration, protein properties, and experimental conditions. It is important to consider these

factors for selection of the appropriate surfactants when studying or manipulating protein systems to ensure desired outcomes and maintain protein integrity.

1.5. References:

1. Chiti, F.; Dobson, C. M. Protein misfolding, functional amyloid, and human disease. *Annu. Rev. Biochem*. **2006**, *75*, 333-366.

2. Dobson, C. M. Getting out of shape. *Nature* **2002**, *418*, 729-730.

3. Dobson, C. M. Protein folding and misfolding. *Nature* **2003**, *426*, 884-890.

4. Pauling, L.; Corey, R. B.; Branson, H. R. The structure of proteins; two hydrogen-bonded helical configurations of the polypeptide chain. *Proc. Natl. Acad. Sci. U. S. A*. **1951**, *37*, 205-211.

5. Dobson, C. M. Protein misfolding, evolution and disease. *Trends Biochem. Sci*. **1999**, *24*, 329-332.

6. Chiti, F.; Taddei, N.; Baroni, F. Kinetic partitioning of protein folding and aggregation. *Nat Struct. Biol*. **2002**, *9*, 137-143.

7. Routledge, K. E.; Tartaglia, G. G.; Platt, G. W.; Vendruscolo, M.; Radford, S. E. Competition between intramolecular and intermolecular interactions in an amyloid-forming protein. *J. Mol. Biol*. **2009**, *389*, 776-786.

8. Amar-Yuli, I.; Azulay, D.; Mishraki, T.; Aserin, A.; Garti, N. The role of glycerol and phosphatidylcholine in solubilizing and enhancing insulin stability in reverse hexagonal mesophases. *J. Colloid. Interface. Sci*. **2011**, *364*, 379-387.

9. Han, Q.; Brown, S. J.; Drummond, C. J.; Greaves, T. L. Protein aggregation and crystallization with ionic liquids: Insights into the influence of solvent properties. *J. Colloid Interface Sci*. **2022**, *608*, 1173-1190.

10. Friedel, G. Les états mésomorphes de la matière. *Ann. Phys.* **1922**, 9, 273-474

11. Gennes, P. G.; Prost, J. *The Physics of Liquid Crystals*, 2nd ed.; Oxford University Press, 1993.

12. Chandrasekhar, S. *Liquid Crystals*, 2nd ed., Cambridge University Press, 1992.

13. Reinitzer, F. Beiträge zur Kenntniss des Cholesterins. *Monatshefte für Chemie* **1888**, *9*, 421–441.

14. Lorentz, H. A. Le partage de l'énergie entre la matière pondérable et l'éther II. *Nuovo Cimento Series 5*. **1908**, 16: 5-34.

15. Van, G.; Iterson Jr. A simple arrangement to demonstrate liquid crystals. *Trans. Faraday Soc.*, **1933**, *29*, 915-919.

16. Gray, G. W. *Molecular structure and the properties of liquid crystals*. New York (NY): Academic Press, 1962.

17. Goodby, J. W.; Gray, G. W. *Guide to the Nomenclature and Classification of Liquid Crystals*, Wiley Online Books, Ch. II, 1998

18. Hussain, Z.; Qazi, F. Liquid crystals based sensing platform-technological aspects. *Biosensors and Bioelectronics*, **2016**, *85*, 110-127.

19. Quan, Li. *Liquid Crystals Beyond Displays: Chemistry, Physics, and Applications*, Wiley Online Books, 2012.

20. Mysliwiec, J.; Szukalska, A.; Szukalski, A.; Sznitko, L. Liquid crystal lasers: the last decade and the future. *Nanophotonics* **2021**, *10*, 2309-2346.

21. Porter, R. S.; Jhonson, J. F. Orientation of nematic mesophases. *J. Phys. Chem.* **1962**, *66*, *10*, 1826–1829.

22. Figueiredo, N.; Antônio, M.; Salinas, R. A. The Nematic And Cholesteric Phases, *The Physics of Lyotropic Liquid Crystals: Phase Transitions and Structural Properties*, Oxford Academic Press, 2010, pp 190-218.

23. Bailly-Reyre, A.; Diep, H. T. Nematic and Smectic Phases: Dynamics and Phase Transition. *Symmetry* **2020**, *12*, 1574.

24. Chandrasekhar, S.; Ranganath, G. S. *Rep. Prog. Phys.* **1990**, *53*, 57.

25. Axenov, K. V.; Laschat, S. Thermotropic Ionic Liquid Crystals. *Materials*, **2011**, *4*, 206-259.

26. Caffrey M. Crystallizing membrane proteins for structure determination: use of lipidic mesophases. *Annu. Rev. Biophys*. **2009**, *38*, 29-51.

27. Victorelli, F. D.; Rodero, C. F.; Lutz-Bueno, V.; Chorilli, M.; Mezzenga, R. Amyloid Fibrils Enhance the Topical Bio-Adhesivity of Liquid Crystalline Mesophase-Based Drug Formulations. *Adv. Health Mater*. **2023**, *12*, 2720.

28. Albayrak, C.; Gülten, G.; Dag, O. Phase separation in liquid crystalline mesophases of $[Co(H_2O)_6]X_2$:P65 Systems (X = NO_3^-, Cl^-, or ClO_4^-). *Langmuir* **2007**, *23*, 855-860.

29. Yaari, A.; Posen, Y.; Shoseyov, O. Liquid crystalline human recombinant collagen: the challenge and the opportunity. *Tissue Engg. Part A*. **2013**, *19*, 1502-1506.

30. Lydon, J. Microtubules: Nature's smartest mesogens- a liquid crystal model for cell division, *Liquid Crystals Today* **2006**, *15*, 1-10.

31. Reich, Z.; Wachtel, E. J.; Minsky, A. Liquid-crystalline mesophases of plasmid DNA in bacteria. *Science* **1994**, *264*, 1460-1463.

32. Kresheck, G. C. Surfactants, *Water A Comprehensive Treatise*, Springer New York, 1975, pp 95-167.

33. Porter M. R. *Handbook of Surfactants*, Springer New York, 1991.

34. Schmitt Th. M., *Analysis of Surfactants*. 2nd ed, Taylor and Francis Online, 2001.

35. Singh, A.; Van H.; Ward, O. P. Surfactants in microbiology and biotechnology: Application aspects, *J. Biotech. Adv.*, **2007**, *25*, 99-121.

36. Tanford, C. *The Hydrophobic Effect*, 2nd ed., Wiley New York, 1980.

37. Rosen, M. J. *Surfactants and Interfacial Phenomena*, 2nd ed., Wiley New York, 1989

38. Israelachvili, J. *Intermolecular and Surface Forces*, 2nd ed., London Academic Press, 1992.

39. Gelbart, W. M.; Ben-Shaul, A. The "New" Science of "Complex Fluids", *J. Phys. Chem.* **1996**, *100*, 13169.

40. Alexander, A. E. The structure of the surfaces of solutions, *Trans. Faraday Soc*. **1942**, *38*, 54-63.

41. Shinoda, K.; Hutchinson, E. Pseudo-phase separation model for thermodynamic calculations on micellar solutions. *J. Phys. Chem.* **1962**, *66*, 577–582.

42. Blandamer, M. J.; Cullis, P. M.; Soldi, L. G.; Engberts, J. B. F. N.; Kacperska, A.; Van Os, N. M.; Subha, M. C. S. Thermodynamics of micellar systems: Comparison of mass action and phase equilibrium models for the calculation of standard Gibbs energies of micelle formation. *Adv. Colloid Interface Sci.* **1995**, 58, 171-209.

43. Ekwall, P.; Mandell, L.; Fontell, K. Solubilization in Micelles and Mesophases and the Transition from Normal to Reversed Structures. *Molecular Crystals* **1969**, 8, 157-213.

44. Maibaum, L.; Dinner, A. R.; Chandler, D. Micelle Formation and the Hydrophobic Effect, *J. Phys. Chem. B* **2004**, *108*, 6778–6781.

45. Tandford, C. Theory of micelle formation in aqueous solutions. *J. Phys. Chem.* **1974**, *78*, 2469–2479.

46. Blanazs, A.; Armes, S. P.; Ryan, A. J. Self-Assembled Block Copolymer Aggregates: From Micelles to Vesicles and their Biological Applications, *Macromol. Rapid Commun.*, **2009**, *30*, 267-277.

47. Otzen, D. Protein-surfactant interactions: A tale of many states. *Biochim. Biophys. Acta.* **2011**, 5, 562-591.

48. Hardy, D.; Desuzinges, M. E.; Rothnie A. J.; Jawhari A. The yin and yang of solubilization and stabilization for wild-type and full-length membrane protein. *Methods* **2018**, *147*, 118-125.

49. Fatma, I.; Kumar, A.; Thakur, R.; Sharma, V. Current Trends in Protein-Surfactant Interactions: A Review. *J. Mol. Liq.* **2021**, *341*, 117344.

50. Otzen, D. E.; Pedersen, J. N.; Rasmussen, H.; Pedersen, J. S. How do surfactants unfold and refold proteins? *Adv. Colloid Interface Sci.* **2022**, *308*, 102754.

51. Mathias, R. A.; Chen, Y. S.; Kapp, E. A.; Greening, D. W.; Mathivanan, S.; Simpson, R. J. Triton X-114 phase separation in the isolation and purification of mouse liver microsomal membrane proteins. *Methods* **2011**, *54*, 396-406.

52. Chamberlain, L. H. Detergents as tools for the purification and classification of lipid rafts. *FEBS Lett.* **2004**, *559*, 1-5.

53. Byrne, B.; Iwata, S. Membrane protein complexes. *Curr. Opin. Struct. Biol*. **2002**, *12*, 239-243.

54. Johansson, J. Structure and properties of surfactant protein C. *Biochim. Biophys. Acta*. **1998**, 1408, 161-172.

55. Hershberger, S. J.; Lee, S. G.; Chmielewski, J. Scaffolds for blocking protein-protein interactions. *Curr. Top. Med. Chem*. **2007**, *7*, 928-942.

CHAPTER 2

Multi-step self-association of monomers in the formation of sodium dodecyl sulfate micelles

Abstract

A step-wise self-association description is used to examine micellization of the anionic surfactant sodium dodecyl sulfate (SDS) at pH 7, 25°C. Experimental data consists of NMR line-broadening and chemical shift of SDS protons, and the hydrodynamic radii of micelles determined by pulsed-field gradient NMR. Detection of premicellar aggregates which are small oligomers at surfactant concentrations lower than the critical micellar concentration (CMC), facilitates the description of multi-step self-association. A linear correlation between the CMC and weight average molecular weight, and hence aggregation number, of SDS micelles is discussed.

2.1 Introduction

The process of spontaneous self-organization of surfactant monomers into micelles is generally described by two models based on thermodynamic theories of micellization, the phase-separation or phase-equilibrium model, and the mass-action model. According to the former, monomers and micelles are two distinct phases, and above the critical micelle concentration (CMC), which represents the point of maximum solubility, the surfactant is a two-phase system.[1,2] The latter describes a micelle as an assembly of surface active ions with bound gegenions formed via mass-action principles.[3-8] The two models are largely similar-

both rest on classical thermodynamics to relate the standard Gibbs energy of micellization to CMC at constant pressure and temperature, but the relation appears confusing when the phase-equilibrium model is examined. While the mass-action model allows the solution state for the reference state of both monomers and micelles, and any other relevant components when considered present in the system, the micellar reference state in the phase-separation model is poorly defined, because the activity coefficient of micellar composition appears zero here.[9] Because of such difficulties, including inconsistency with Gibbs phase rule, the phase-equilibrium model is often also called a pseudo-phase model. Nevertheless, the phase-equilibrium model is very useful in practice for providing mathematically simple analyses of surfactant solution properties.

The micelle literature is vastly rich, and the scope of this work delimits even a brief review of numerous discussions on experimental results and theoretical models of micellization. The rationale of this study is not to prove or disprove a model, rather to look for an analytical description of surfactant aggregation in relation to their hydrodynamic and molecular properties across the range of total molar concentration of monomeric surfactant. The surfactant chosen is sodium dodecyl sulfate, perhaps the most widely used ionic surfactant in molecular biology and clinical laboratories. Fluorescence and NMR spectroscopy have been used to experimentally follow micellization. Analysis of NMR chemical shift of SDS resonances, line-broadening, and mass-average molecular weight as a function of SDS concentration provide evidence for the occurrence of premicellar aggregates. Results are analyzed by a multi-step version of the mass action model in which the monomers can diffusively enter into and exit from the micelle in a sequential manner.

2.2. Experimental section

2.2.1. *Fluorescence measurement*

Solutions of SDS in the 0-140 mM range each containing 15 μM ANS ((8-anilinonaphthalene sulfonate) were prepared in 0.1 M sodium phosphate, pH 7.0. Fluorescence emission spectra were taken in a photon counting instrument (Fluoromax P4, Jobin-Yvon, Horiba) at 25°C by exciting ANS fluorescence at 360 nm.

2.2.2. *NMR spectroscopy*

One-dimensional ^{1}H spectra of SDS solutions in the 0.5-70 mM range prepared in D_2O containing 0.1 M phosphate, pH 7.0, were recorded at 25°C. Pulsed-field-gradient NMR (PFG NMR) diffusion measurements were performed using the water-sLED pulse sequence[10] with diffusion gradient (*z*-gradient) strength varying in the 8-50 Gauss cm^{-1} range. About 1 mM 1,4-dioxane added to the SDS samples served as the internal R_H standard. Values of R_H were calculated by

$$\mathrm{I}(g) = A\mathrm{e}^{-dg^2}$$

$$R_{\mathrm{H}}^{\mathrm{SDS}} = R_{\mathrm{H}}^{\mathrm{dioxane}} \left(\frac{d_{\mathrm{dioxane}}}{d_{\mathrm{SDS}}}\right) \quad (1)$$

where, *I* is the NMR signal intensity, *g* is the gradient strength, and the decay constant, *d*, is proportional to the diffusion coefficient, *D*. All spectra were recorded at 25°C in a 500 MHz Avance III (Bruker) spectrometer.

2.3. Results and discussion

2.3.1. *Micelle formation probed by ANS fluorescence and ^{1}H–NMR*

The monomer-micelle equilibrium is measured simply by monitoring the fluorescence of the hydrophobic dye ANS (8-anilinonaphthalene sulfonate), which fluoresces when bound to micellar aggregates (Figure 1a). As shown by the ANS-docked micellar structure generated by molecular dynamics, the dye-micelle interaction is dominated by hydrophobic effect, and presumably involves a positive entropy change originating from the association of ANS with the hydrophobic environment of SDS aggregates. Here, the interest lies in the SDS concentration dependence of three spectral parameters of ANS fluorescence.

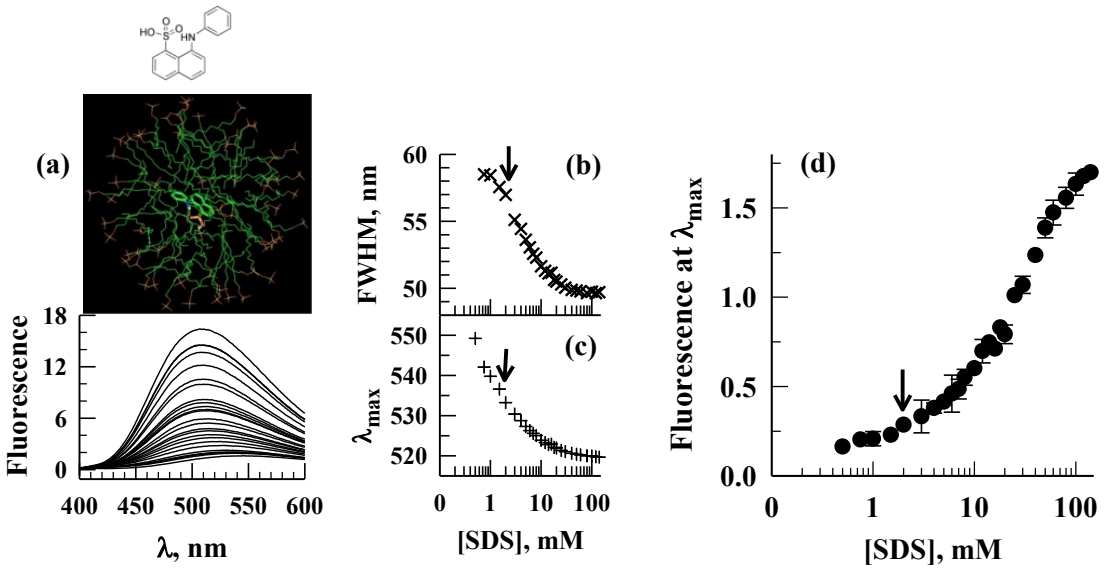

Figure 1. (a) ANS-docked structure of a SDS micelle obtained from molecular dynamics simulation, and steady-state ANS fluorescence spectra at various concentration of SDS in the 0-140 mM range. (b) and (c) Variation of the FWHM and emission maximum, respectively. The arrow heads point to the value of CMC under the present experimental conditions, 0.1 M phosphate, pH 7. (d) Changes in fluorescence intensity at the respective emission maximum does not show a sharp change in the CMC region (arrowhead).

One, the SDS dependence of FWHM of the skewed Gaussian band (Figure 1b) suggests that the distribution of small changes in the environment of the ANS molecule, which is the basis of the inhomogeneous broadening, shifts with the total monomer concentration. Two, the shift of the emission maximum to higher energy (Figure 1c) indicates large-scale burial of ANS in low dielectric environment of SDS aggregates. Three, higher quantum yield of ANS fluorescence (Figure 1d) should mean reduced collisional quenching due to increasingly rigid micellar environment as the surfactant concentration increases. The observed properties vary rather gradually at concentrations near the CMC of ~ 1.7 mM (Figure 1d).

The ^{1}H resonances in the NMR spectra are identified by the carbon atom numbering scheme shown below.

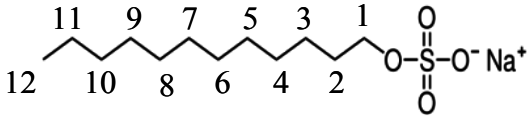

The SDS concentration dependence of spectral changes is illustrated for two resonances in Figure 2. Expectedly, the intensities grow with increasing concentration of the surfactant. The triplet for the methyl protons (H12) shifts downfield by 0.0317 ppm as the SDS concentration is raised from 0.2 to 20 mM, and remains constant thereafter (Figure 2). Two more triplets appear at ~10 mM SDS, and both shift slightly upfield. Similar spectral changes are observed for H3-11 protons. While the physical origins of observed chemical shifts are changes in magnetic susceptibility, local magnetic anisotropies, and polarization of the electron cloud near the hydrogens accompanied by the micelle aggregation process, the appearance of additional triplets must mean the existence of a heterogeneous ensemble in terms of the aggregation number, *n*. On the other hand, the chemical shift of the H2 resonance that appears as a pentate changes little (Figure 2), suggesting that micelle aggregation does not significantly change the

environment of this part of the chain. However, the pentate broadens somewhat even in the submicellar concentrations of the surfactant. Such broadening occurs for all SDS peaks, but the complexity of spectra renders quantification difficult. The broadening suggests that the alkyl chain experiences restricted motion resulting from self-association of monomers. The fact that line-broadening begins to appear even at very low concentration of the surfactant should mean the formation of small premicellar oligomers, and such behavior suggests that micellization could involves sequential or multi-step association of monomers.

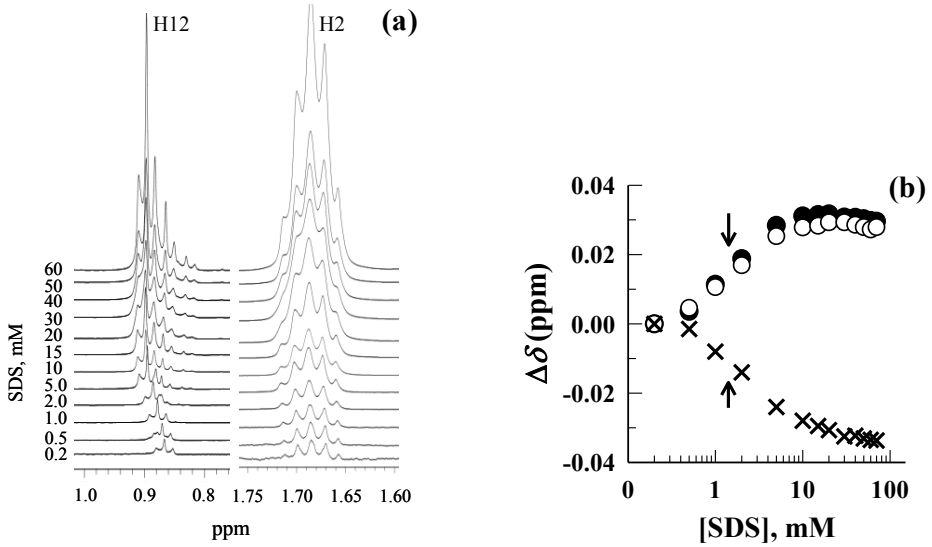

Figure 2. (a) Regions of ^{1}H NMR spectrum of SDS showing chemical shift of the H12 resonance and line-broadening for the H2 resonance at the indicated concentrations of SDS. Spectra were recorded in D_2O at pH 7, 25 °C. (b) Plots of micellization dependent chemical shifts for the proton resonances indicated. δΔ is the observed chemical shift minus the chemical shift of the proton resonance in the monomeric state of SDS. Thus, positive and negative values of δΔ mean low-field and high-field shifts, respectively. Data presented are for H12 methyl protons (●), H3-11 methylene protons (○), and H1 methylene protons (×).

Figure 2 also plots the chemical shift differences, $\Delta\delta$, the observed chemical shift minus the corresponding monomer chemical shift, for H12, H3-11, and H1 protons as a function of SDS concentration. Consistent with the observations made earlier for the fluorescence data (Figure 1), the micelle properties reported by the chemical shifts near the CMC do not change as sharply. Such spectral features and their changes as a function of the surfactant concentration, even though useful for a qualitative description of micellization, cannot be directly used to understand the mechanism of surfactant aggregation. Nor do they provide adequate proof in support of one or the other of thermodynamic models of micellization.

2.3.2. *Hydrodynamic radii (R_H) of micellar aggregates*

Looking for molecular parameters so as to model the process of micelle formation, sizes of micellar aggregates at different monomer concentration of SDS were quantified by pulsed-field-gradient NMR diffusion measurements. Figure 3a shows a representative set of primary data. The variation of R_H values with SDS concentration (Figure 3b) reveals a significant size difference for the aggregate species at submicellar concentrations. It is implicit that a measured value of R_H is the mean distribution value for aggregates of different size. The Gaussian distribution of micelle size varies continuously with SDS concentration, apparently atypical of a phase separation process.

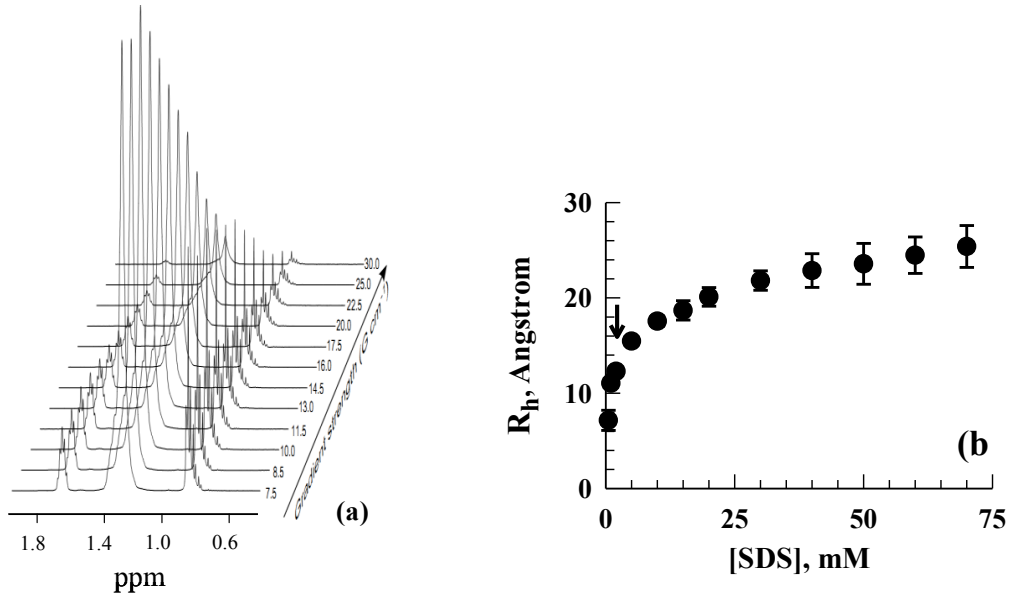

Figure 3. (a) High-field region of PFG NMR spectra of a D_2O solution of 70 mM SDS showing signal decay with increasing gradient strength. (b) Plot of hydrodynamic radius (R_H) of the micelle aggregate ensemble at various SDS concentration.

2.3.3. Step-wise self-association of monomers

For a model description of micelle formation, we consider multiple equilibria involving multimers b_i formed by association of i monomers,

$$[b] + [b] \overset{K_1}{\rightleftharpoons} [b_2] + [b] \overset{K_2}{\rightleftharpoons} [b_3] + [b] \overset{K_3}{\rightleftharpoons} [b_4] + [b] \overset{K_4}{\rightleftharpoons} [b_5] + [b] \rightleftharpoons \cdots \quad (1)$$

where, [b] and [b_i] are molar concentrations of free monomers and multimers, and K_i are association equilibrium constants for dimerization, trimerization, tetramerization, and so on for i = 1, 2, 3, …, respectively. The equilibria provide the molar concentration of total monomers, free and associated together, $[b]_{total}$.

$$[\mathbf{b}]_{\mathbf{total}} = [\mathbf{b}] + \mathbf{2}[\mathbf{b_2}] + \mathbf{3}[\mathbf{b_3}] + \mathbf{4}[\mathbf{b_4}] + \cdots$$

$$= [b] + 2K_1[b]^2 + 3K_1K_2[b]^3 + 4K_1K_2K_3[b]^4 + \cdots \quad (2)$$

Since $[b]_{total}$ is a function of all equilibrium constants in the sequence, the number of K_i can be reduced by considering the variation of free-energy of micellization, ΔG, with $[b]_{total}$. In general, $\Delta G=\Delta G_{tail}+\Delta G_{head}+\Delta G_{elec}$, where ΔG_{tail} and ΔG_{head} represent free energy changes for association of the hydrocarbon tail and the sulfate head, respectively. The free-energy component arising from ionic repulsions, ΔG_{elec}, opposes micelle formation. If the addition of a monomer to a multimer does not add much to ΔG, as might occur for large-size micelles, the sequential model of micellization may be reduced to a single value of K ($K \approx K_2 \approx K_3 \approx K_4 \approx K_5$ …) along with a hypothetical dimerization constant, K_1.[6] In the limit of smaller-size aggregates however, the assumption of independence of ΔG on $[b]_{total}$ becomes less obvious. In this case, ΔG is expected to vary non-linearly and gradually at low monomer concentrations, characteristic of molecular binding processes. Naively, a monomer would establish only one unit of contact with another monomer to form a dimer, and the same monomer could have two units of contact in a trimer, and so on. If ΔG is taken due to the size of inter-monomeric contacts, then K-values for smaller aggregates cannot be equated. At higher monomer concentrations, the assumption of linearity and independence of ΔG can still be made. Hence, we let $K_1 \neq K_2 \neq K$, where $K=K_3=K_4=K_5\cdots$, and simplify the expression for $[b]_{total}$.

$$[\mathbf{b}]_{\mathbf{total}} = [\mathbf{b}] + \mathbf{2}\boldsymbol{K_1}[\mathbf{b}]^{\mathbf{2}} + \mathbf{3}\boldsymbol{K_1K_2}[\mathbf{b}]^{\mathbf{3}} + \frac{\boldsymbol{K_1K_2}}{\boldsymbol{K^2}}[\mathbf{b}]\left\{\frac{\mathbf{1}}{(\mathbf{1}-\boldsymbol{K}[\mathbf{b}])^{\mathbf{2}}} - (\mathbf{1}+\mathbf{2}\boldsymbol{K}[\mathbf{b}]+\mathbf{3}\boldsymbol{K}^{\mathbf{2}}[\mathbf{b}]^{\mathbf{2}})\right\} \qquad (\mathbf{3})$$

This general equation for a sequential processes provides for the variation of free-monomer, [b], as a function of total monomer concentration, $[b]_{total}$. At a fixed $[b]_{total}$, the larger the magnitude of K_1K_2/K^2, the smaller the value of [b], and hence larger is the deviation from a

phase separation characteristic. The assumption of $K_1 \neq K_2 \neq K$, and $K = K_3 = K_4 = K_5 \cdots$ is arbitrary. Expressions for $[b]_{total}$ can also be written letting $K_1 \neq K_2 \neq K_3 \neq K$, without loss of generality.

2.3.4. Micelle molecular weights, equilibrium constants, and total monomer concentration

One of the predictions of the step-wise self-association model of micellization is the proportionality of the weight-average value of the molecular weight, M_w, to the square root of the total molar concentration, $([b]_{total})^{0.5}$, of all surfactant species, including the monomers[6]. For the present sequential model, the proportionality is given by

$$M_w \propto \sqrt{\frac{K^2}{K_1 K_2}} \sqrt{\frac{[b]_{total}}{CMC}} \quad (4)$$

This approximation relies on the assumption of $K = K_3 = K_4 = K_5 \cdots$, which means the free energy change, ΔG, becomes independent of entry of a monomer to an existing aggregate because the local structure around the micellized monomer does not change. To test the predicted $M_w \propto \sqrt{[b]_{total}}$ relation originally derived for large-size micelles,[6] molecular weights of micellar aggregates at different monomer concentration were calculated from NMR-derived hydrodynamic radii using the relation $R_H \sim (M_w)^a$, where $a = 1/3$ for spherical micelles. As shown in Figure 4, the plot of M_w and $([b]_{total})^{0.5}$ indeed provides an excellent linear correlation ($r^2 = 0.99$).

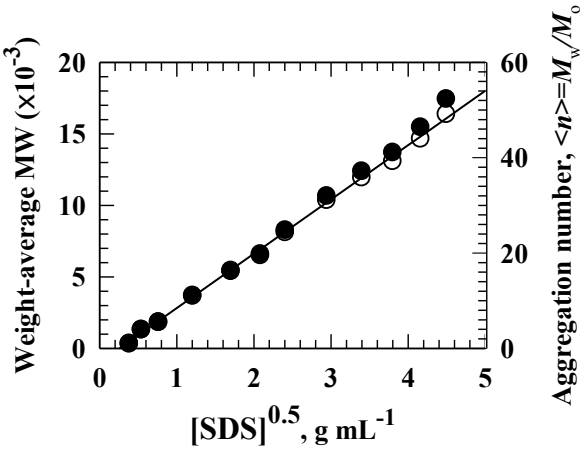

Figure 4. Plot of micellar molecular weight (and aggregation number) *vs* $\sqrt{C}$ (where C is SDS concentration) provides an excellent linear correlation (r^2=0.99). The uncorrected solvated molecular weight (○) differs little from that corrected for second virial coefficient (●).

Conversion of the apparent solvated molecular weight to the true solvated molecular weight by using the second virial coefficient (B_2 = 0.0016) affects the slope little. It is clear that for a given concentration of the total monomer, smaller values of the initial equilibrium constants, say K_1 and K_2, or relatively larger value of K, will lead to formation of micelles of higher aggregation number.

2.3.5. *Aggregation number, premicellar aggregates, and micelle shape*

The mean aggregation number of the micelle is $\langle n \rangle = M_w/M_o$, where M_o is the molecular weight of SDS monomer. Under the experimental conditions of 0.1 M sodium-phosphate, pH 7, 25°C employed here, $\langle n \rangle$ ranges from 1 to 57 for $([b]_{total})^{0.5}$ varying from 0.37 to 4.5 g mL^{-1} [1] (Figure 4b). While the literature consistently reports $n \sim 60$ for a maximally organized spherical micelle in pure water at 25 °C,[11,12] the range of aggregation numbers observed here on either side of CMC must mean the existence of a range of small micellar aggregates which grow, most likely by a stepwise process, to produce large micelles. The presence of aggregates

with fewer monomers is possible regardless of the mean value representation of aggregation numbers, because the width of the Gaussian distribution of the micelles is unlikely to deviate largely from the observed mean value.[13] The concentration of such premicellar aggregates in the sub-CMC region is much lower than the monomers,[13-15] but builds up substantially around the CMC region,[16] and dwindles thereafter.[15]

Since prolate micelles appear only under high ionic strength and surfactant concentration,[17] the maximally assembled micelle under the present conditions of experiments ($<n> \sim 57$) should be spherical or nearly so as indicated by numerous earlier studies on the size and shape of micelles.[17,18] The interest however lies in the mode of monomer association and the resultant shape of premicellar aggregates. In all likelihood, the individual monomers cluster by a tail-to-tail association.[19] Considering the general constraints on hydrocarbon chain packing in the process of amphiphile aggregation,[20,21] these small micellar aggregates could be lamellar. The shape of a dimer is then highly aspherical. The asphericity rapidly diminishes with increasing aggregation number,[18] and the shape turns to be spheroidal or nearly spherical for a fully assembled micelle.

2.3.6. *Instability of premicellar aggregates is the reason for their depleted level*

Low concentration of small oligomers in the sub-CMC region could arise from reduced thermodynamic stability of a low order assembly of SDS monomers when compared with a higher order one.[13-15] This is qualitatively understood from the differences in hydrophobic solvation [20,22] and heat capacity of oligomers of different aggregation number. The unfavorable interactions between water and alkyl chains are alleviated as increasing number of monomers enter the micelle,[23] meaning that the heat capacity change for micellization, ΔC_p, defined as

the heat capacity of the micelle minus the heat capacity of the monomer, becomes more negative as the micelle size grows. Clearly, the population of small oligomers will be low.

2.4. Conclusions

Small premicellar aggregates of SDS exist below CMC, in apparent conformity with the mass-action model of micellization. The step-wise self-association process of micellization consistently shows linear variation of weight average molecular weights of micelles having aggregation number in the limit of ~ 60.

2.5. References

1. Alexander, A. E. The Structure of the Surfaces of Solutions. *Trans. Faraday Soc.* **1942**, *38*, 54.

2. Shinoda, K.; Hutchinson, E. Pseudo-Phase Separation Model for Thermodynamic Calculations on Micellar Solutions. *J. Phys. Chem.* **1962**, *66*, 577–582.

3. Philips, J. N. *Trans. Faraday Soc.* **1955**, *51*, 561.

4. Bashford, M. T.; Woolley, E. M. Enthalpies of Dilution of Aqueous Decyl-, Dodecyl-, Tetradecyl-, and Hexadecyltrimethylammonium Bromides at 10, 25, 40, and 55 °C. *J. Phys. Chem.* **1985**, *89*, 3173–3179.

5. Dearden, L. V.; Woolley, E. M. Heat Capacities of Aqueous Decyl-, Dodecyl-, Tetradecyl-and Hexadecyltrimethylammonium Bromides at 10, 25, 40, and 55 °C. *J. Phys. Chem.* **1987**, *91*, 4123–4127.

6. Mukerjee, P. Size Distribution of Small and Large Micelles. Multiple Equilibrium Analysis. *J. Phys. Chem.* **1972**, *76,* 565–570.

7. Desnoyers, J. E.; Caron, G.; DeLisi, R.; Roberts, D.; Roux, A.; Perron, G. Thermodynamic Properties of Alkyldimethylamine Oxides in Water: Application of a Mass-Action Model for Micellization. *J. Phys. Chem.* **1983**, *87*, 1397–1406.

8. Rosenholm, J. B.; Burchfield, T. E.; Hepler, L. G. Thermodynamics of Micelle Formation: Standard States, Temperature Dependence of the Critical Micelle Concentration, and Thermal Expansion of the Solvent. *J. Colloid Interface Sci.* **1980**, *78,* 191–194.

9. Blandamer, M. J.; Cullis, P. M.; Soldi, L. G.; Engberts, J. B. F. N.; Kacperska, A.; Van Os, N. M.; Subha, M. C. S. Thermodynamics of Micellar Systems: Comparison of Mass Action and Phase Equilibrium Models for the Calculation of Standard Gibbs Energies of Micelle Formation. *Adv. Colloid Interface Sci.* **1995**, *58,* 171–209.

10. Altieri, A. S.; Hinton, D. P.; Byrd, R. A. Association of Biomolecular Systems via Pulsed Field Gradient NMR Self-Diffusion Measurements. *J. Am. Chem. Soc.* **1995**, *117,* 7566–7567.

11. Chiang, H. C.; Lukton, A. Interaction of Sodium Dodecyl Sulfate with the Hydrophobic Fluorescent Probe, 2-p-Toluidinylnaphthalene-6-Sulfonate. *J. Phys. Chem.* **1975**, *79,* 1935–1939.

12. Chen, J. M.; Su, T. M.; Mou, C. Y. Size of Sodium Dodecyl Sulfate Micelle in Concentrated Salt Solutions. *J. Phys. Chem.* **1986**, *90,* 2418–2421.

13. Aniansson, E. A. G.; Wall, S. N.; Almgren, M.; Hoffmann, H.; Kielmann, I.; Ulbricht, W.; Zana, R.; Lang, J.; Tondre, C. Theory of the Kinetics of Micellar Equilibria and Quantitative Interpretation of Chemical Relaxation Studies of Micellar Solutions of Ionic Surfactants. *J. Phys. Chem.* **1976**, *80*, 905–922.

14. Aniansson, E. A. G.; Wall, S. N. Kinetics of Step-Wise Micelle Association. *J. Phys. Chem.* **1974**, *78*, 1024–1030.

15. Cui, X.; Mao, S.; Liu, M.; Yuan, H.; Du, Y. Mechanism of Surfactant Micelle Formation. *Langmuir* **2008**, *24,* 10771–10775.

16. Hadgiivanova, R.; Diamant, H. Premicellar Aggregation of Amphiphilic Molecules. *J. Phys. Chem. B* **2007**, *111,* 8854–8859.

17. Mazer, N. A.; Olofsson, G. Calorimetric Studies of Micelle Formation and Micellar Growth in Sodium Dodecyl Sulfate Solutions. *J. Phys. Chem.* **1982**, *86,* 4584–4593.

18. Colafemmina, G.; Fiorentino, D.; Ceglie, A.; Carretti, E.; Fratini, E.; Dei, L.; Baglioni, P.; Palazzo, G. Structure of SDS Micelles with Propylene Carbonate as Co-solvent: A PGSE-NMR and SAXS Study. *J. Phys. Chem. B* **2007**, *111,* 7184–7193.

19. Yoshii, N.; Okazaki, S. A. Molecular Dynamics Study of Structural Stability of Spherical SDS Micelle as a Function of Its Size. *Chem. Phys. Lett.* **2006**, *425,* 58–61.

20. Israelachvili, J. N.; Mitchell, D. J.; Ninham, B. N. *J. Chem. Soc. Faraday Trans.* **1976**, *72*, 1525.

21. Israelachvili, J. N.; Mitchell, D. J.; Ninham, B. W. Theory of Self-Assembly of Lipid Bilayers and Vesicles. *Biochim. Biophys. Acta* **1977**, *470,* 185–201.

22. Tanford, C. *The Hydrophobic Effect*; Wiley, 1973.

23. Mukerjee, P. *Adv. Colloid Interface Sci.* **1967**, *1*, 241.

CHAPTER 3

Completion of all structural, conformational, and fibrillation transitions in proteins at submicellar SDS

Abstract

In the continued engagement with the interaction of sodium dodecyl sulfate (SDS) with proteins and the reaction of the latter thereof ambiguities exist regarding the level of the surfactant adequate to obtain complete structural and functional response of the protein. Uncertainties also appear concerning the role of protein charge and micellar surfactant concentration on amyloid fibrillation. To examine these issues this study reports on equilibrium and kinetic measurements of SDS interaction with six model proteins, and analyzes the results to obtain a united view of tertiary conformational breakdown, reorganization and restructuration of secondary structure, and entry into the crystal-like amyloid fibrillar state. Significantly, all of these responses are entirely resolved at much lower than the critical micellar concentration (CMC) of SDS. Adequate number of electrostatic interaction of dodceyl sulfate anion (DS^-) with positive charges on the protein can destroy both secondary and tertiary structures completely followed by restructuration preferentially to α-helices. Invariably all proteins are driven by SDS to aggregate which can be amorphous or crystal-like corresponding to low or high concentration of the surfactant.

3.1. Introduction

The age-old area of protein–SDS interactions has witnessed volumes of studies due to numerous applications of the system ranging from fundamental understanding of molecular

structure in micelle mimetic of membranes to industrial production of washes and hygiene merchandise. More recent studies on thermodynamics and kinetics of protein–surfactant interactions,[1-16] forces involved therein,[17,18] and the complexity of changes brought about in the protein structure,[13,14,19,20] are continuing to provide advances in the topic. Still persisting are however some basic-level obscurity that includes the structure content of the SDS-interacted protein, the resistance of β-sheet proteins to denaturation,[3,8] shift and restructuration of β→α secondary structure,[18] the role of electrostatic versus hydrophobic interactions in altering the conformational landscape,[20] and the mystery of SDS-to-protein ratio dependent aggregation of the complex.[2] The difficulties arise partly from protein-specific manifest of SDS-resistance that has been dubbed kinetic stability,[3] anomalous SDS effect,[21] and the strong binding of the ionic surfactant to protein side chain which produces only a narrow window in the submillimolar concentration to work with.

The central objective of this study is to provide a unified conceptual understanding of the action of SDS on protein structure and conformation with references to the surfactant binding isotherm and possible modes of binding. Experiments have been performed uniformly with a set of six protein paradigms – lysozyme, cytochrome *c*, myoglobin, α-lactalbumin, β-lactoglobulin, and trypsin, held under conditions that provide a broad range of net charge content. But for trypsin, these proteins have been widely by authors in the field to study protein-SDS interactions. We first looked into the general belief that global protein unfolding occurs above the CMC of SDS, since only a few proteins have been found to unfold at sub-CMC level.[1,13] The idea that secondary structure shifts to all α-helix in SDS-denatured protein has also been considered. These analyses have been carried out by equilibrium and kinetic measurements probed with basic CD and fluorescence methods. The emerging idea that SDS binding drives protein fibrillation universally has been studied next by fibrillation kinetics and electron microscopy.[22,23] Evidence for charge-based response of proteins to the extent of

complete loss of all structures has been obtained. Importantly, we resolve all of these processes lower in the submicellar concentration of SDS showing that the micellar regime may not at all be relevant for protein conformational changes and fibrillation.

3.2. Materials and methods

All proteins were purchased from Sigma Chemical Company, and SDS was from Calbiochem. Experiments were performed at 25(±1)°C using water at pH 3.8 (lysozyme), 100 mM sodium phosphate, pH 5.7 (cytochrome *c*), 20 mM sodium phosphate, pH 7 (myoglobin), 100 mM Tris, pH 7 (α-lactalbumin), 20 mM sodium phosphate, pH 7 (β-lactoglobulin), and 10 mM sodium phosphate, pH 8 (Trypsin).

3.2.1. *Determination of CMC*

Solutions containing ~8 μM protein, the dye rhodamine B fixed to a concentration that yields ideal fluorescence signal and variable SDS under the pH and buffer conditions mentioned above were incubated for 2 h in dark at 25(±1)°C, and the dye fluorescence spectra were recorded by exiting at 310 nm. The control experiment excluded protein in the solution. The CMC value is determined by plotting the fluorescence values at the dye emission maximum as a function of SDS concentration.

3.2.2. *Equilibrium measurements*

Titration of a protein with SDS involved the use of two stock solutions – the native protein solution and the denatured protein solution containing the highest concentration of SDS employed. The stock solutions were prepared carefully to obtain considerable uniformity in both protein concentration and the buffer pH, and samples of different SDS concentration

were obtained by appropriate mixing of the two stock solutions. This procedure of sample preparation ensures reversibility of the protein-SDS reaction. Final protein concentrations were 4–8, 7, 7, 8, 8, and 7 μM for lysozyme, cytochrome *c*, myoglobin, α-lactalbumin, β-lactoglobulin, and trypsin, respectively. Samples were equilibrated typically overnight at 25(±1)°C, and CD, fluorescence, and turbidity measurements were done successively. Measurements were performed at 25 °C using AVIV SF420 instrument for CD, Jasco FP-8300 for fluorescence, and a CARY 100 UV-Visible spectrophotometer for turbidity measurement. Sample pH was checked once more after completion of the experiment.

3.2.3. *Kinetics measured by manual mixing*

As a prelude to faster kinetics, the SDS-induced conformational changes in seconds of time-scale were measured by manually mixing the protein solution with the appropriate buffer so as to raise and lower the surfactant concentration. The final protein concentration in the mixed solution was 9 μM. The mixing dead time was ~10 s, and kinetics were monitored at 25°C by both far-UV CD and tryptophan fluorescence.

3.2.4. *Stopped-flow kinetics*

Since the equilibrium experiments provide two phases of conformational transitions across the SDS scale, kinetics were measured by diluting the protein solutions held at the two ends of each transition. For example, lysozyme unfolding measurements were carried out in two sets corresponding to the two phases – one involving dilution of the native protein solution that contained no SDS with different buffers of increasing surfactant level, and the other requiring dilution of the initial protein solution that had 1.5 mM with buffers of lower level of SDS. However, refolding was carried out by diluting the initial protein solution prepared in 0.2 mM SDS so as to variably decrease (phase 1) and increase (phase 2) the final surfactant

concentration. The mixing ratio of one part of the protein solution (38 μL) to seven parts of the buffer (267 μL) was held constant, and the final protein concentration was ~8 μM. Kinetics were monitored by tryptophan fluorescence at 25 °C using a SFM–400 BioLogic instrument the mixing dead-time of which was found to be 1.7 ms for a 0.8 mm cuvette (FC 08). Each kinetic trace obtained finally was an average of a minimum of seven traces.

3.2.5. *Kinetics of fibrillation and FESEM imaging*

To determine the time and type of protein aggregation a manually mixed solution containing 8 μM protein, 50 μM dye ThT (4-[3,6-dimethyl benzothiazol-2-yl]-N,N-dimethylaniline), and variable SDS in 0.015 to 1 mM range was excited at 432 nm, and the 478-nm emission of the dye was measured with time. The experiment was done at 25 °C for all proteins using the respective buffer system mentioned above. Fibers were however imaged availing the same samples that were used for equilibrium measurements described earlier. Gold coated samples were imaged in a ZEISS Ultra 55 FESEM instrument operating at 30 kV.

3.2.6. *Determination of SDS activity*

Mean activity coefficients for SDS at 25°C available from the work of Burchfield and Wooley[24] were analyzed to obtain the following empirical equation valid for concentrations at least up to CMC

$$\ln \gamma_{\pm} = a + \left(\frac{1}{b + c\sqrt{[\mathrm{SDS}]}}\right), \qquad (1)$$

in which a = 0.054125, b = –13.866168, c = 2.577401, and [SDS] is surfactant molality. Instability of the function appears above 20 mM SDS.

3.3. Results

3.3.1. *CMC of SDS in buffered protein solutions*

Since this study seeks details of events at submicellar concentrations of SDS, it is desirable to know the CMC of the surfactant even if a value above 5 could be easily assumed. In view of the fact that the protein perturbs the chemical potential of SDS in the three-component water-protein-SDS solution, the CMC of SDS is expected to shift to a lower value. Figure 1 shows the extraction of CMC values in lysozyme, cytochrome *c*, myoglobin, and trypsin solutions at respective buffered pH used for experiments throughout.

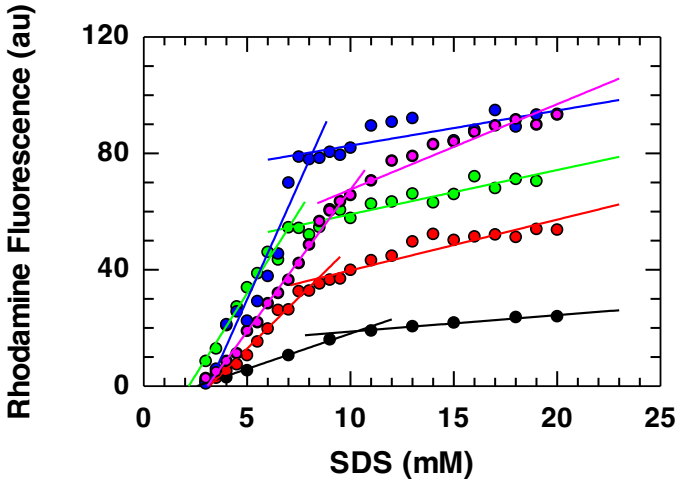

Figure 1. SDS dependence of rhodamine-B fluorescence in water solution (black) compared with the fluorescence of protein–SDS–rhodamine-B solutions. Red, green, pink, and blue symbols correspond to lysozyme (aqueous, pH 3.8), cytochrome *c* (100 mM sodium phosphate, pH 5.7) myoglobin (20 mM sodium phosphate, pH 7), and trypsin (10 mM sodium phosphate, pH 8), respectively. The break point of rhodamine-B fluorescence, determined by linear extrapolation of data from each side, approximates CMC values of 10.1, 8.4, 7.25, 10, and 8.3 for no protein, lysozyme, cytochrome *c*, myoglobin, and trypsin, respectively.

The values are in the range of ~ 7.0 for cytochrome *c* to ~ 9.9 for myoglobin, which are somewhat lower than the CMC of ~ 10.1 for water solution of SDS. As our experiments described below are performed at lower than 3 mM SDS, all results correspond to surfactant concentrations substantially lower than the CMC.

3.3.2. *Far-UV CD bands of proteins at submicellar SDS*

The negative CD bands centered at 222 and 207 nm, the former showing relatively larger ellipticity, are associated with α-helical protein structure. But the prominence of the 222-nm band with little ellipticity at 207 nm is indicative of overwhelming β-sheet content of the protein. Thus both 222 and 207-nm bands can be used to monitor the extent of secondary structure content in protein conformational studies. Figure 2 uses lysozyme, cytochrome *c*, and β-lactoglobulin to exemplify changes in the far-UV CD spectrum brought about by sub-CMC concentrations. For lysozyme and cytochrome *c* the initial band intensity at both 222 and 207 nm gradually disappears, indicating virtually complete loss of secondary structure. The bands however reappear as the SDS concentration continues to rise up to the CMC, implying recovery of the lost secondary structure. In the case of predominantly β-sheeted β-lactoglobulin that shows a major band centered at 218 nm the first event of band disappearance is not seen, but SDS causes the initial 218-nm spectral minimum to shift to a strongly growing negative band at 207 nm and a commensurate weaker 222-nm shoulder, suggesting SDS-induced β→α structural transition apparently complemented by denaturation.

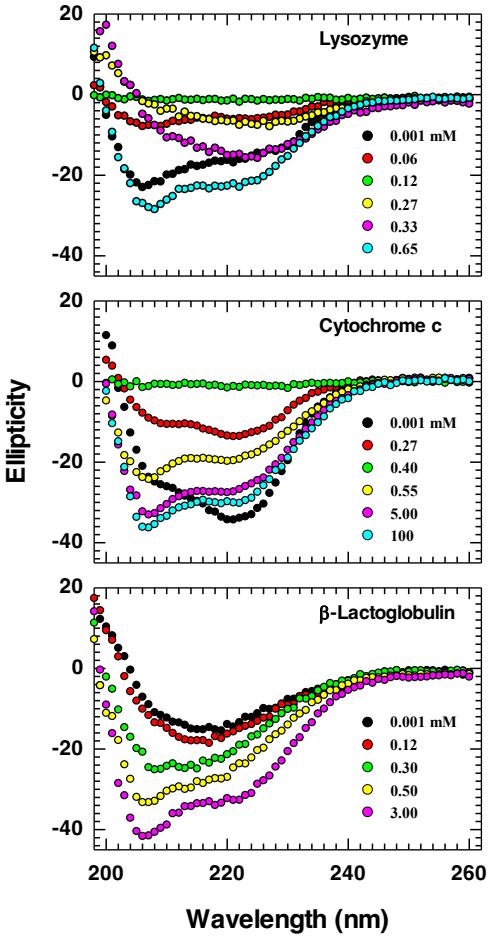

Figure 2. Far-UV CD spectra of lysozyme, cytochrome *c*, and β-lactoglobulin at indicated SDS concentrations showing band intensities near 222 and 207 nm.

3.3.3. *Successive unfolding and reformation of secondary structure within the CMC*

The spectral observations above led to a series of careful protein-SDS titrations, of which the 222-nm monitored data for six proteins are provided in Figure 3 where we choose to plot natural logarithm of activity rather than molality, ln a_{SDS}, because SDS is highly non-ideal in aqueous solution and its effect on protein need not be linear in concentration. Results for lysozyme (pH 3.8) and cytochrome *c* (pH 5.8) show abrupt loss of ellipticity within an extremely narrow region of the surfactant concentration, suggesting virtually complete removal of secondary structure by ~ 0.21 mM SDS. The cooperativity of structure loss is more pronounced in the case of lysozyme where a small but distinct plateau region of SDS is identified in which the protein stays unfolded. Passing the plateau region the secondary

structure is restored cooperatively and at least completely at ~ 0.42 mM SDS. Cytochrome *c* produces identical result except for the lack of a plateau region to straddle the unfolding and reforming transitions of secondary structure. Clearly, SDS has acted to both first unfold and then extensively reform the secondary structure. The regain of secondary structure here does not necessarily mean refolding to the same native state in the absence of SDS that was started with. The results do not provide specific information regarding the extent of SDS-induced secondary structure and conformation of the protein. Hence we call this 'newly secondary-structured' protein denatured or D, and propose the existence of a three-state equilibrium N $\rightleftharpoons$ U $\rightleftharpoons$ D at submicellar SDS.

Myoglobin at pH 7 is also unfolded by ~ 0.42 mM SDS cooperatively but partially accounting for the breakdown of roughly one-third of the secondary structure. Restoration of secondary structure ensues immediately, but the 222-nm ellipticity is recovered only in part, suggesting partly unfolded myoglobin at SDS levels higher than CMC.

The other three proteins – α-lactalbumin (pH 7), β-lactoglobulin (pH 6.3), and Trypsin (pH 8) – show little change in 222-nm CD up to ~0.2 mM SDS followed by a cooperative increase of ellipticity to the extent of 30, 160, and 320% of the initial value for the respective proteins. Such changes in secondary structure are consistent with earlier report of SDS action on α-lactalbumin[11] and the "α-state" structure of β-lactoglobulin in the presence of organic solvents and alcohols.[25] Clearly, SDS has induced additional secondary structure, but this change is not attributed to refolding because these three proteins in aqueous medium at respective pH are known to be functionally active native protein, which at first sight would provide little scope for further conformational folding. However, the transition for all three proteins is highly cooperative with well-defined baselines, characteristic of a stabilizing conformational transition accompanied by a substantial increase in secondary structure. Thus,

it is tempting to assign these transitions to further folding of the proteins, a claim that cannot be generalized when further analyses are carried out. They are rather denaturation transitions that lead to excessive secondary restructuration involving a β→α switch.

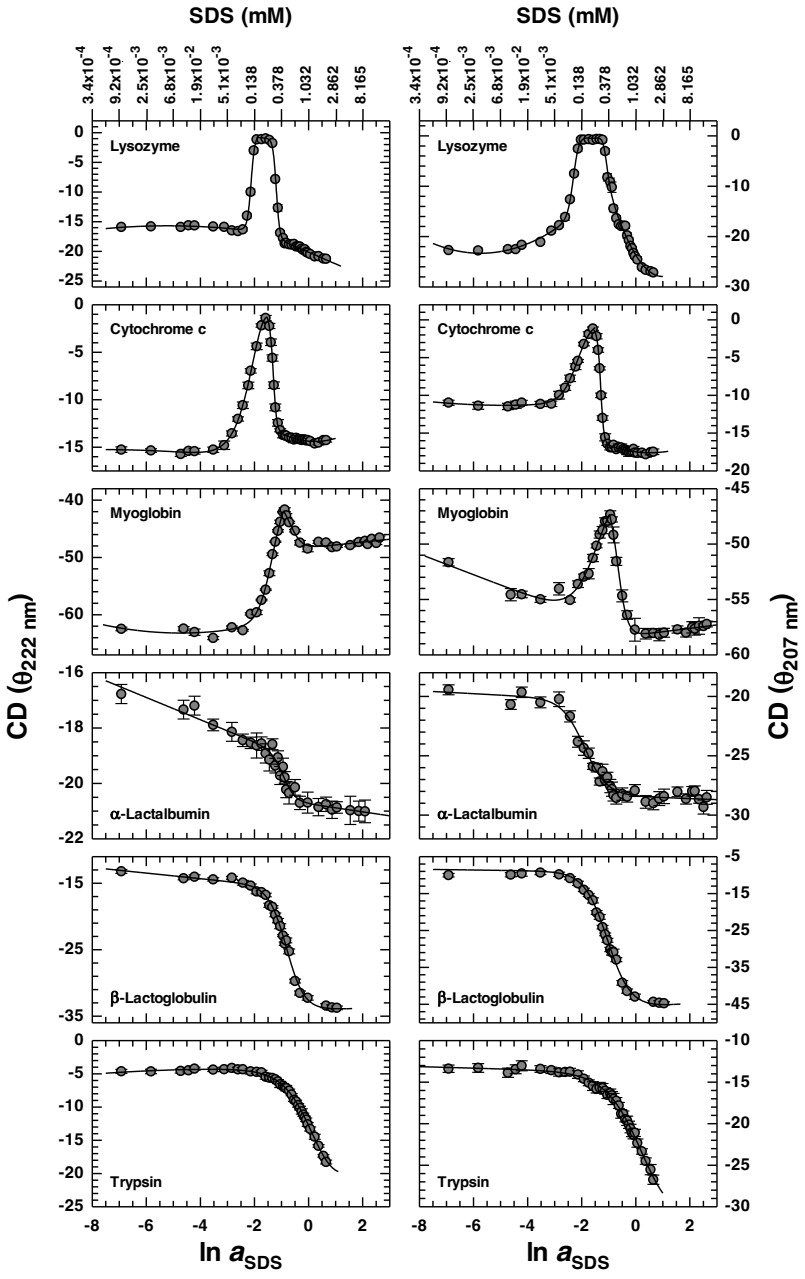

Figure 3. The SDS dependence of 222 and 207-nm ellipticity for the proteins indicated. The data are plotted with natural logarithm of SDS activity (a_{SDS}) because of highly non-ideal

behavior of the surfactant solution. Molar concentrations corresponding to some ln a_{SDS} are shown on top. Since the effect of SDS should not be linear because of the non-ideality in solution behavior, the solid lines drawn through data points are according to a two-state transition that assumes linearity of the protein effect on ln a_{SDS}.

3.3.4. *β-sheet ⇌ α-helix transition in SDS: no general rule for β-sheet → α-helix transition*

An assessment of SDS-induced preferential secondary structure type for the six proteins is provided in Figure 5 that plots R_θ – the ratio of ellipticity at 207 to 222 nm – with the surfactant level below CMC. The premise is that R_θ will increase with α-helix preference. For lysozyme the ratio initially decreases to zero, indicating favored breakdown of α-helix over β-sheet up to the point of complete disappearance of both secondary structure types.

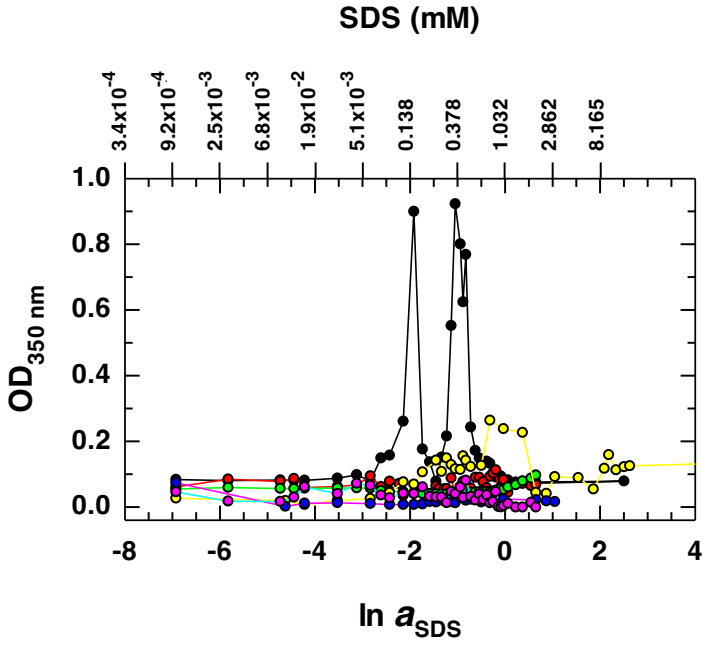

Figure 4. Turbidity measurement of the same set of protein solutions that were used for equilibrium measurements. Symbols colored in black, red, green, yellow, blue, and pink

stand for lysozyme, cytochrome *c*, myoglobin, α-lactalbumin, β-lactoglobulin, and trypsin, respectively.

This cooperative decrease of R_θ with SDS is associated with complete unfolding of lysozyme leaving no residual structure (see also Figure 5). In the refolding phase next R_θ is recovered cooperatively, indicating preferential α-helix formation over β-sheet. The hatched region in the graph shows scattered data points corresponding to a few turbid samples (Figure 4). The R_θ recovery in the SDS-denatured protein or D state however does not assert excess helicity relative to its content in the native state.

The biphasic change of R_θ observed for lysozyme is not reproduced in results for cytochrome *c* despite the fact that cytochrome *c* undergoes the same successive stages of unfolding and denaturation in the presence of SDS. The two stages are smeared in a single cooperative increase of R_θ the midpoint of which corresponds to the unfolding concentration of SDS (Figure 5), meaning preferential α-helical propensity and higher content of α-helix in the denatured state.

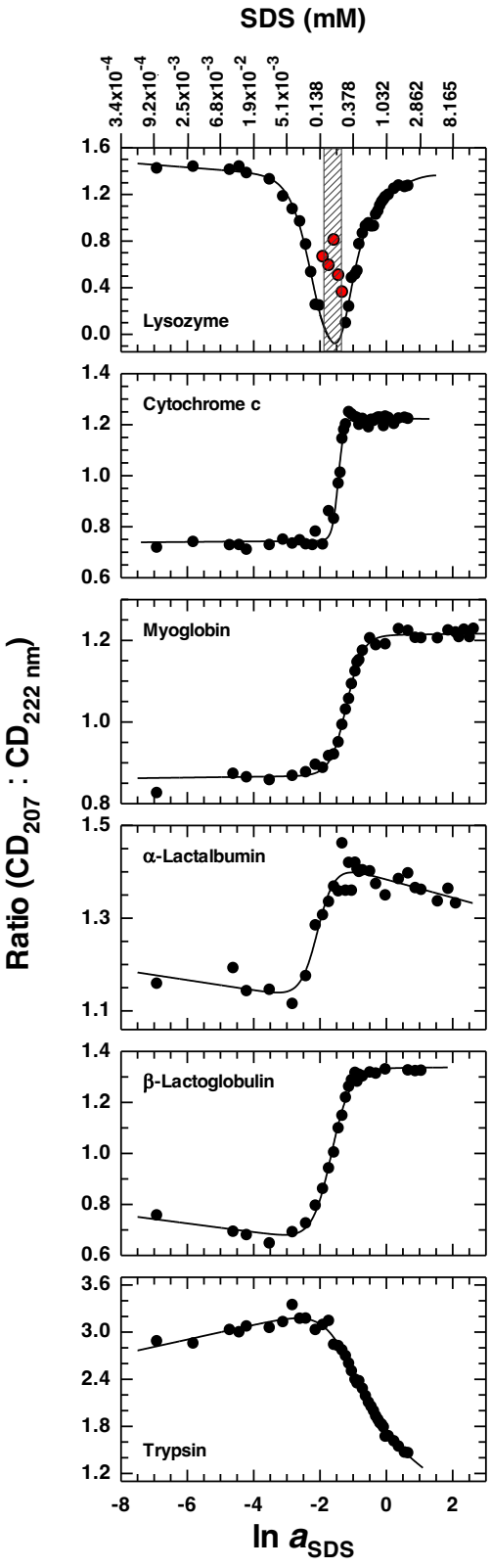

Figure 5. The ratio of 207 to 222-nm ellipticity with ln a_{SDS} for the proteins indicated. Solid lines through data are drawn to show a simple two-state transition that assumes linearity of effect on ln a_{SDS}. The hatched strip in the lysozyme graph shows data for a few turbid samples (see Figure 4).

The increase of R_θ with SDS for the all β-sheet protein myoglobin, α-helix and β-sheet mixed α-lactalbumin, and predominantly β-sheet β-lactoglobulin is very similar to that for cytochrome *c*, suggesting variable β-sheet → α-helix transition. The increase occurs in a single cooperative phase, although the midpoint and the slope of the transition vary expectedly from one to another protein. The largely β-sheet trypsin shows a cooperative decrease of R_θ with increasing concentration of SDS, suggesting the surfactant-induced formation of additional β-sheet structure. The results suggest that SDS binding to these proteins causes a cooperative β-

sheet → α-helix structural transition, consistent with the belief that SDS-denatured proteins contain abundant α-helices.[13] However, the change of R_0 for trypsin with SDS exemplifies the case for an α-helix → β-sheet transition, which together with the result for lysozyme indicates that β-sheet → α-helix structural transition accompanying SD denaturation need not be a general rule.

3.3.5. *Successive unfolding and refolding of tertiary structures of lysozyme and apo-α-lactalbumin within the CMC*

Action of SDS on the tertiary structure of all six proteins was studied by tryptophan fluorescence of the same samples that were used for CD measurements. Figure 6 organizes the data into fluorescence spectra (left row), fluorescence emission maxima (middle row), and fluorescence intensity read at a fixed wavelength which corresponds to either no SDS or in the presence of highest concentration of SDS (right row). In general, each emission spectrum is inhomogeneous-broadened Gaussian made up of several overlapping bands that correspond to differences in the environment of the tryptophan side chain in different molecules.

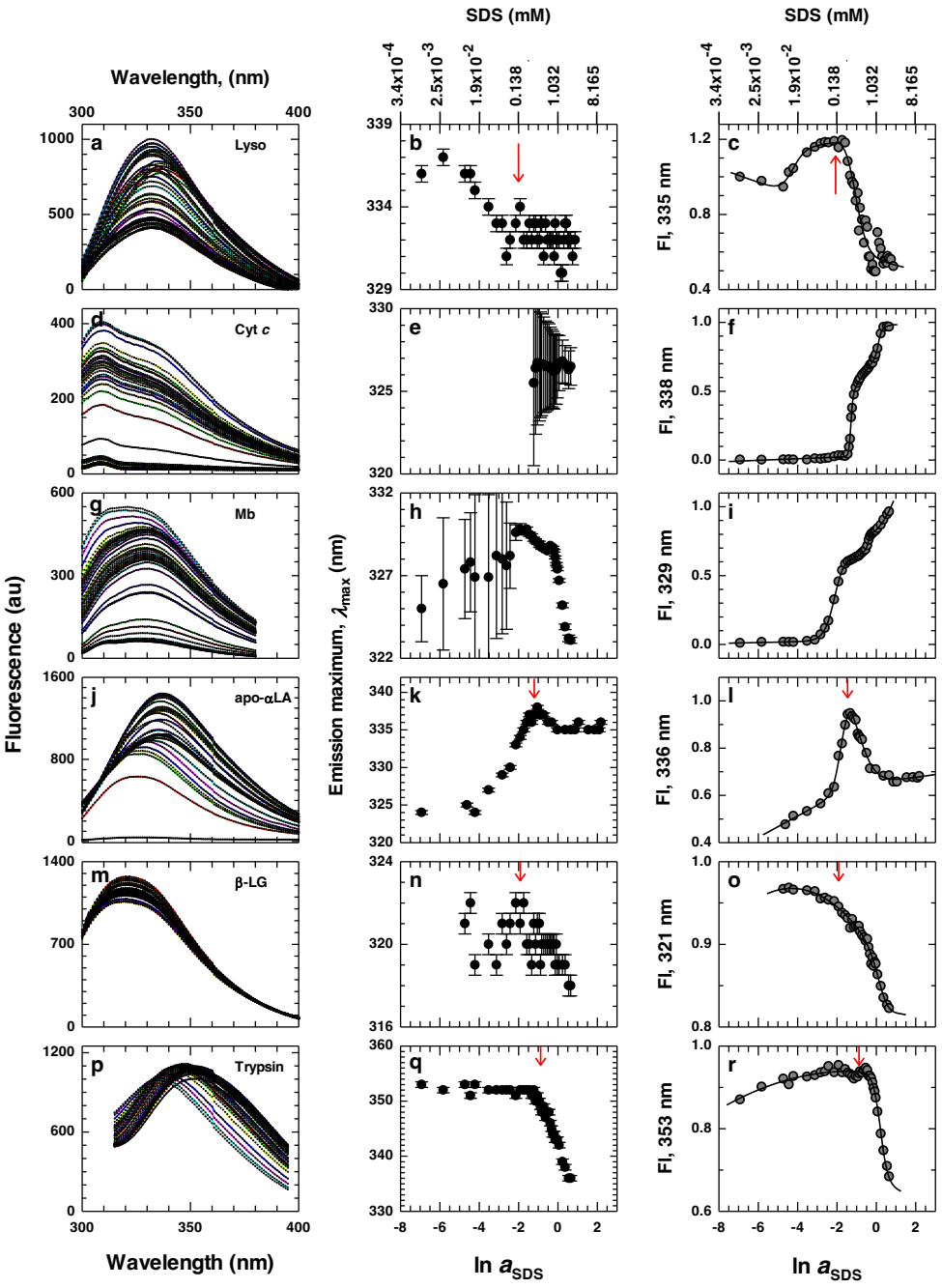

Figure 6. Details of tryptophan fluorescence with SDS. Spectra for cytochrome *c* (d) are relatively less resolved resulting in virtually no resolution of λ_{max} (e). Spectral quality for myoglobin greatly improves at higher SDS. Red arrows indicate correspondence of SDS dependence of λ_{max} and conformational transition which is least clear in the case of cytochrome *c*.

The SDS dependence of the wavelength of maximum emission, λ_{max}, was read by inspection or Gaussian fits of the spectra. For cytochrome *c* and myoglobin, whose native-state fluorescence is quenched by resonance energy transfer to the heme, λ_{max} values at low concentration of SDS are in large error (Figure 6e,h). The tryptophan emission band of cytochrome *c* which appears as a shoulder (Figure 6d) compounds the difficulty. The fluorescence increase for both cytochrome *c* and myoglobin (Figure 6f,i) indicates tertiary structure unfolding via structural intermediates that populate near 0.15 mM SDS.

Results for β-LG and trypsin are relatively easier to interpret. Constant λ_{max} at low SDS for both (Figure 6n,q) is an indication that tertiary structures of the two proteins are not considerably perturbed, but the decrease of λ_{max} at SDS concentration higher than ~0.15 mM suggests greater burial of the tryptophan side chain (Figure 6o,r). The fluorescence decrease at 321 and 353 nm for β-lactoglobulin and trypsin is associated with structure unfolding[26,27] and refolding,[28] respectively.

Even clearer are results for lysozyme and apo-αLA. For lysozyme, a 4-nm emission blue-shift up to ~0.15 mM SDS accompanies tertiary structure unfolding, the λ_{max} remains nearly constant thereafter, and the tertiary structure appears to fold up at SDS concentration much lower than the CMC (Figure 6b,c). The λ_{max} of apo-αLA red-shifts by ~14 nm at low SDS concentration but sharply turns to blue after ~0.3 mM SDS (Figure 6k), and the two transitions correspond to tertiary structure unfolding and refolding, respectively (Figure 6l). The two transitions of apo-αLA at sub-CMC level were observed in an earlier 350-nm fluorescence data as well,[11] but the authors interpreted the transitions as indicative of a two-step binding of SDS leading to denaturation. Since the increase and decrease in fluorescence emission read at 335 and 336 nm for lysozyme and apo-αLA, respectively, are consistent with those seen in guanidine-induced equilibrium unfolding of the two proteins,[29,30] we find

successive unfolding and refolding of tertiary structures of these two proteins at sub-CMC level of SDS. In the absence of information about the extent and the nature of this refolded tertiary structure we call the state D for denatured and propose a submicellar equilibrium N $\rightleftharpoons$ U $\rightleftharpoons$ D, which is consistent with results for secondary structure.

3.3.6. *Free energy of unfolding and refolding (denaturation) at submicellar SDS*

Because of strong and stoichiometric binding of SDS monomers to protein side chains a useful theoretical form for the excess free energy of binding is based on the binding polynomial analysis.[31] Using subscripts 1, 2, and 3 for water, protein, and SDS, respectively, the chemical potential of the protein μ_2 is given by

$$\mu_2 = \mu_2^{\circ} + RT \ln m_2 + RT\beta_2 \tag{2}$$

where μ_2° is the standard-state chemical potential, m_2 is molal concentration of the protein, and β_2 represents the excess free energy of the protein arising from its binding to SDS monomers. The formula for β_2 based on mutual perturbation of chemical potentials of protein and ligand takes the form[32,33]

$$\beta_2 \equiv \Gamma_{23} \cong \left(\frac{\partial m_3}{\partial m_2}\right)_{T,P,\mu_3}$$

in which Γ_{23} is the thermodynamic binding coefficient. Because the difference in the chemical potentials of the protein in the presence of two different concentrations of the ligand gives the change in the free energy of the protein, the free energy of folding, ΔG, determined from SDS unfolding results can be written as

$$\Delta G_{\circ} = \mu_2^{\mathrm{D}} - \mu_2^{\mathrm{N}} = -RT(\Gamma_{23}^{\mathrm{D}} - \Gamma_{23}^{\mathrm{N}}) = -RT\Delta\Gamma_{23}, \tag{3}$$

where μ_2^{D} and μ_2^{N} are chemical potentials of the protein in the presence and absence of SDS, and Γ_{23}^{D} and Γ_{23}^{N} are corresponding thermodynamic binding coefficients. When information about Γ_{23} is not available, $\Delta\Gamma_{23}$ can be estimated from the Wyman linkage equation[34] expressed in terms of SDS activity

$$-RT\left(\frac{\partial \ln K}{\partial \ln a_3}\right)_{m_2} = -RT\Delta\Gamma_{23} = \Delta G, \quad (4)$$

where K is the equilibrium constant of the reaction, and a_3 is SDS activity. Thus, determination of K of the folding-unfolding reaction across the activity a_3 allows for the calculation of ΔG for the SDS-induced folding-unfolding process.

To apply the approach each of the SDS-induced unfolding and/or denaturation curves was plotted as fraction unfolded (f_u) as a function of natural logarithm of SDS activity. This exercise was less straightforward for cytochrome *c* and myoglobin data which provide no baselines for the unfolded state (Figure 3), and were constructed assuming no change in the ellipticity on either side of the point of the lowest CD signal. The K values were thus extracted across the sharp transition region, and the slope $\left(\frac{\partial \ln K}{\partial \ln a_3}\right)$ times $-RT$ provided the ΔG value. A representative set of analysis corresponding to the 207-nm CD data is provided in Figure 7, and values of ΔG yielded by all probes of measurement for the six proteins are listed in Table 1.

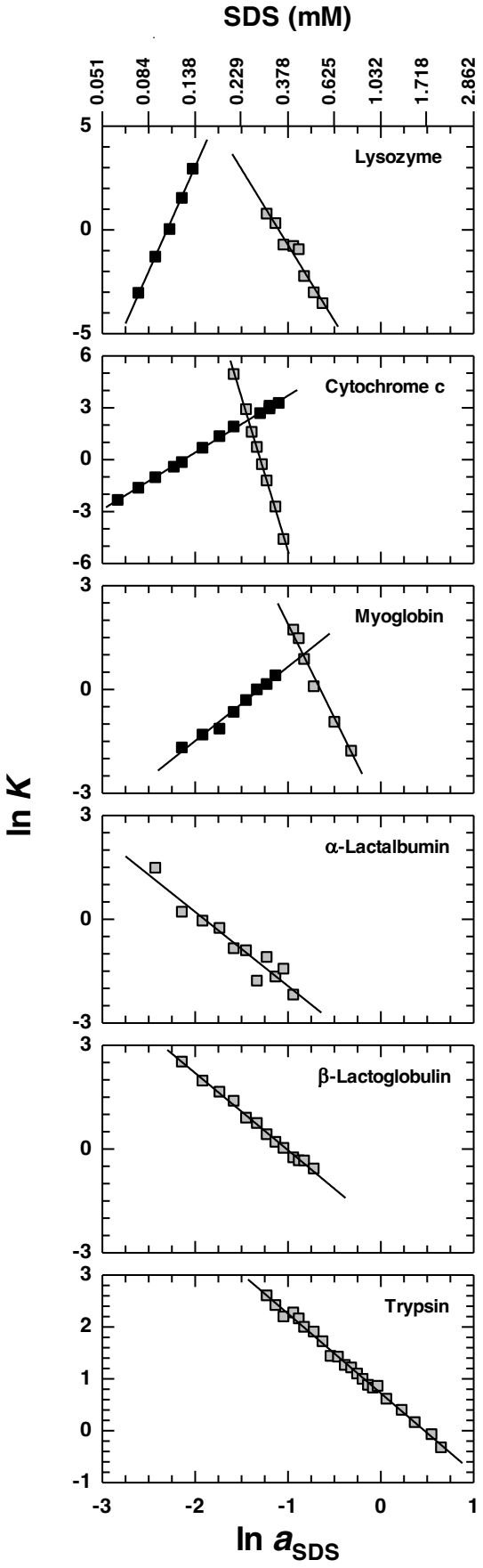

Figure 7. Linearity of natural logarithms of equilibrium constants for unfolding and/or denaturation with the natural logarithm of SDS activity. The slope of each line provides the free energy of the corresponding transition (see Table 1).

The sizable free energy difference between the native and the initial unfolded state of lysozyme is consistent with the result that secondary and tertiary structures are completely unfolded. The corresponding ΔG value for myoglobin is less, indicative of the fact that myoglobin undergoes only partial unfolding. Cytochrome *c* also undergoes complete unfolding, the lower value of 2.7 kcal mol^{-1} is in large error. The denaturation process of the unfolded again shows large values for lysozyme and cytochrome *c*, which is consistent with the reality of restructuration and reorganization of secondary structure starting from a

completely unfolded protein. The denaturation ΔG value of myoglobin is not that substantial because myoglobin is only partially unfolded initially. Values of ΔG for denaturation of α-lactalbumin, β-lactoglobulin, and trypsin are even lower, which is a reflection of the fact that native-state secondary structures of these three proteins are reorganized during denaturation.

3.3.7. *Kinetics of conformational changes during unfolding and refolding at submicellar SDS*

Conformational changes across the equilibrium $N \rightleftharpoons U \rightleftharpoons D$ for lysozyme and cytochrome *c* at submicellar SDS were studied by both manual mixing and stopped-flow fluorescence methods. According to the three-state equilibrium, unfolding kinetics were initiated from both N and N_1 states, and refolding and folding were initiated from the U state. Manual mixing experiments employed both far-UV CD and fluorescence, analyses of which are provided as Supporting Information (Figures 8−11).

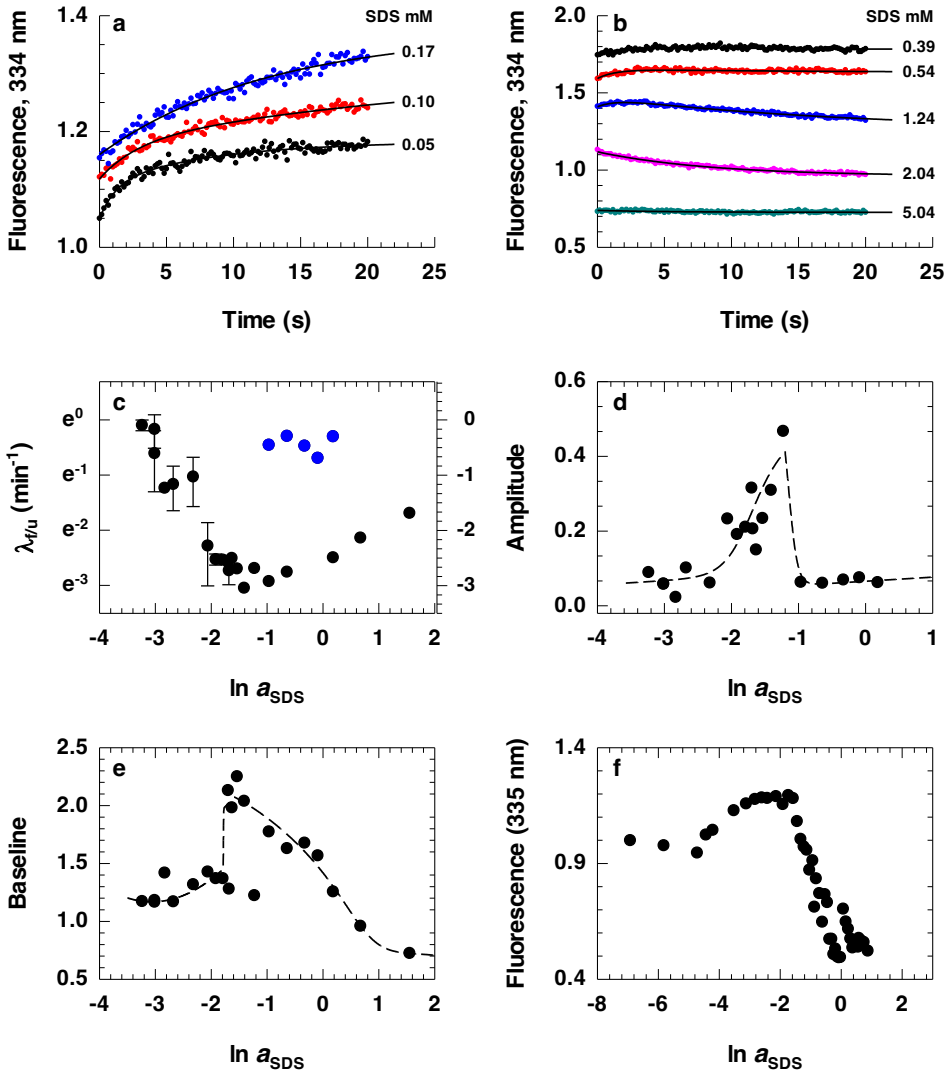

Figure 8. Fluorescence-monitored manually mixed kinetics of lysozyme conformational changes in SDS. (a) Traces fitted to a single-exponential showing unfolding of the native protein containing no SDS initially. (b) Denaturation from the initial condition of 0.2 mM SDS fits to two-exponentials, and occasionally to one. (c) The bottom of the chevron corresponds to ~0.4 mM SDS. (d) The amplitude maximum also occurs at ~0.4 mM SDS. (e) The SDS dependence of baseline fluorescence, corresponding to time t_∞, shows similarity with the equilibrium transition (f), which is reproduced from Figure 6c.

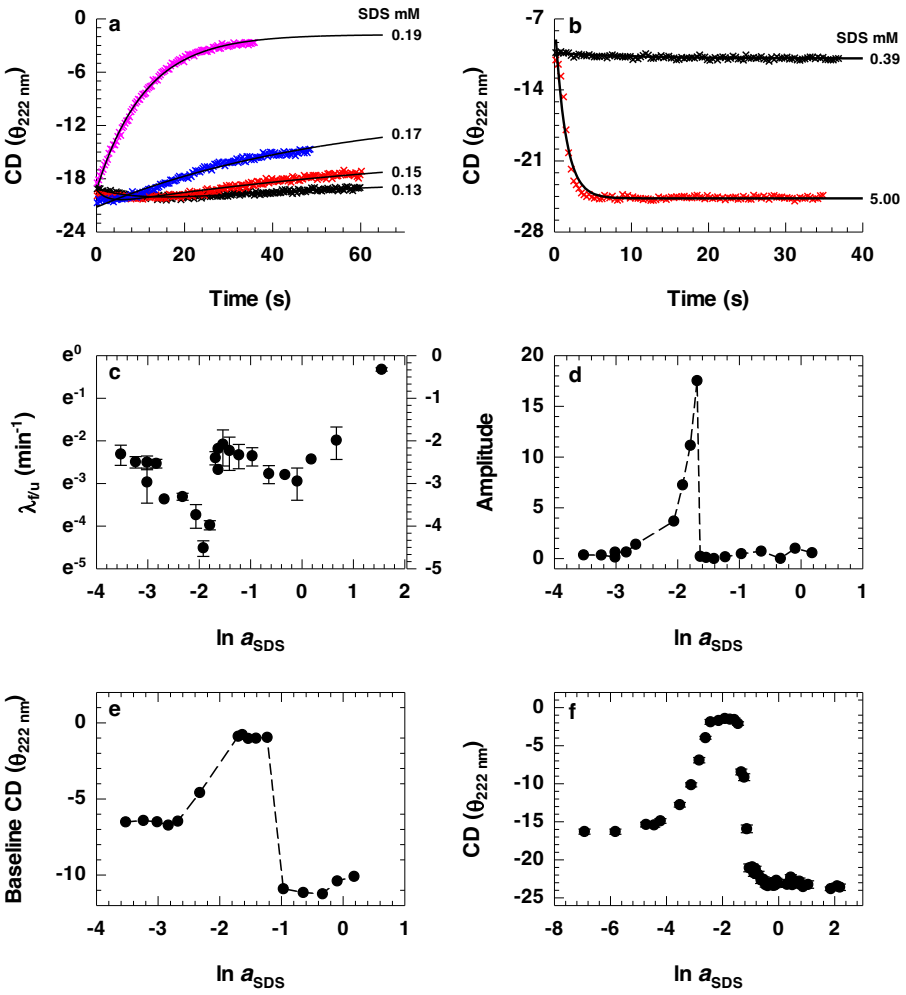

Figure 9. Manual-mixing slow kinetics of lysozyme monitored by 222-nm CD. (a) Unfolding of the native protein initially held at no SDS to the indicated concentrations of the surfactant. Kinetics are described by a single exponential at higher SDS, but a second exponential sets in as the concentration falls lower. (b) Denaturation measured by changing the protein at 0.2 mM to higher SDS occurs by a single phase. (c) The observed rate with SDS goes through two minima appearing near 0.15 and 0.9 mM SDS. (d) Maximum of the amplitude occurs near 0.15 mM SDS. (e) SDS dependence of t_∞ baseline values (outliers not shown) shows the same trend observed in CD-monitored equilibrium measurements (f).

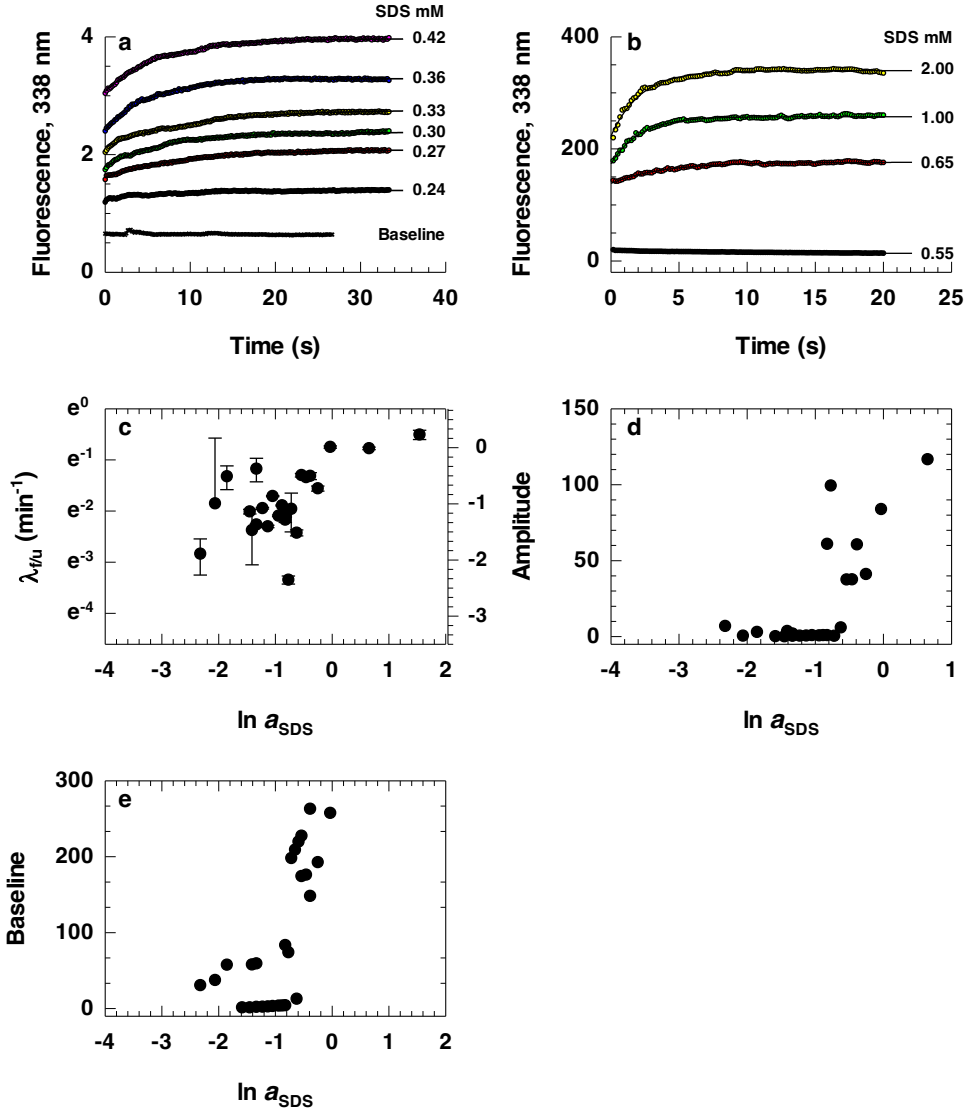

Figure 10. Cytochrome *c* slow kinetics monitored by fluorescence. (a) Unfolding of the native protein to indicated SDS concentrations occurs by one exponential phase. (b) Denaturation initiated by transferring the protein from 0.45 mM to the indicated SDS also occurs by a single kinetic phase. (c) The chevron limb at lower SDS is not quite clear due to noise in data. SDS dependence of kinetic amplitude and baseline fluorescence (d and e, respectively) also appear featureless.

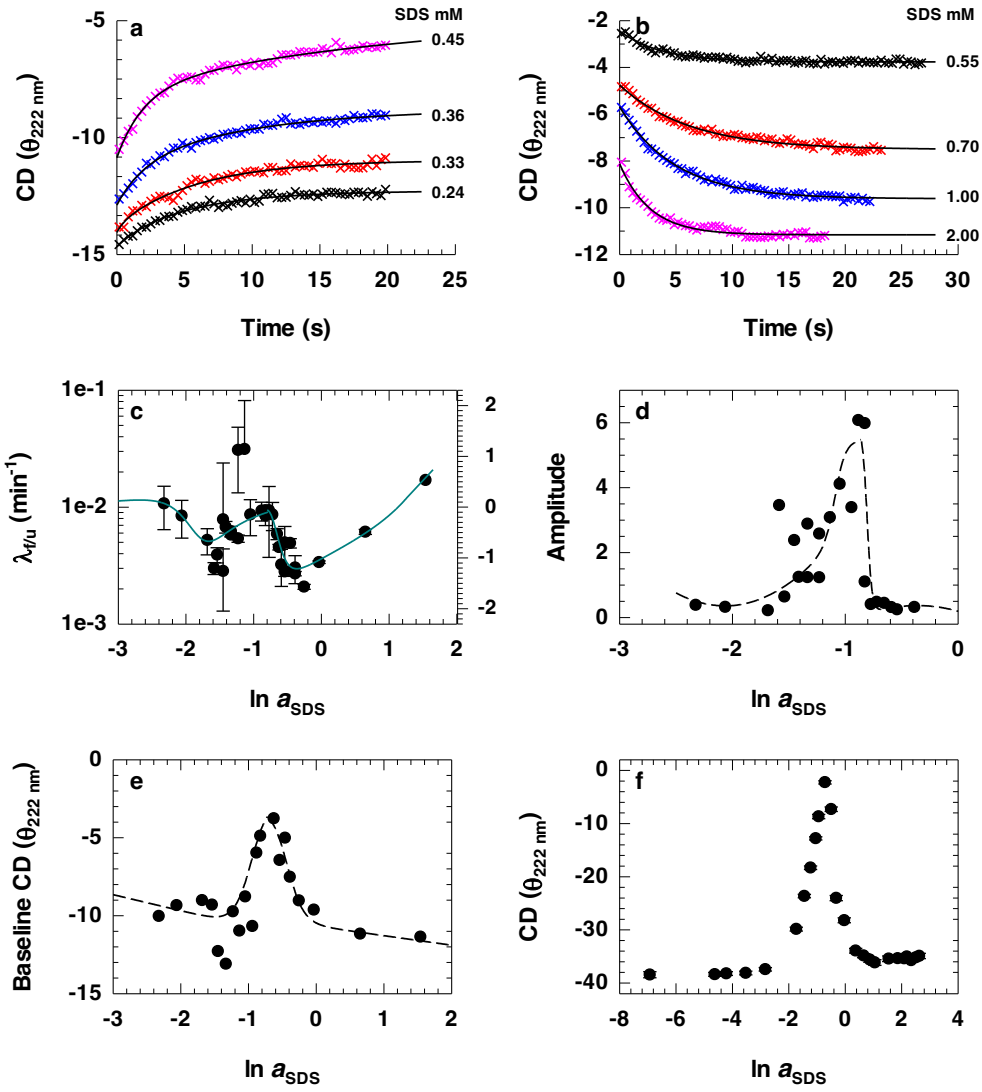

Figure 11. Cytochrome *c* slow kinetics monitored by 222-nm CD. (a) Unfolding of the native protein to indicated SDS concentrations occurs in two kinetic phases. (b) Denaturation initiated by jumps in solution conditions from the initial 0.45 mM to the indicated SDS occurs by a single kinetic phase. (c) Chevron minima occur near 0.2 and 0.7 mM SDS. The solid line is drawn to guide the eye, and has no physical meaning. (d) The peak of the kinetic amplitude appears near 0.4 mM SDS. (e) SDS dependence of the t_∞ baseline CD signal fairly reproduces the equilibrium data observed in an independent experiment under identical solution conditions.

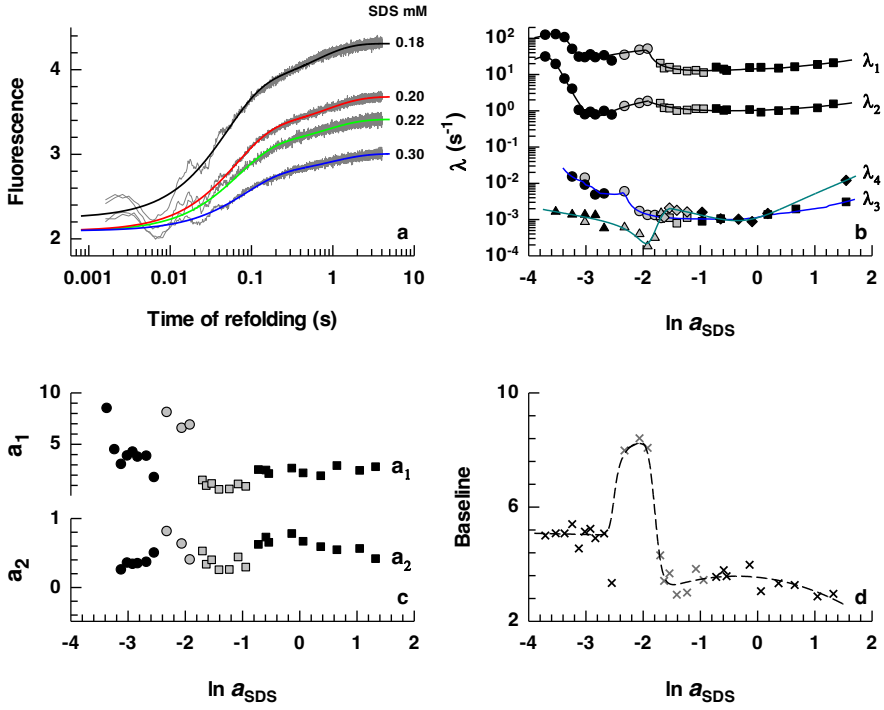

Figure 12. Kinetics of SDS-induced conformational transitions in lysozyme. (a) Representative stopped-flow traces for unfolding ($N_1 \rightarrow U$) from the initial denatured protein N_1 held at 1.5 mM to the indicated final concentrations of SDS. The traces are fitted to two exponentials. (b) Chevrons constructed from observed rate constants by stopped-flow fluorescence (λ_1 and λ_2) and manual mixing (λ_3 and λ_4) experiments: refolding from 0.2 mM SDS-unfolded protein (●), unfolding from 0 mM SDS (●), unfolding from 1.5 mM SDS (■), denaturation from 0.2 mM SDS (■), denaturation from 0.2 mM SDS (♦), unfolding from 1.5 mM SDS monitored by 222-nm CD (♦), refolding from 0.2 mM SDS monitored by 222-nm CD (▲), and unfolding from 0 mM SDS monitored by 222-nm CD (▲). Solid lines through data have been drawn using empirical functions, and have no physical basis. (c) Amplitudes a_1 and a_2 for the two phases observed in stopped-flow kinetics are plotted with ln a_{sds} to indicate occurrence of parallel kinetic pathways. Amplitudes related to manual-mixing kinetics are sufficiently small compared with the stopped-flow kinetics, and are not shown. (d) Baseline or t_∞ values read from stopped-flow kinetic traces are plotted with ln a_{sds} to show the reproducibility of the equilibrium data (see Figure 3).

Figure 12 shows results of millisecond reaction kinetics for lysozyme across the $N \rightleftharpoons U \rightleftharpoons N_1$ equilibrium. Typical kinetic traces for unfolding from N_1 to U (Figure 12a) show

no burst kinetics, and are fitted to two exponentials with occasional inclusion of a third one (Figure 12b). The SDS distribution of each of the observed rate constants (λ_1 and λ_2) corresponding to the two kinetic phases shows features of a sharp chevron at low SDS followed by a shallow one at high SDS (Figure 12b). The appearance of chevrons is an indication of reversibility of the transitions. Macroscopic rate constants λ_3 and λ_4 in the figure, reproduced from fluorescence and CD-monitored manual mixing data given in the Supporting Information (Figures 8,9), also show the two consecutive chevrons, although the first chevron in the CD-monitored kinetics appears a little shifted to higher SDS. The first chevron of CD-monitored λ_4 is vertically shifted downward relative to the corresponding fluorescence-monitored λ_3, but the second chevron of both λ_3 and λ_4 appears comparable. We do not have stopped-flow CD data, but on the basis of the comparison of λ_3 and λ_4 one can cogitate on the existence of two more rate constants, say λ_5 and λ_6, corresponding to the two stopped-flow fluorescence rate constants λ_1 and λ_2 such that $\lambda_5 \neq \lambda_2$ and $\lambda_6 \neq \lambda_1$ all through submicellar SDS. This is an expectation the validity of which remains to be seen. The interpretation of these results and assumptions are done as follows. Two consecutive chevrons for each λ correspond to the three-state N $\rightleftharpoons$ U $\rightleftharpoons$ D unfolding and folding mechanism seen in equilibrium experiments, and the observation of three λ's for tertiary and presumably for secondary structures would mean three parallel kinetic pathways, which is in accordance with amplitudes of the kinetic phases obtained from stopped-flow experiments (Figure 12c). The comparison of λ_3 and λ_4 already hints at the existence of a kinetic intermediate I for the N $\rightleftharpoons$ U half of the N $\rightleftharpoons$ U $\rightleftharpoons$ D equilibria, so that the N $\rightleftharpoons$ U transition in kinetic terms becomes N $\rightleftharpoons$ I $\rightleftharpoons$ U, where the intermediate I lacks tertiary structure but is secondary-structured. Whether an intermediate populates in the U $\rightleftharpoons$ D half is not certain because the second chevron for λ_3 and λ_4 is little different, and hence no temporal intermediate is invoked for this transition. By the assumption and the argument above that CD-monitored fast kinetics should yield λ_5

and λ_6 such that $\lambda_5<\lambda_2$ and $\lambda_6<\lambda_1$, a kinetic intermediate devoid of tertiary structure needs invoked for each parallel pathway. These interpretations, subject to establishing the assumptions, allow writing the following parallel-pathway minimal mechanism for unfolding and refolding of lysozyme at submicellar SDS.

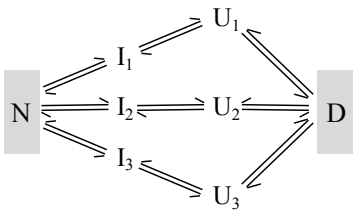

We also note that the baseline values extracted from end times (t_∞) of kinetic traces at different SDS concentration (Figure 12d) reproduce the features of the equilibrium transition shown in Figure 12c, underlining the successive unfolding and refolding model N $\rightleftharpoons$ U $\rightleftharpoons$ D at submicellar SDS.

Results for cytochrome *c* are presented in the same manner. Analyses of manual mixing slow kinetics are provided in the Figures 10,11 and stopped-flow fluorescence results are shown in Figure 13.

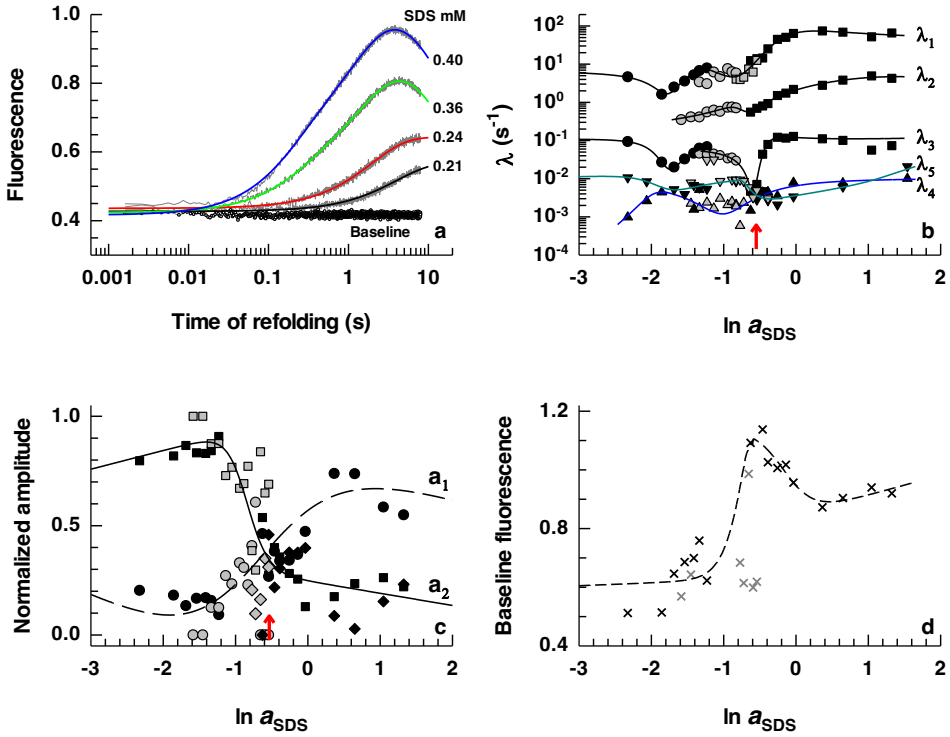

Figure 13. Kinetics of conformational transitions in cytochrome *c*. (a) A few traces showing unfolding from the native state initially in 0 mM to the indicated final concentrations of SDS. All traces fit to two exponentials, but the fit with a third exponential showing reversal of fluorescence that appears at higher final SDS is associated with large uncertainty. (b) Observed rate constants by stopped-flow fluorescence (λ_1, λ_2, and λ_3) and manual mixing kinetics monitored by fluorescence (λ_4) and 222-nm CD (λ_5) experiments with ln a_{SDS} : refolding from 0.45 mM SDS-unfolded protein (●), unfolding from 0 mM SDS (●), unfolding from 3 mM SDS (■), denaturation from 0.45 mM SDS (■). Manual mixing kinetics results are fluorescence-monitored refolding and denturation from the intial condition of 0.45 mM SDS (▲) and unfolding from the native protein initially in 0 mM SDS (▲), and 222-nm CD-monitored refolding and denturation from the intial condition of 0.45 mM SDS (▼) and unfolding from the initial condition of 0 mM SDS (▼). (c) Titration of the two stopped-flow amplitudes associated with λ_1 and λ_2 shows prevalence of a sequential pathway with intermediate population. (d) The baseline values of the stopped-flow traces reproduce the

equilibrium curve (see Figure 2). Substantially outlying data points have been omitted from this graph.

Time traces were generally fitted to three exponentials (Figure 13a), and the SDS variation of the macroscopic rate constants λ_1, λ_2, and λ_3 each entails two chevrons, one each at low and high SDS (Figure 13b). The lower SDS chevron for λ_2 is not clearly developed due to minor contribution of the second kinetic phase at lower concentration. The amplitudes corresponding to λ_1 and λ_2 are plotted in Figure 13c, where the amplitude for λ_3 was excluded due to considerable uncertainty. Nevertheless, the two amplitudes titrate out with SDS. This result and the appearance of the three stopped-flow kinetic phases in SDS-induced folding-unfolding of cytochrome *c* is consistent with an earlier study,[12] but that study did not particularly focus on submicellar SDS and detected only one chevron. Figure 12b also includes λ_4 and λ_5 that correspond to manual-mixing kinetics monitored by fluorescence and 222-nm CD, respectively (Figure 10,11). The crossovers in the vertical shifts of λ_4 and λ_5 at high SDS suggest no uniform sequence for dissolution and formation of secondary and tertiary structures across the SDS scale. The interpretation of these results is similar to that done for lysozyme above – two chevrons for each λ is consistent with the equilibrium $N \rightleftharpoons U \rightleftharpoons D$ mechanism at submicellar SDS which is also evident from the fluorescence values at t_∞ of the kinetic traces (Figure 13d), but is different with respect to the titration of the amplitudes seen for cytochrome *c*. Growth or suppression of a kinetic amplitude at the expense of another (Figure 13c) suggests sequential pathway with intermediate population. We also notice that the SDS concentration at which the amplitudes cross over corresponds to the minimum of the second chevron, indicated by arrowheads in Figures 13b,c, which suggests that the intermediate may be placed in the $U \rightleftharpoons N_1$ half of the $N \rightleftharpoons U \rightleftharpoons D$ equilibrium. However,

we do not have complete information about all amplitudes including that of the slowest kinetic phase λ_4. The available information enables writing the following minimal representation of a kinetic mechanism

$$N \rightleftharpoons I_1 \rightleftharpoons U \rightleftharpoons I_2 \rightleftharpoons D$$

where I_1 possibly lacks secondary structure as the manual-mixing slow-kinetics would suggest, and I_2 may have both secondary and tertiary structures the extent of which is different from D. Further studies will be needed to see if additional parallel pathways similar to those for lysozyme operate.

3.3.8. *Protein Fibrillation at submicellar SDS*

To find out the amount of SDS required for fibrillation we measured fibrillation kinetics by time-base fluorescence of the dye ThT at 25°C. In a manual mixing procedure, solutions of the protein, SDS, and ThT were rapidly mixed in a way that final concentrations were 8 μM protein and 50 μM ThT constantly, but the concentration of SDS varied from 0.015 to 5 mM. The time-dependence of the 478-nm ThT fluorescence in the mixed solution is shown in Figure 14 for lysozyme and cytochrome *c* at the indicated SDS. All concentrations of the surfactant produce kinetics suggesting protein aggregation, but they are distinguished on the basis of whether a lag phase appears. Kinetics with no lag phase, lysozyme in 0.015 mM SDS, for example, suggests rapid formation of amorphous aggregates. A lag phase precedes at higher SDS concentrations, suggesting the formation of crystal-like amyloid aggregates. Cytochrome *c* kinetics are relatively faster and the lag phase at intermediate SDS concentrations, 0.55 and 0.7 mM, is shorter compared to others. Apparently amorphous aggregation occurs at very low concentrations of SDS where the interaction with the protein

is predominantly electrostatic, but amyloid fibrillation is prevalent at intermediate to higher concentrations where SDS-protein interactions are hydrophobic and the protein unfolds and reorganizes the secondary structure. The shorter duration at higher SDS concentrations presumably arises from the α-helical nature of the reorganized structure.

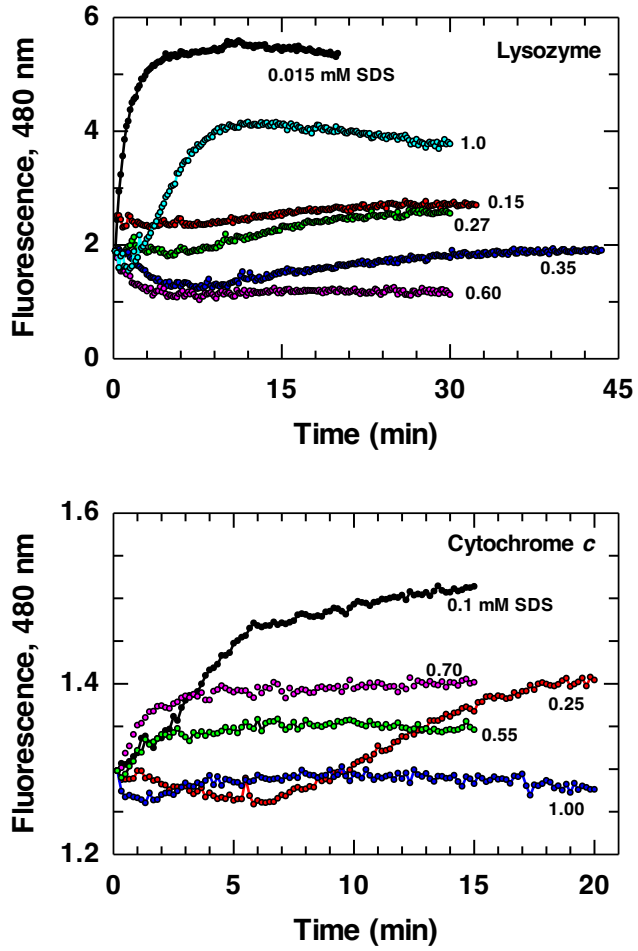

Figure 14. Fibrillation kinetics monitored by fluorescence of the dye ThT at the indicated final SDS concentrations. The reaction is monitored at 25°C, and the final protein and dye concentrations are 8 μM and 50 μM, respectively. The lysozyme reaction was set up in water at pH 3.8, and the cytochrome c reaction was done in 100 mM phosphate buffer, pH 5.8.

The same set of samples for each of the six proteins used for equilibrium measurements were imaged by microscopy. Sample age varied randomly, from few hours to days. Only those samples that contained denaturing amount of SDS, more than ~0.3 mM, showed evidences of fibrillation. FESEM images sampled in Figure 15 illustrate different forms and topology of fibers at varying magnification.

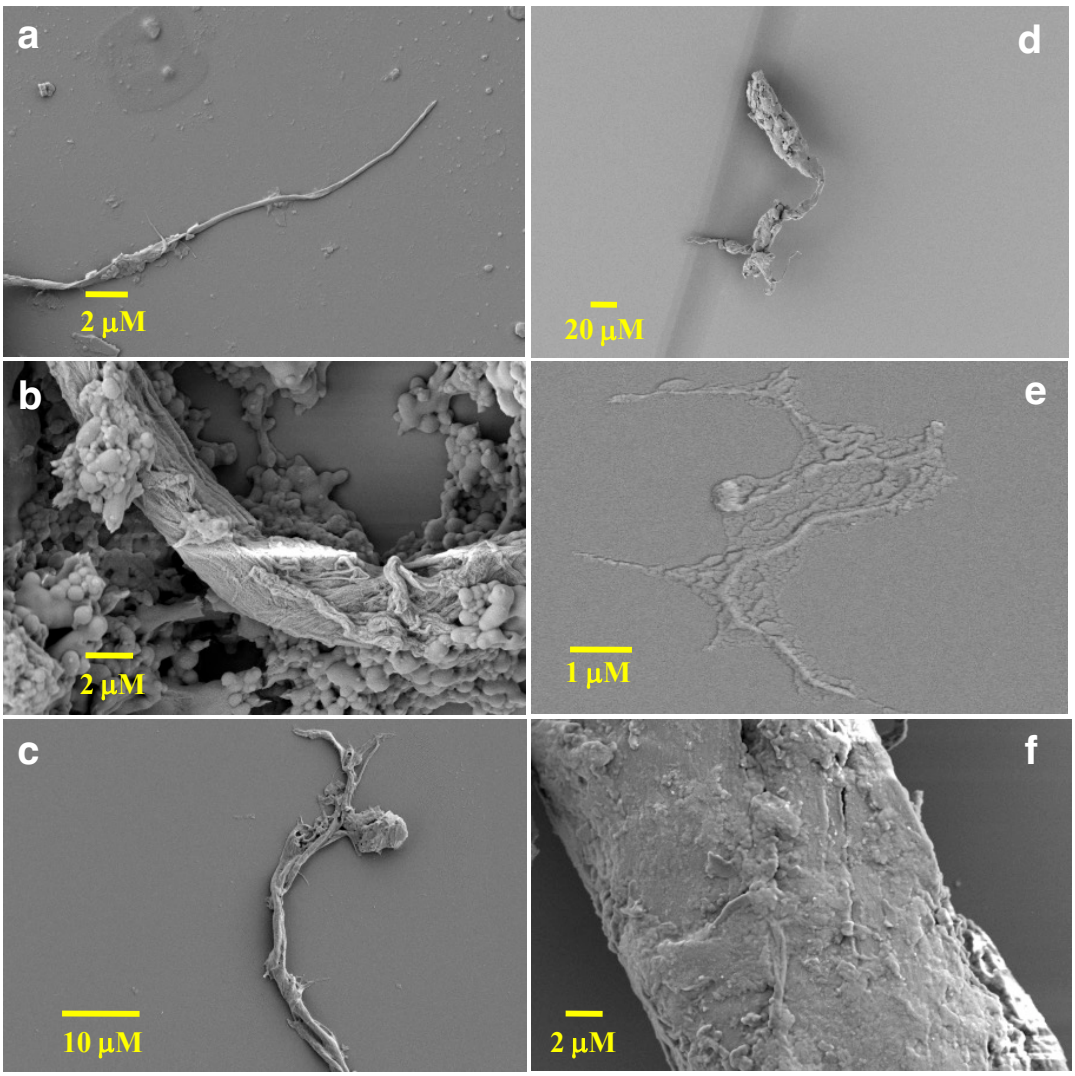

Figure 15. FESEM images of fibrils in samples that were used for equilibrium experiments. Hence, the fibers grew in respective buffers at 25°C with no extra condition. The age of the samples varied from a few hours to ~2 days, and the magnification in each image is chosen to provide clarity. Image labels and corresponding SDS concentrations in mM are (a) lysozyme 0.9, (b) cytochrome *c* 1.0, (c) myoglobin 0.4, (d) α-lactalbumin 1.0, (e) β-lactoglobulin 1.0, and (f) trypsin 2.0.

3.4. Discussions

3.4.1. *Protein unfolding and refolding (denaturation) at submicellar SDS.*

The key result provided here is dramatic changes in both secondary and tertiary structure of proteins due to binding of a few SDS monomers which otherwise is taken as a sub-denaturing load. In Figure 16 that reproduces a SDS-lysozyme binding isotherm from the work of Jones[35] we have partitioned the SDS scale according to the type and nature of changes we note for the six proteins. Although the binding isotherm changes with pH and ionic strength, and will also vary a bit from one to another protein under identical conditions, the SDS-lysozyme curve is taken here as a prototype. In zone A that corresponds the 0–0.04 mM range of free surfactant concentration cooperative binding of SDS monomers that numbers up to ~15 perturbs the structure a little but gives rise to detectable changes in spectroscopic signals in the baseline region of the titration curve for all six proteins. In the ensuing zone B covering about 0.04 to 0.4 mM free surfactant, where the isotherm is nearly flat due to the binding of just about 5 additional SDS monomers leading to a tally of ~20, secondary structures of lysozyme and cytochrome *c* are completely unfolded, and myoglobin is partly unfolded. Reformation of secondary structure of the unfolded proteins and the other three native proteins also begins in this range, although cytochrome *c* has already undergone substantial restructuring of secondary structure. In zone C that drapes ~0.4 to 3 mM free surfactant concentration and where cooperative binding of SDS reappears and a total of ~60 monomers bind, the restructuring of secondary structure nears completion.

Although we are able to partition the submicellar SDS scale into these three zones with respect to protein conformational changes, it must be noted that the consecutive unfolding and reformation of secondary structure is established for half of the proteins we scanned (Figure 3).

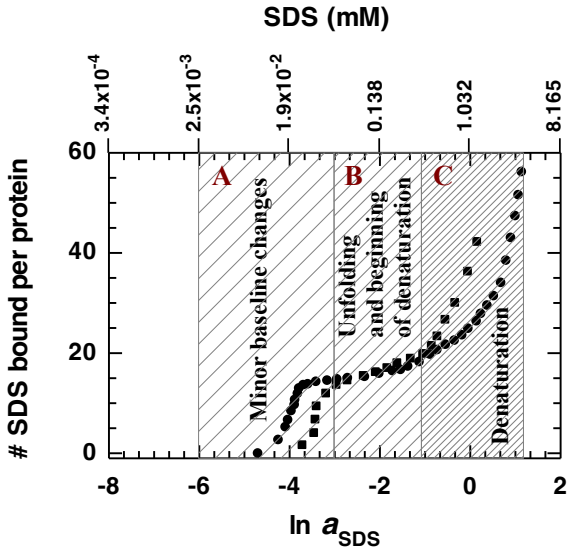

Figure 16. Protein conformational changes due to SDS binding. Zone demarcation should be taken as approximates only. The binding isotherms for lysozyme-SDS interaction at pH 3.2, 25°C, and ionic strength values of 12 (●) and 212 (■) mM are reconstructed after Jones.[35]

The first stage of secondary structure unfolding is not detected for the other three proteins. Concerning the response of tertiary structure, only two proteins – lysozyme and apo-α-lactalbumin – undergoes unfolding and refolding in succession. Tertiary structures of cytochrome *c* and myoglobin do not refold after the initial unfolding, and those of β-lactoglobulin and trypsin do not unfold initially but the former unfolds and the latter folds further in zone C (Figure 5). These observations thus do not provide a common pattern of protein conformational changes in the submicellar limit of SDS. A generic phenomenon however clearly emerge – secondary and tertiary structures are reformed and (or) restructured, and the restructuring of the latter may involve unfolding or further folding of the native state.

3.4.2. *Restructuration, refolding or denaturation?*

With regard to the transition in zone C (Figure 16) the use of terminology is fumbled. Secondary structure is either reformed in zone C from the unfolded state in zone B as for lysozyme, cytochrome *c*, and myoglobin or restructured directly in zone C from the initial native state in zone A. In both cases, the structure type in the resultant state is predominantly α-helical irrespective of the type in the native state (Figure 5), and that too in excess of the content in the initial state. Therefore, the secondary structure transition in zone C is more appropriately labeled denaturation rather than refolding. This terminology may not seem fitting with respect to the tertiary structure transition, which results in unfolding as for cytochrome *c*, myoglobin, and β-lactoglobulin or folding to more compact states of lysozyme, α-lactalbumin, and trypsin. The fact that the final protein state in zone C cannot structurally be the same initial native state qualifies the use of 'denaturation' to describe the structural transition in zone C.

3.4.3 *Structural organization in the submicellar vis a vis micellar SDS.*

A generalized view of the action of SDS on protein structure and conformation is tertiary structure unfolding at submicellar and protein chain expansion at micellar levels of SDS.[12,13] The denaturation of secondary structure observed up to micellar concentration of SDS produces an expanded chain rich in α-helices.[11,13,36,37,38] The submicellar observations here are consistent with tertiary structure denaturation and higher α-helical content (Figure 5), but we have no information about hydrodynamics of the denatured chain. Since micellization on the protein surface is thought to give rise to chain expansion,[12] the denatured protein at submicellar limit is likely to be compact.

3.4.4. *The basis for unfolding and denaturation at submicellar SDS.*

It occurs to us that submicellar SDS effect on protein unfolding observed here originates from favored ionic interaction of DS^- with positive charges on amino acid side chains. The initial unfolding process largely exposes the apolar surfaces of the protein facilitating their hydrophobic interaction with the alkyl chain of DS^- leading to denaturation. Although the involvement of both ionic and hydrophobic interactions in the SDS perturbation of protein structure is widely recognized,[35,39,40] it is important to realize that the prevalence of each of the two and the stages of their occurrence are decidedly dependent on the net charge the protein carries. Even as trivial as it seems, the present dataset reflects the relative importance of the two interactions with regard to the net protein charge. As Table 1 shows positive charges on lysozyme, cytochrome *c*, and myoglobin offer ion sites to which DS^- monomers bind electrostatically. The binding is cooperative and presumably weak with dissociation constant approaching as high as 1 mM.[8] The consequence of this electrostatic interaction with specific binding sites on the protein surface is neutralization of the net positive charge, which may be one of the factors causing precipitation of SDS-lysozyme complex.[2,41] Lysozyme solubility is intricately related to protein concentration and solution conditions. We have also sensed some degree of precipitation of the lysozyme-SDS complex (Figure 5) even when the protein concentration was lowered to 5.5 μM (Figure 4). The origin of this precipitation is not definitely known, but supposedly follows from aggregation of lysozyme which is consistent with the fact that precipitation is protein concentration dependent.[42] We suggest that the precipitation is the result of substantial protein unfolding due to electrostatic binding of DS^- such that the unfolded protein chains aggregate by hydrophobic interactions, which is substantiated by studies on aggregation of partly folded or unfolded lysozyme.[43–47] Thus the observation of aggregation in a few unfolded samples (Figure 5) provides a clue that saturating electrostatic interactions of ~14 DS^- ions with one molecule of lysozyme completely unfolds

the protein. This must also be the basis of complete unfolding of cytochrome *c* and partial unfolding of myoglobin whose net charge content is +12 and +4.8, respectively. Myoglobin does not unfold completely simply because of its less positive net charge content so that DS^- interacts to a lesser extent. Proteins α-lactalbumin, β-lactoglobulin, and trypsin, whose net charge is negative (Table 1) and could offer only a fewer positively charged side chains for the initial ionic interactions with DS^- do not unfold.

Next in zone C of Figure 16 the hydrophobic surfaces of unfolded lysozyme, cytochrome *c*, and myoglobin support cooperative binding of the alkyl chain and consequent denaturation that involves preferential reformation of α-helices. Evidences exist that disordered or unstructured proteins and peptides can adopt α-helical structure in the presence of SDS.[39,48,49] The hydrophibic binding and restructuring also tips the unfolded aggregate – monomer equilibrium to the right. The cooperativity of hydrophobic binding of the surfactant alkyl chain with the apolar sites of those proteins including α-lactalbumin, β-lactoglobulin, and trypsin that are structurally destabilized but not unfolded due to interaction with a fewer DS^- monomers is relatively less, and restructuration of their existing secondary structure into α-helices occurs at relatively higher SDS concentration (Figure 3). Our conclusion that SDS binds in two stages – electrostatic and hydrophobic in order – is consistent with the proposal of Burkhard and Stolzenberg,[50] and proteins can unfold completely in submillimolar SDS concentration if they possess adequate positive charges to establish electrostatic interaction with DS^-. Unfolding in turn facilitates subsequent denaturation.

3.5. Summary and prospect

All generic structural changes of proteins occur completely at submicellar limit of SDS, meaning binding with the surfactant monomers suffices. Micelle aggregation along the protein chain that occurs at higher concentration of SDS causes chain expansion. Complete unfolding at submillimolar SDS can occur when the protein carries sufficient positive charges for supporting the initial ionic interactions. The resulting unfolded chains tend to aggregate and hence establish a monomer ↔ aggregate equilibrium, which is shifted to the monomer side in the ensuing hydrophobic binding of surfactant alkyl chains with the apolar surfaces in the unfolded protein. Binding of alkyl chain will occur even if the chains are not completely unfolded, but the binding should be less cooperative. This second stage of SDS-protein apolar interactions that may extend up to 2–3 mM SDS depending upon the net charge content on the protein results in reformation of lost secondary structure or reorganization of existing secondary structures to give rise to α-helices. These observations can be used to tune charges simply by placing the protein at a different pH so as to study further details of protein-SDS interactions, structure modulation, protein fibrillation, electrophoretic migration, and SDS-resistance phenomena.

3.6. References

1. Otzen, D. E. Protein Unfolding in Detergents: Effect of Micelle Structure, Ionic Strength, pH, and Temperature. *Biophys. J.* **2002**, *83*, 2219–2230.

2. Lad, M. D.; Ledger, V. M.; Briggs, B.; Green, R. J.; Frazier, R. A. Analysis of the SDS-Lysozyme Binding Isotherm. *Langmuir* **2003**, *19,* 5098–5103.

3. Manning, M.; Colón, W. Structural Basis of Protein Kinetic Stability: Resistance to Sodium Dodecyl Sulfate Suggests a Central Role for Rigidity and a Bias Toward Beta-Sheet Structure. *Biochemistry* **2004**, *43,* 11248–11254.

4. Nielsen, A. D.; Arleth, L.; Westh, P. Analysis of Proein-Surfactant Interactions – A Titration Calorimetric and Fluorescence Spectroscopic Investigation of Interactions Between *Humicola insolens* Cutinase and an Anionic Surfactant. *Biochim. Biophys. Acta.* **2005**, *1752*, 124–132.

5. Xu, Q.; Keiderling, T. A. Stop-Flow Kinetics Studies of the Denaturation of Surfactant, Sodium Dodecyl Sulfate, with Acid-Denatured Cytochrome c. *Proteins* **2006**, *63,* 571–580.

6. Sehgal, P.; Otzen, D. E. Thermodynamics of Unfolding of an Integral Membrane Protein in Mixed Micelles. *Protein Sci.* **2006**, *15*, 890–899.

7. Droghetti, E.; Oellerich, S.; Hildebrandt, P.; Smulevich, G. Heme Coordination States of Unfolded Ferrous Cytochrome c. *Biophys. J.* **2006**, *91*, 3022–3031.

8. Nielsen, M. M.; Andersen, K. K.; Westh, P.; Otzen, D. E. Unfolding of b-Sheet Proteins in SDS. *Biophys. J.* **2007**, *92*, 3674–3685.

9. Chen, E.; Van Vranken, V.; Kliger, D. S. The Folding Kinetics of the SDS-Induced Molten Globule Form of Reduced Cytochrome c. *Biochemistry* **2008**, *47*, 5450–5459.

10. Badraghi, J.; Yousefi, R.; Saboury, A. A.; Sharifzadeh, A.; Haertlé, T.; Ahmad, F.; Moosavi-Movahedi, A. A. Effect of Salts and Sodium Dodecyl Sulfate on Chaperone Activity of Camel aS_1-CN:Insulin as the Target Protein. *Colloids Surf. B Biointerfaces* **2009**, *71*, 300–305.

11. Otzen, D. E.; Sehgal, P.; Westh, P. J. a-Lactalbumine Is Unfolded by All Classes of Detergents but with Different Mechanism. *J. Colloid Interface Sci.* **2009**, *329,* 273–283.

12. Bhuyan, A. K. On the Mechanism of SDS-Induced Protein Denaturation. *Biopolymers* **2010**, *93*, 186–199.

13. Otzen, D. E. Protein-Surfactant Interactions: A Tale of Many States. *Biochim. Biophys. Acta* **2011**, *1814,* 562–591.

14. Naidu, K. T.; Prabhu, N. P. Protein –surfactant Interactions: Sodium Didecyl Sulfate-Induced Unfolding of Ribonuclease A. *J. Phys. Chem. B* **2011**, *115,* 14760–14767.

15. Sun, Y.; Filho, P. L. O.; Bozelli, J. C.; Carvalho, J.; Schreier, S.; Oliveira, C. L. P. Unfolding and folding pathway of lysozyme induced by sodium dodecyl sulfate. *Soft Matter* **2015**, *11*, 7769-7777.

16. Kaspersen, J. D.; Søndergaard, A.; Madsen, D. J.; Otzen, D. E.; Pedersen, J. S. Refodlign of SDS-Unfolded Proteins by Nonionic Surfactants. *Biophys. J.* **2017**, *112,* 1609–1620.

17. Gudiksen, K. L.; Gitlin, I.; Moustakas, D. T.; Whitesides, G. M. Increasing the Net Charge and Decreasing the Hydrophobicity of Bovine Carbonic Anhydrase Decreases the Rate of Denaturation with Sodium Dodecyl Sulfate. *Biophys. J.* **2006**, *91*, 298–310.

18. Takeda, K.; Moriyama, Y. Kinetic Aspects of Surfactant-Induced Structural Changes of Proteins – Unsolved Problems of Two-State Model for Protein Denaturation. *J. Oleo Sci.* **2015**, *64,* 1143–1158.

19. Kumar, E. K.; Prabhu, N. P. Differential Effects of Ionic and Non-ionic Surfactants on Lysozyme Fibrillation. *Phys. Chem. Chem. Phys.* **2014**, *16,* 24076–24088.

20. Jafari, M.; Mehrnejad, F.; Rahimi, F.; Asghari, S. M. The Molecular Basis of the Sodium Dodecyl Sulfate Effect on Human Ubiquitin Structure: A Molecular Dynamics Simulation Study. *Sci. Rep.* **2018**, *8,* 2150.

21. Gentile, F.; Amodeo, P.; Febbraio, F.; Picaro, F.; Motta, A.; Formisano, S.; Nucci, R. SDS-Resistant Active and Thermostable Dimers Are Obtained from the Dissociation of Homotetrameric b-Glycosidase from Hyperthermophilic *Sulfolobus solfataricus* in SDS. *J. Biol. Chem.* **2002**, *277,* 44050–44060.

22. Khan, J. M.; Qadeer, A.; Chaturvedi, S. K.; Ahmad, E.; Rehman, S. A. A.; Gourinath, S.; Khan, R. H. SDS Can Be Utilizedas an Amyloid Inducer: A Case Study on Diverse Proteins. *PLOS ONE* **2012**, *7,* 9694.

23. Khan, J. M.; Sharma, P.; Arora, K.; Kishor, N.; Kaila, P.; Guptasarma, P. The Achilles' Heel of Ultrstable Hyperthermophile Proteins: Submillimolar Concentrations of SDS

Stimulate Rapid Conformational Changes, Aggregation, and Amyloid Formation in Proteins Carrying Overall Positive Charge. *Biochemistry* **2016**, *55*, 3920–3936.

24. Burchfield, T. E.; Woolley, E. M. Models for Thermodynamics of Ionic Surfactant Solutions. 1. Osmotic and Activity Coefficients. *J. Phys. Chem.* **1984**, *88,* 2149–2155.

25. Viseu, Melo, E. P.; Carvalho, T. I.; Correia, R. F.; Costa, S. M. B. Unfolding kinetics of b-lactoglobulin induced by surfactant and denaturant: a stopped-flow/fluorescence study. *Biophys*. *J*. **2007**, *93*, 3601-3612.

26. D'Alfonso, L.; Collini, M.; Ragona, L.; Ugolini, R.; Baldini, G.; Molinari, H. Porcine Beta-Lactoglobulin Chemical Unfolding: Identification of a Non-native A-Helical Intermediate. *Proteins* **2005**, *58,* 70–79.

27. Yagi, M.; Sakurai, K.; Kalidas, C.; Batt, C. A.; Goto, Y. Reversible Unfolding of Bovine b-Lactoglobulin Mutants Without a Free Thiol Group. *J. Biol. Chem.* **2003**, *278,* 47009–47015.

28. Outzen, H.; Berglund, G. I.; Smalas, A. O.; Willassen, N. P. Temperature Nad pH Sensitivity of Trypsins from Atlantic Salmon (*Salmo salar*) in Comparison with Bovine and Porcine Trypsin. *Comp*. *Biochem. Physiol.* **1996**, *115*, 33–45.

29. Rao, M. T.; Bhuyan, A. K.; Venu, K.; Sastry, V. S. S. Nonlinear Effect of GdnHCl on Hydration Dynamics of Proteins: A H Magnetic Relaxation Dispersion Study. *J. Phys. Chem. B* **2009**, *113*, 6994–7002.

30. Arai, M.; Kuwajima, K. Rapid Formation of a Molten Globule Intermediate in Refolding of a-Lactalbumine. *Fold. Des.* **1996**, *1,* 275–287.

31. Schellman, J. A. The Relation Between the Free Energy of Interaction and Binding. *Biophys. Chem.* **1993**, *45*, 273–279.

32. Schellman, J. A. Selective Binding and Solvent Denaturation. *Biopolymers* **1987**, *26*, 549–559.

33. Timasheff, S. N. Protein-Solvent Preferential Interactions, Protein Hydration, and the Modulation of Biochemical Reactions by Solvent Components. *Proc. Natl. Acad. Sci. U. S. A.* **2002**, *99*, 9721–9726.

34. Wyman, J., Linked Functions and Reciprocal Effects in Hemoglobin: A Second Look. *Adv. Protein Chem.* **1964**, *19*, 223–286.

35. Jones, M. N. Surfactant Interactions with Biomembranes and Proteins. *Chem. Soc. Rev.* **1992**, *21*, 127–136.

36. Hiramatsu, K.; Yang, J. T. Cooperative Binding of Hexadecyltrimethylammonium Chloride and Sodium Dodecyl Sulfate to Cytochrome c and the Resultant Change in Protein Conformation. *Biochim. Biophys. Acta* **1983**, *743*, 106–114.

37. Andersen, K. K.; Oliveira, C. L.; Larsen, K. L.; Poulsen, F. M.; Callisen, T. H.; Westh, P.; Pedersen, J. S.; Otzen, D. The Role of Decorated SDS Micelles in Sub-CMC Protein Denaturation and Association. *J. Mol. Biol.* **2009**, *391*, 207–226.

38. Halskau, O.; Underhaug, J.; Frøystein, N. A.; Martínez, A. Conformational Stability of a-Lactalbumine Related to Its Membrane Binding Capacity. *J. Mol. Biol.* **2005**, *349*, 1072–1086.

39. Hamada, S.; Takeda, K. Conformational Changes of Alpha-Lactalbumine and Its Fragments, Phe31–Ile59 Induced by Sodium Dodecyl Sulfate. *J. Protein Chem.* **1993**, *12*, 477–482.

40. Chattopadhyay, K.; Mazumdar, S. Stabilization of Partially Folded States of Cytochrome c in Aqueous Surfactant: Effects of Ionic and Hydrophobic Interactions. *Biochemistry* **2003**, *42*, 14606–14613.

41. Morén, A. K.; Khan, A. Phase Equilibria of an Anionic Surfactant (Sodium Dodecyl Sulfate) and an Oppositely Charged Protein (Lysozyme) in Water. *Langmuir* **1995**, *11*, 3636–3643.

42. Jones, M. N.; Manley, P. Interaction Between Lysozyme and n-alkylsulphates in Aqueous Solution. *J. Chem. Soc. Faraday Trans. 1* **1980**, *76*, 654–664.

43. Booth, D. R.; Sunde, M.; Bellotti, V.; Robinson, C. V.; Hutchinson, W. L.; Fraser, P. E.; Hawkins, P. N.; Dobson, C. M.; Radford, S. E.; Blake, C. C. F.; Pepys, M. B. Instability, Unfolding, and Aggregation of Human Lysozyme Variants Underlying Amyloid Fibrillogenesis. *Nature* **1997**, *385*, 787–793.

44. Arakawa, T.; Tsumoto, K. The Effects of Arginine on Refolding of Aggregated Proteins: Not Facilitate Refolding, but Suppress Aggregation. *Biochem. Biophys. Res. Commun.* **2003**, *304*, 148–152.

45. Petersen, S. B.; Jonson, V.; Fojan, P.; Wimmer, R.; Pedersen, S. Sorbitol Prevents the Self-Aggregation of Unfolded Lysozyme Leading to an up to 13°C Stabilization of the Folded Form. *J. Biotechnol.* **2004**, *114*, 269–278.

46. Sassi, P.; Giugliarelli, A.; Paolantoni, M.; Morresi, A.; Onori, G. Unfolding and Aggregation of Lysozyme: A Thermodynamic and Kinetic Study by FTIR Spectroscopy. *Biophys. Chem.* **2011**, *158*, 46–53.

47. Patel, D.; Kuyucak, S. Computational Study of Aggregation Mechanism in Human Lysozyme[D67H]. *PLOS ONE* **2017**, 12, 6886.

48. Eliezer, D.; Kutluay, E.; Bussell, R.; Browne, G. Conformational Properties of a-Synuclein in Its Free and Lipid-Associated States. *J. Mol. Biol.* **2001**, *307*, 1061–1073.

49. Maiti, N. C.; Apetri, M. M.; Zagorski, M. G.; Carey, P. R.; Anderson, V. E. Raman Spectroscopic Characterization of Secondary Structure in Natively Unfolded Proteins: a-Synuclein. *J. Am. Chem. Soc.* **2004**, *126*, 2399–2408.

50. Burkhard, R. K.; Stolzenberg, G. E. Interaction Between Sodium Dodecyl Sulfate and Ferricytochrome *c*. *Biochemistry* **1972**, *11*, 1672–1677.

CHAPTER 4

Mechanical unfolding and amorphous aggregation of proteins in very low-strength DC field

Abstract

A common theme for the effect of electric field on the structure and conformation of proteins is lacking due to a myriad of conflicting reports emerging from different protein systems subjected to different frequency and strength of the field (0.8 –10^8 V cm^{-1}), which may be pulsed for a few nano- to microseconds or steady state extending to several hours. It is however necessary to find a common theme because of increasing use of electric field not only to understand Stark-like electro-optic effects in large molecules, but also in food processing technology, and perhaps in the disruption of amyloid bodies in Alzheimer condition. This study finds an optimized condition of 1.3 V cm^{-1} DC field, in which the electrophoretic mobility is ~1.2 mm h^{-1}, and systematically shows electrophoretic, electrochemical, and unfolding effects at different levels of cytochrome *c* structure within ~90 minutes of turning the field on. Interestingly, the protein undergoes amorphous aggregation concomitant with a high degree of denaturation. In support of this suggestion, data for myoglobin and trypsin are also presented. Effort has been made to separate out the chemical and physical effects of the electric field.

4.1. Introduction

Stark effect, the splitting of spectral lines due to energy level perturbation in atoms and molecules subjected to electric field (EF), has contributed enormously to develop the fundamental principles of molecular spectroscopy.[1] The description of EF effect on large molecules in aqueous solutions or embedded in gel matrix is, however, fraught with hydrodynamic, electrophoretic, and confinement factors compounded by changes in molecular conformation and motional mechanics. Analysis of macromolecules subjected to steady-state electric field must therefore include the codes of electrochemistry in conjunction with additional forces on the molecular structural elements exerted by the field. These complexities may appear to overshadow the classical definition of Stark effect, although energy term values at rotational, vibrational, and electronic levels are perturbed in the case of macromolecules as well. The associated spectral lines can still be probed by appropriately designed spectroscopic methods, but the Stark-perturbed band structures are expected to change continuously as the steady-state current flow is maintained. To note, spectroscopic observation of Stark effect generally requires much higher field, at least hundreds of V cm^{-1},[2] compared to the field used to detect EF effect in biological macromolecules. Very high pulsed field of the order of tens of kV cm^{-1} has however been used for electric dichroism measurements in DNA.[3,4] Since field gradients used to detect EF effect on biological molecules are very small (~1–10 V cm^{-1}), and the objective of such experiments is to study motional, conformational, and symmetry perturbations, it is more useful to analyze the results by electrochemical principles and molecular relaxation in conjunction with classical mechanics rather than considering the Stark-split band structures or electro-optic effects. The term 'EF effect' is used to refer to local and global changes in structure, function, conformation, solvation, and thermodynamic and kinetic properties of the molecular systems subjected to steady state electric field.

Having come across a surging body of reports of EF effect on various proteins and

peptides based on both experimental and molecular dynamics (MD) simulation studies, we briefly mention the main results of some typical studies. Electric field brings about helical to β-structure transition in the β amyloid peptide,[5] but the incidence of β→α structural transition in a V3-loop peptide has also been documented immediately after.[6] In both of these studies, the authors suggest the occurrence of a global rearrangement of peptide dipoles affecting hydrogen bonding and hence an altered peptide structure. Oscillating motion of the peptide chingolin placed in unusually high oscillating field (10^7 V cm^{-1}) is observed, but the peptide retains native-state structure when the frequency of the field is very high.[7] Experiments with the archetypal globular lysozyme subjected to pulsed EF show cleavage of disulfide bonds, loss of α-helical structure and protein aggregation.[8,9] The results of secondary structure destabilization concomitant with H-bond breakage as a consequence of alignment of protein dipole moments of lysozyme with the field was also observed in earlier MD simulation.[10,11] Simulations of a single myoglobin molecule in water subjected to pulsed or steady field of the order ~10^7–10^8 V cm^{-1} has been used to describe protein unfolding thermodynamics with a suggestion of similar behavior for other globular proteins.[12,13] Low fields (0.8–5 V cm^{-1}) oscillating at 10 or 500 Hz are found to destabilize secondary and tertiary structures causing unfolding of both bovine serum albumin (BSA) and lysozyme.[14] Several other reports have mentioned protein destabilization and aggregation in electric field of medium to high strength; β-lactoglobulin in medium field,[15,16] and wheat gluten and peanut proteins in very high field[17,18] are examples. Activity of enzymes pectin methyltransferase and polygalacturonase is reduced in the presence of lower field (~0.4 V cm^{-1}) of frequency in the 0–60 Hz range.[19] The effect on the enzyme activity at higher frequencies appears negligible, which the authors explain by invoking lower amplitude of field-induced molecular motion. Structural modification, changes in functional properties, and aggregation for other proteins have also been documented.[20–22] The use of electric field to create thermo-electric effect, i.e., Joule

heating, in food processing technology has also led to experiments to understand as to how proteins in foodstuffs are affected,[23] and the basic observation made in all such studies is that electric field somehow disturbs protein conformation. High-frequency radio waves are suggested to offer protection and reverse cognitive impairment in Alzheimer's disease mice,[24] although the mechanism of fiber disintegration remains unexplained.

A review of these reports would show the lack of a coherent description of the EF effect on functional native proteins. A part of the reason for the host of conflicting reports of EF effect on proteins is diverse response of the protein systems to the magnitude of the field and frequency and the duration of field application. It may also appear irrational to use fields as high as ~10^7 or 10^8 V cm^{-1} unless simulation settings require such large values.[11,25] It is possible that experiments that employed this order of field were inspired by simulation studies. Another significant problem associated with description of results has been the failure to account for electrophoretic mobility and clearly separate the chemical and physical effects elicited by EF.

This work studies cytochrome *c* in aqueous solution of low ionic strength subjected to low DC field (0.8–1.3 V cm^{-1}). Electrochemical reduction of the heme iron, and unfolding of tertiary and secondary structures have been systematically probed by using appropriate spectroscopic markers. Within ~90 min of application of the steady field, the protein unfolds to produce amorphous aggregates as observed in electron micrographs. Unfolding and amorphous aggregation as generic EF effects are documented for myoglobin and trypsin as well.

4.2. Experimental section

Experiments performed are fairly simple and totally reproducible for different proteins. A 7 μM aqueous solution each of commercial preparations of cytochrome *c* (pH 5.8)

myoglobin (pH 7), and trypsin (pH 8) buffered with 20 mM sodium phosphate was placed in a 1-cm quartz cuvette, two opposite faces of which contained platinum meshes acting as electrodes. Homogenous electric field throughout the solution was obtained from a DC supply monitored by an oscilloscope. The cuvette was positioned in the sample chamber of spectrometers for optical absorption, fluorescence, CD, IR, and light scattering measurements at 25 °C. The placement of the electrodes was calibrated so as not to obstruct the light beams in spectrometers. Samples for SEM were obtained by re-suspending the protein solution at the end of each set of optical measurement. Gold coated samples were imaged in a ZEISS Ultra 55 FESEM instrument operating at 30 kV.

4.3. Results and discussion

4.3.1 *Protein mobility in low electric field.*

The instantaneous velocity of the protein molecule of mass m in the presence of an external electric field **E** is given by the Langevin equation

$$-m\gamma v + R + f = 0, \quad (1)$$

in which γ in the drag-force term is the friction coefficient, R is the random force due to protein-solvent collisions, and f is the external force arising from the electric field. The external force can be separated into f_{E} and $f_{\mathrm{counterion}}$, which are the forces arising directly from the electric field and the counterion cloud. The inertial force has been neglected in the Langevin equation. Using the Stokes formula

$$m\gamma = 6\pi r_g \eta, \quad (2)$$

where r_g is the radius of gyration of the protein and η is the viscosity of the solution, the Langevin equation reads

$$-6\pi r_g \eta \frac{dx}{dt} + R + f_{\mathrm{E}} + f_{\mathrm{counterion}} = 0. \quad (3)$$

The solution for the velocity of the fluid $\mathbf{v}(\mathbf{r})$ at a distance $\mathbf{r}$ from the center of the protein typically starts with the steady-state Navier-Stokes equation containing the Laplace operator

$$-\eta\nabla^2\mathbf{v}(\mathbf{r}) + \nabla p(\mathbf{r}) = \rho(\mathbf{r})\mathbf{E}(\mathbf{r}), \tag{4}$$

where p is pressure, ρ is the ion charge density outside the protein, and $\mathbf{E}(\mathbf{r})$ is the electric field on the protein surface. Since the velocity is considered only along the laboratory (space) x-axis, the magnitude of the electric field can be taken as E_x (=$E\hat{x}$). The Hückel solution[26] for the mean velocity of the protein is

$$6\pi r_g \eta \left\langle \frac{dx}{dt} \right\rangle = QE - \frac{\kappa r_g}{(1+\kappa r_g)} QE, \tag{5}$$

in which Q is the protein charge and κ is the screening parameter (inverse Debye length)

$$\kappa = \sqrt{\frac{2e^2 N_\mathrm{A}}{\varepsilon k_\mathrm{B} T}} \times \sqrt{I}, \tag{6}$$

where e is the charge on a proton, N_A is Avogadro's constant, ε is the dielectric constant of the medium, and I is ionic strength. Under our experimental conditions of 20 mM sodium phosphate aqueous buffer, pH 5.8, 298 K, the numerical value of κ is ~0.49 nm^{-1}.

In Hückel's derivation of the ion velocity,[26] the first and second terms on the right-hand side of Eq. 5 arise from f_E and $f_{\mathrm{counterion}}$, respectively. The quantity QE is the familiar Stark Hamiltonian used to describe steady-state electric field perturbation of atomic and molecular energy levels. In the present case, however, the effect of protein-counterion dynamics that produces a net electric field needs a mention. This is realized when the two terms are combined to obtain

$$\left\langle \frac{dx}{dt} \right\rangle = \frac{E}{6\pi r_g \eta} \left[\frac{Q}{(1+\kappa r_g)} \right], \tag{7}$$

where $Q/(1+\kappa r_g)$ is often called Q_eff,[27,28] whose smallness with respect to the actual Q will depend on both the size of the protein and the Debye length. This expression formally predicts the electrophoretic mobility of a globular (spherical) protein in the presence of an equilibrium electric potential, even though a slight improvement on the Hückel result is made by including

in the numerator a factor called Henry correction function $X_1(\kappa r_g)$ tabulated in literature.[29]

The electrophoretic velocity of cytochrome *c* under conditions employed in this study is ~1.2 mm h^{-1} when E=1.3 V cm^{-1}, which is expected to be lowered substantially by the much faster relaxation of the counterion cloud. Hence, electrode deposition of the protein migrating from the bulk solution in a few hours should not be large. Moreover, apart from the presence of the electric potential gradient, the interaction of ion atmospheres with protein charges should lower the chemical potential of the latter, thus lowering its free energy relative to its uncharged state. These considerations suggest that low potential gradient of the order applied here is not detrimental to structure and conformation of the protein in solution.

4.3.2. *Reduction of cytochrome c in electric field.*

In addition to the normal electrophoretic mobility, reactions innate to electrochemistry will be observed; the most obvious one for cytochrome *c* is the reduction of the heme iron. The redox reaction

$$\text{cytochrome } c\ \text{Fe}^{3+} + e^- \rightleftharpoons \text{cytochrome } c\ \text{Fe}^{2+}$$

is characterized by the standard redox potential $E^o \sim +263$ mV with respect to the standard hydrogen electrode,[30] implying moderately high affinity of the oxidized iron for electron. Reduction of the heme iron in the applied field of 1.3 V cm^{-1} is shown in Figure 1. The 409-to-412 nm red-shift of the heme Soret band ($\pi \rightarrow \pi^*$), and the appearance of much weaker *Q* bands ($\pi \rightarrow \pi^*$) at 549 nm due to configurational interaction between $a_{1u} \rightarrow e_g$ and $a_{2u} \rightarrow e_g$ and at 521 nm which is vibronic,[31] indicates reduction of cytochrome *c* (Figure 1a). The single-exponential rise of the 412-nm absorbance with time provides a reduction time τ_{red} ~ 27 min (Figure 1b), which is expected to be smaller with higher magnitude of the electric field (current density).

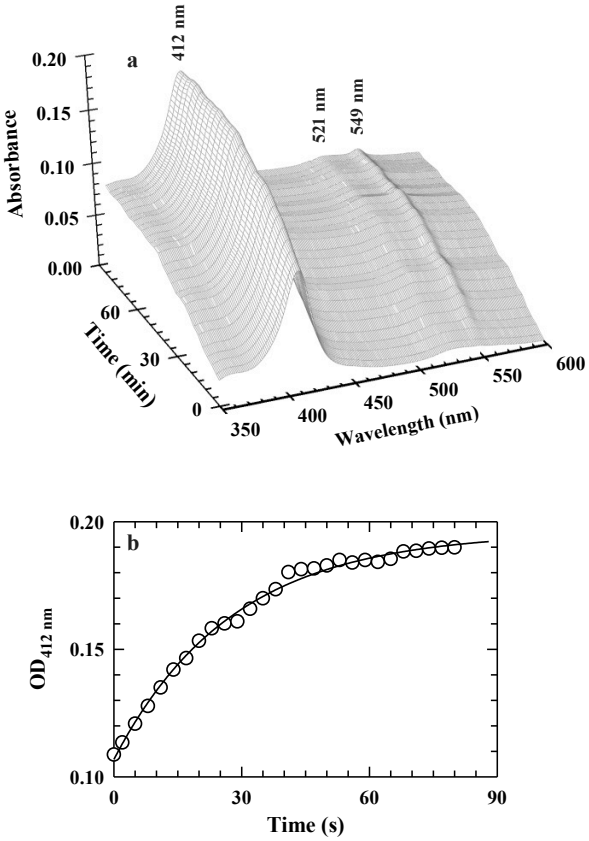

Figure 1. (a) Time-base absorption spectrum of cytochrome *c* depicting reduction of the heme iron ($Fe^{3+} \rightarrow Fe^{2+}$) by red-shift of the Soret band from the initial 409 nm, and the appearance of the *Q* band at 549 nm. (b) The absorption at 412 nm increases apparently exponentially with a time constant of ~ 27 min.

The heme reduction increases the energetic stability of the native protein,[32] arising from Gibbs free energy of electrochemical reduction ($\Delta G = -nFE_o \sim -5.9$ kcal mol^{-1}) and the relief of losing a +ve charge ($Fe^{3+} \rightarrow Fe^{2+}$) from the low dielectric protein interior. This result also suggests that the protein in the electric field gradient should migrate electrophoretically without any perturbation to its structure and conformation. Interestingly and to the contrary of these indications, the protein undergoes slow denaturation losing both tertiary and secondary structures, the time taken for which varies with the magnitude of the applied electric field. In this following, we produce some basic experimental results that establish a high degree of

protein denaturation by the same field of 1.3 V cm^{-1}.

4.3.3. *Unfolding of tertiary structure.*

Figure 2 shows real-time unfolding of tertiary structure monitored by fluorescence signals of tyrosine (Tyr) and tryptophan (Trp), the former undergoing a 310→299 nm shift of the emission maximum and the latter merely increasing at 386 nm from a quenched state. These spectral features have simple interpretations. The higher emission intensity of Tyr compared with that of Trp approximates the relative occurrence of the former and the latter (4:1) in the amino acid sequence. The 9-nm blue-shift of the Tyr emission maximum should imply relocation of the phenolic side chains in a nonpolar (rigid) environment of the denaturing protein. The Trp fluorescence at 386 nm is initially quenched when the protein is native, but increases with time because of tertiary structure unfolding that widens the center-to-center distance between the indole ring and the heme ring so that quenching of the former's fluorescence due to resonance energy transfer between the two rings decreases. In fact, the increase of fluorescence of the lone Trp of cytochrome *c* is known as a distinguished marker of chain expansion and unfolding of tertiary structure.[33] Thus we have the results for kinetic unfolding of tertiary structure in 1.3 V cm^{-1} electric field (Figure 2c,d). The rate constant for unfolding obtained from Tyr fluorescence (k = 0.068 min^{-1}) is nearly two-fold higher than that yielded by Trp fluorescence (k = 0.037 min^{-1}).

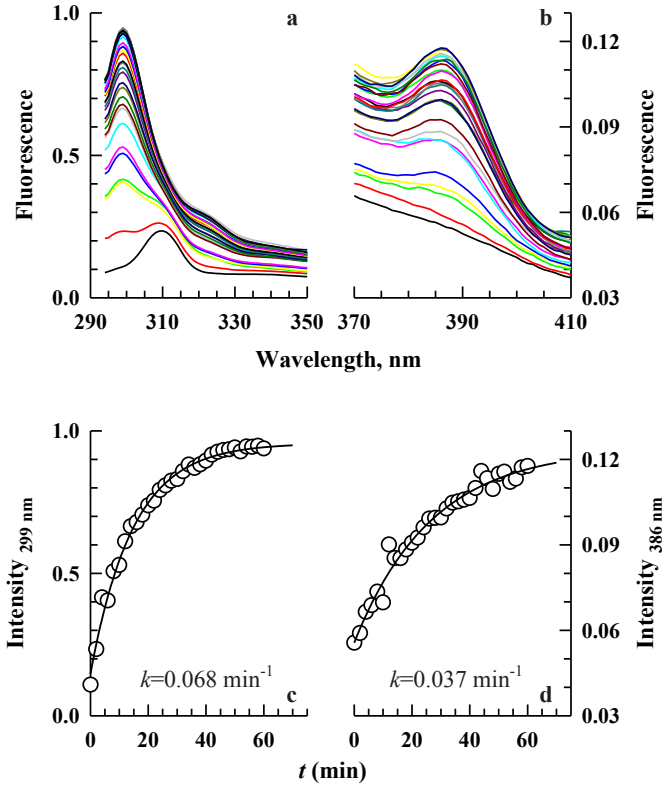

Figure 2. Changes in the fluorescence spectrum of cytochrome *c* with the time of application of the electric field. (a) Blue-shift (310→299 nm) of Tyr emission, (b) increase in the emission of Trp fluorescence at 386 nm due to a lift of quenching, (c) time-base Tyr emission at 299-nm, and (d) time-base lift of quenching of Trp emission at 386 nm.

The tertiary structure unfolding monitored by steady-state IR bands under identical conditions provides similar result; the bands centered at 1213 and 1365 cm^{-1}, both assigned to indole ν(CC), and 1740 cm^{-1} assigned to Asp/Glu ν(C=O)[34] give an apparent unfolding rate constants in the range 0.043 to 0.062 min^{-1} (Figure 3). Protein folding literature considers such probe-dependent rate constant as a hallmark of multistate kinetics involving multiple transition states, generally observed in slow folding and unfolding processes often limited by proline isomerization and chain misconfiguration that act as kinetic traps.[35,36] Proline isomerization and heme-misligation implicated in the folding of cytochrome *c*[37] are not expected to occur here because of accompanying reduction of the heme iron by the electric field. We thought it could be a change in the distribution of side chain charges in response to the external electric

field that produces a variation in the rate of unfolding of different parts of the tertiary structure. The applied potential can be thought to polarize the intra-protein charges akin to charging a capacitor, even though large separation of charges in the protein will be hindered by limited flexibility of covalently bonded side chains. Substantial charge separation is possible only when the stiffness of the covalent bond is reduced to an extent that the protein mechanically unfolds. The charge distribution at best is perturbed by the potential gradient, leading to a variation in the unfolding speed of different regions of tertiary structure.

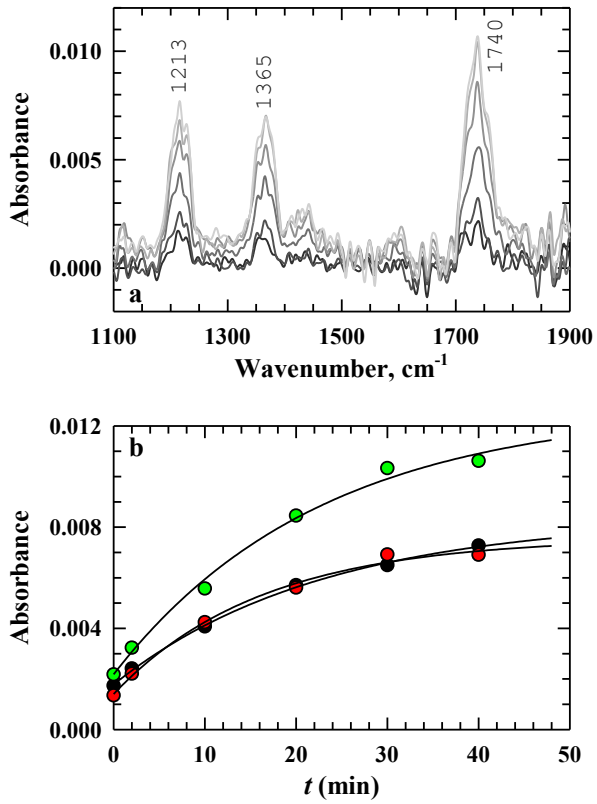

Figure 3. Changes with time in the IR absorption of indole ν(CC), and Asp/Glu ν(C=O) of cytochrome *c*. (a) Relevant region of the convoluted spectrum, and (b) time-base absorption intensity at 1213 (red), 1365 (black), and 1740 (green) cm^{-1}.

4.3.4. *Unfolding of secondary structure.*

Figure 4a shows the changes in the far-UV CD spectrum of cytochrome *c* at the indicated time intervals after placing the protein solution in the electric field, suggesting plainly the melting of secondary structure with time. Single wavelength absorbance at 207 and 222 nm

were taken without averaging the individual points up to ~110 minutes of subjecting the protein solution to potential gradient (Figure 4b). For simplicity, the CD signals are assumed to disappear by a single exponential; the possibility of occurrence of stretched or multi exponential kinetics is not verified because of low resolution of data. The estimated rate constant (10% error) for secondary structure unfolding is 0.009 cm^{-1}, which is at least four-fold smaller than the range of rate constants measured for tertiary structure unfolding. Clearly, the results present a sequential unfolding process with multiple intermediates, eventually losing the secondary structure entirely (Figure 4c).

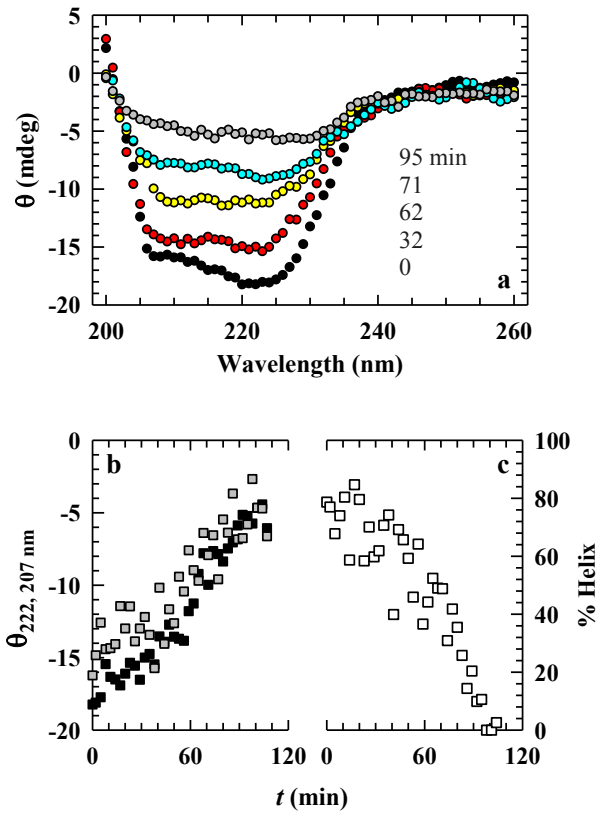

Figure 4. (a) Changes in the far-UV CD spectrum at the indicated times after the field (1.3 V cm^{-1}) application; (b) Ellipticity at 222- and 207 nm with time; (c) The helix content decreases to zero in ~100 min.

The preceded loss of tertiary structure is not the reason for unfolding of secondary structure; there is no theory that relates the occurrence of the latter at the expense of the former, although the interplay between the two determines the cooperativity of folding.[38] To interpret the present results obtained without the use of chemical denaturants, one can invoke the mechanics of motion of secondary structure elements under the influence of the external field. If the field is flat over the charge distribution in an element, a helix for example, the magnitude of the helix dipole moment μ is obtained as the integral of the charge distribution.

The electrical potential energy of the helix is the work done to rotate the helix dipole by an angle θ with reference to an initial value. The energy is first order with respect to μ and E, i.e, to the first power of (μE). If the field direction is taken along the space x-axis the potential energy will be

$$U = -\mu_x E_x \cos\theta, \tag{8}$$

and because the field gradient $\partial E/\partial x$ exists, the force experienced by the helix dipole along x is $F_x = \partial U/\partial x$. The helices thus tend to align with the electric field. A 15-residue α-helical segment having a dipole of ~70 D when placed in a field of 1.3 V cm^{-1} experiences a force of ~3×10^{-23} N to rotate the helix mass of ~0.2×10^{-23} kg. The reoriented alignment of the dipoles is adverse to structure folding, because the electrostatic energy of the protein is highly sensitive to the relative orientation of peptide dipoles in α-helix and β-sheet,[39] causing the loss of secondary structure. This proposition also states that electric field induced mechanical unfolding can be qualitatively understood with classical mechanics, unlike chemical denaturation in which denaturants bind to multifunctional protein groups to disrupt hydrogen bonding and hydrophobic interactions.

4.3.5. *Double perturbation by electric field and chemical denaturants.*

To further qualify the electric field gradient as an effective physical denaturant, a double perturbation experiment was performed in which cytochrome *c* already denatured variably by the use of different levels of the non-ionic chemical denaturant urea was subjected to electric field. Double perturbation experiments are widely used to study thermodynamics and kinetics of protein unfolding,[40] but the objective here is only to check if the two unfolding agents produce a cumulative effect so as to project the electric field as a physical denaturant. The field

is expected to reduce the effective level of a chemical denaturant required to perturb the structure.

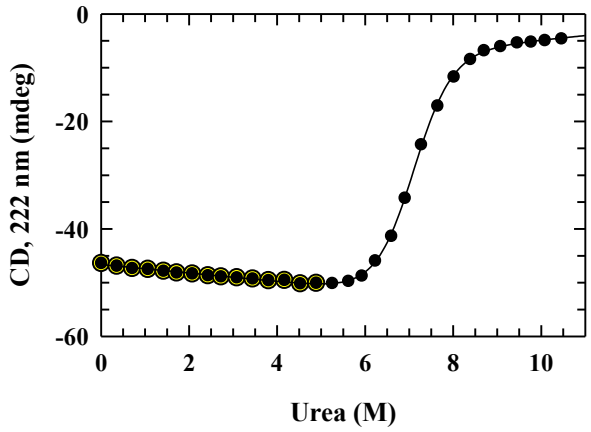

Figure 5. The pre-transition baseline region (large symbols) in the urea-induced unfolding of cytochrome c at 25°C, 20 mM sodium phosphate, pH 5.8. The solid line through data is drawn according to a two-state (N ↔ U) transition.

To look into the double perturbation effect, we first develop the denaturation isotherm of cytochrome *c* with the non-ionic chemical denaturant urea. The pre-transition baseline of the isotherm extends up to ~5 M urea (Figure 5), and the changes in the properties of native and unfolded ensembles in this baseline region generally remain silent to common spectroscopic probes, including fluorescence and CD. Cytochrome *c* samples prepared in variable urea (0.5, 1.0, 2.0, 3.0, and 4.0 M) that correspond to the pre-transition baseline were probed for their response to a fixed field of 1.3 V cm^{-1} by monitoring fluorescence spectra with time (Figure 6a).

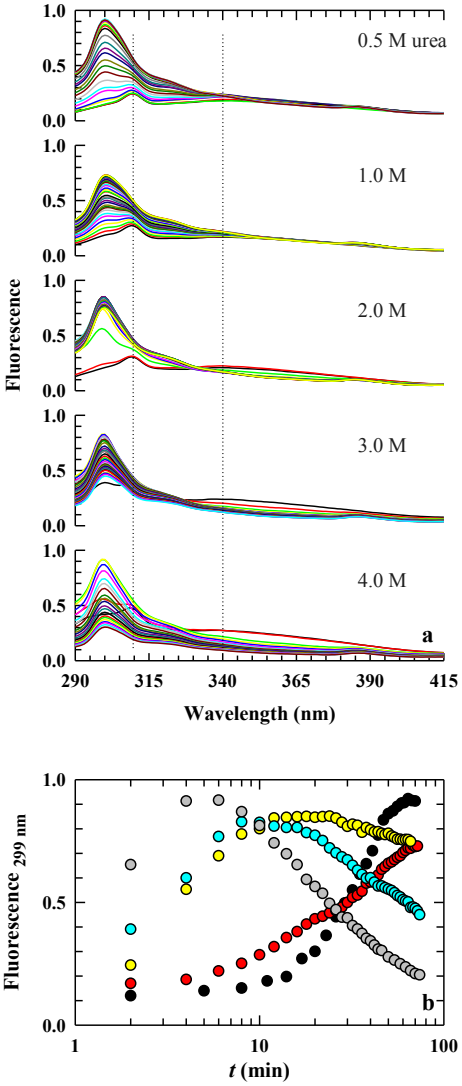

Figure 6. (a) Effect of 1.3 V cm^{-1} field on the emission spectra of cytochrome *c* predenatuerd with the indicated levels of urea. The dotted line at 430 nm indicates Trp fluorescence that marginally increases with urea, but decrease with time of field application. The dotted line at 309 nm indicates Tyr fluorescence that blue-shifts under the influence of the field. (b) Time dependence of Tyr fluorescence at 299 nm for the protein predenatured in 0.5 (black), 1.0 (red), 2.0 (yellow), 3.0 (cyan), and 4.0 (gray) M urea.

As discussed already, the spectrum is dominated by Tyr fluorescence characterized by a shift of the native-state emission peak at 309 nm to the unfolded-state peak at 299 nm, the former tending to disappear with increasing urea-induced destabilization. The broad tryptophan emission peak centered at ~340 nm is absent or strongly quenched at low urea (0.5 and 1.0 M) because of resonance energy transfer with the heme, but turns fluorescent as the indole-heme distance increases due to denaturation by higher urea (Figure 6a).

The time course of the 299-nm fluorescence intensity in the presence of the electric field shows tertiary structure unfolding (Figure 6b). The traces should be exponential in general; the field-induced rate of unfolding is faster with urea that has already perturbed the structure. The

amplitude however rolls over at higher levels of urea, the turning point being shorter in time. This brings us to another interesting property of electric field-unfolded protein. We have consistently observed in all experiments, even in those where no urea was used, that the protein begins to aggregate and precipitate as soon as electric field unfolding was complete. In the present double perturbation results (Figure 6b), the rollover amplitude arise from fluorescence of the aggregating unfolded species. Clearly, the side-chain fluorophores in the aggregating protein are relocated so as to quench their fluorescence. To summarize this section, electric field is a physical denaturant, the rate of unfolding by which increases with decreasing stability of the protein. The aggregation must be a characteristic of electric field unfolding, because chemically unfolded cytochrome *c* is not known to aggregate.[33,41–44]

4.3.6. *Kinetics of unfolded-state aggregation.*

Aggregation of the unfolded protein was probed by including the aggregate-staining dye ThT commonly used to study kinetics of protein fibrillation.[45,46] The protein solution containing ~25 μM ThT was subjected to electric field, and time-base emission of the dye was taken at 478 nm (Figure 7a). The fluorescence remains unchanged up to ~ 2 h with a potential gradient of 0.28 V cm^{-1}, suggesting that the protein has not unfolded yet. The unfolding at higher electric field is accompanied by aggregation without a lag phase; the apparent lag phase is expected to disappear as the field strength is made higher. The formation of aggregates was also studied by 350-nm light scattering in the presence of electric field (Figure 7b). Here again, fluorescence changes little up to ~ 2 h with 0.28 V cm^{-1}, but the emission increases and reaches the steady-state in ~80 min after passing 0.8 or 1.3 V cm^{-1}. Clearly, the apparent lag phase will shorten increasingly with higher field strength.

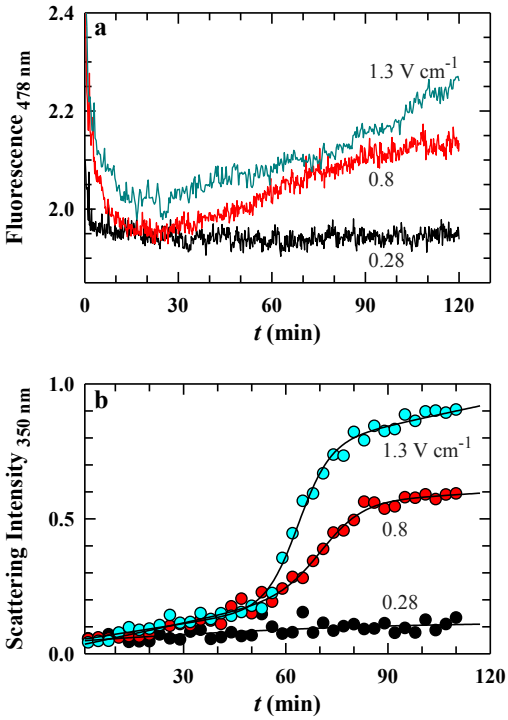

Figure 7. (a) Time-base fluorescence of ThT included in the cytochrome *c* solution and subjected to indicated electric fields. (b) Time dependence of 350-nm static light scattering of cytochrome c subjected to the fields indicated.

The lack of a lag time in the kinetics of ThT fluorescence and light scattering suggests amorphous aggregation of the unfolded proteins, the kinetics of which is field dependent. The absence of the lag phase is taken as a hallmark of the formation of nucleation-independent glass-like amorphous assemblies that are different from nucleation-dependent ordered crystalline amyloid that are ordered and highly structured. The possibility that a part of the population of amorphous fibrils is reconfigured at later times to produce rigid amyloid fibers also exists,[47] in which case the total fibril population will be represented by both amorphous and crystalline aggregates. To check if such is the case, the unfolded protein solution containing the precipitated aggregates was stirred and the re-suspended aggregates were viewed by SEM. The morphology in the micrograph (Figure 8a) shows variable-size smaller aggregates held on to larger ones. Most of the former that could be as small as ~100 nm appear as protruded overhangs, which produce more secondary electrons so as to appear brighter than the latter in the SEM image. Several smaller aggregates coming together for attachment are also visible, possibly leading to the formation of larger mass of aggregates. The zoom out of the micrograph shows an irregular mesh formed of the aggregates with varying dimensions of interstitial voids (Figure 8b), the origin of which – whether intrinsic

or an effect due to the electron beam of the microscope, remains uncertain. The mode(s) of interaction in the aggregate network has not been studied in this work, but the asymmetry in the attachment of the smaller proto-aggregates suggests that they interact by hydrophobic or dispersion forces rather than electrostatic interactions.

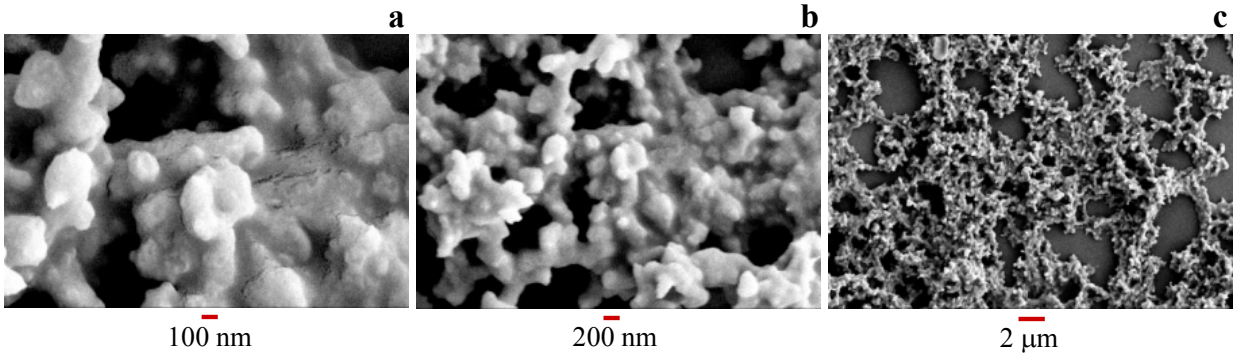

Figure 8. (a) Morphology of cytochrome c aggregates formed due to unfolding by 1.3 V cm^{-1} electric field. (b and c) Zoom outs showing irregular mesh-like morphology of the aggregates with interstitial voids of varying dimension.

4.3.7. *All proteins should unfold in electric field.*

If the results produced for cytochrome *c* are considered prototypical, similar effects of electric field on the structure and conformation of other proteins should also be established. We examined half a dozen globular proteins to find that all follow the same suit. Briefly presented in Figure 9 are results for two of these proteins. The tertiary structure perturbation of myoglobin and trypsin were monitored by fluorescence up to ~90 min after the application of the same potential of 1.3 V cm^{-1} (Figure 9). For myoglobin at pH 7 (charge +4.8) Trp fluorescence quenches and Tyr fluorescence increases. Similarly, the Trp fluorescence of trypsin (pH 8, charge –2.0) starts out with an initial steady-state baseline extending to ~20 min and then quenches by apparently exponential courses to reach the final steady state in ~ 1 h.

The apparent exponential nature of signal changes for both proteins is a sign of tertiary structure unfolding. Note that the observed changes in fluorescence, whether quenched or increased, with electric field need not be consistent with protein specific canonical changes for chemical or thermal unfolding. The SEM images of the unfolded proteins (Figure 9) show aggregates similar to those observed for cytochrome *c* above (Figure 8b).

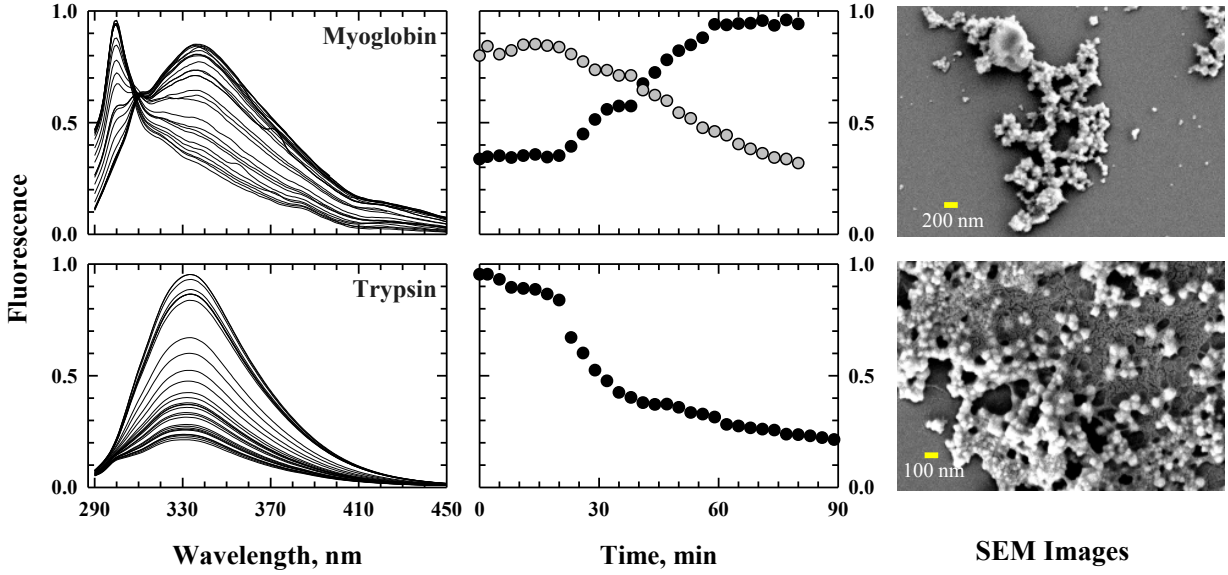

Figure 8. Unfolding and amorphous aggregation of myoglobin (top row), and trypsin (bottom row). The middle panel of the myoglobin row shows emission intensity at 337 (gray) and 300 (black) nm.

At this stage, we believe that unfolding and amorphous aggregation is a generic EF effect expected for other protein systems as well. We simply mention that this pathway leading to amorphous aggregation is likely to be in competition with another process of nucleation-dependent crystalline aggregation arising from the concentration gradient across the electrodes established by electrophoresis. In such a case, one expects to find both amorphous and crystalline aggregates, a full-fledged description of which along with experimental proof is being worked out.

4.4. References

1. Bhuyan, A. K. *Fundamental Concepts of Molecular Spectroscopy*; CRC Press, Taylor & Francis Group, 2023.

2. Townes, C. H.; Schawlow, A. L. *Microwave Spectroscopy*; Dover Publications Inc., 1975

3. Porschke, D.; Obst, A. An Electric Field Jump Apparatus with ns Time Resolution for Electro-Optical Measurements at Physiological Salt Concentrations. *Rev. Sci. Instrum.* **1991**, *62,* 818–820.

4. Porschke, D. Microdipoles: Unusual Electric Properties of Biological Molecules. *Biophys. Chem.* **1997**, *66*, 241–257.

5. Toschi, F.; Ugli, F; Biscarini, F; Zerbetto, F. Effects of Electric Field Stress on a b-Amyloid Peptide. *J. Phys. Chem. B* **2009**, *113*, 369–376.

6. Ojeda-May, P.; Garcia, M. E. Electric Field-Driven Disruption of a Native b-Sheet Protein Conformation and Generation of a Helix Structure. *Biophys. J.* **2010**, *99*, 595–599.

7. Astrakas, L. G.; Gousias, C.; Tzaphlidou, M. Structural Destabilization of Chingolin Under the Influence of Oscillating Electric Fields. *J. Appl. Phys.* **2012**, *111*, 074702.

8. Zhao, W.; Yang, R.; Lu, R.; Tang, Y.; Zhang, W. Investigation of the Mechanisms of Pulsed Electric Fields on Inactivation of Enzyme: Lysozyme. *J. Agric. Food Chem.* **2007**, *55*, 9850–9858.

9. Zhao, W.; Yang, R. Experimental Study on Conformational Changes of Lysozyme in Solution Induced by Pulsed Electric Field and Thermal Stresses. *J. Phys. Chem. B* **2010**, *114*, 503–510.

10. English, N. J.; Mooney, D. A. Denaturation of Hen Egg White Lysozyme in Electromagnetic Fields: A Molecular Dynamics Study. *J. Chem. Phys.* **2007**, *126*, 091105.

11. English, N. J.; Waldron, C. J. Perspectives on External Electric Fields in Molecular Simulation: Progress, Prospects, and Challenges. *Phys. Chem. Chem. Phys.* **2015**, *17*, 12407–12440.

12. Marracino, P.; Apollonio, F.; Liberti, M.; D'Inzeo, G.; Amadei, A. Effect of High Exogenous Electric Pulses on Protein Conformation: Myoglobin as a Case Study. *J. Phys. Chem. B* **2013**, *117*, 2273–2279.

13. Amadei, A.; Marracino, P. Theoretical-Computational Modeling of the Electric Field Effects on Protein Unfolding Thermodynamics. *RSc. Adv.* **2015**, *5*, 96551–96561.

14. Bekard, I.; Dunstan, D. E. Electric Field Induced Changes in Protein Conformation. *Soft Matter* **2014**, *10*, 431–437.

15. Rodrigues, R. M.; Vicente, A. A.; Petersen, S. B.; Pereira, R. N. Electric Field Effects on b-Lactoglobulin Thermal Unfolding as a Function of pH – Impact on Protein Functionality. *Innov. Food Sci. Emerg. Tech.* **2019**, *52*, 1–7.

16. Rodrigues, R. M.; Avelar, Z.; Vicente, A. A.; Petersen, S. B.; Pereira, R. N. Influence of Moderate Electric Fields in b-Lactoglobulin Thermal Unfolding and Interactions. *Food Chem.* **2020**, *304*, 125442.

17. Vanga, S. K.; Singh, A.; Raghavan, V. Effect of Thermal and Electric Field Treatment on the Conformation of Ara h 6 Peanut Protein Allergen. *Innov. Food Sci. Emerg. Tech.* **2015**, *30*, 79–88.

18. Vanga, S. K.; Singh, A.; Raghavan, V. Review of Conventional and Novel Food Processing Methods on Food Allergens. *Crit. Rev. Food Sci. Nutr.* **2017**, *57*, 2077–2094.

19. Samaranayake, C. P.; Sastry, S. K. Effects of Controlled-Frequency Moderate Electric Fields on Pectin Methyltransferase and Polygalacturonase Activities in Tomato Homogenate. *Food Chem.* **2016**, *199*, 265–272.

20. Wu, L.; Zhao, W.; Yang, R.; Chen, X. Effects of Pulsed Electric Fields Processing on Stability of Egg White Proteins. *J. Food Eng.* **2014**, *139*, 13–18.

21. Liu, Y. F.; Oey, I.; Bremer, P.; Carne, A.; Silcock, P. Effect of pH, Temperature, and Pulsed Electric Fields on the Turbidity and Protein Aggregation of Ovomucin-Depleted Egg White. *Food Res. Int.* **2017**, *91*, 161–170.

22. Han, Z.; Cai, M.; Cheng, J.-H.; Sun, D.-W. Effects of Electric Fields and Electromagnetic Wave on Food Protein Structure and Functionality: A Review. *Trends Food Sci. Technol.* **2018**, *75*, 1–9.

23. Rodrigues, R. M.; Avelar, Z.; Machado, L.; Pereira, R. N.; Vicente, A. A. Electric Field Effects on Proteins - Novel Perspectives on Food and Potential Health Implications. *Food Res. Int.* **2020**, *137*, 109709.

24. Arendash, G. W.; Sanchez-Ramos, J.; Mori, T.; Mamcarz, M.; Lin, X.; Runfeldt, M.; Wang, L.; Zhang, G.; Sava, V.; Tan, J.; Cao, C. Electromagnetic Field Tretment Protects Against and Reverses Cognitive Impairment in Alzheimer's Disease Mice. *J. Alzheimers Dis.* **2010**, *19*, 191–210.

25. Zhang, Q.; Shao, D.; Xu, P.; Jiang, Z. Effects of an Electric Field on the Conformational Transition of the Protein: Pulsed and Oscillating Electric Fields with Different Frequencies. *Polymers* **2021**, *14*, 123.

26. Hückel, E. Die Kataphorese Der Kuge. *Physik. Z* **1924**, *25*, 204–210.

27. Ohshima, H. Electrophoretic Mobility of a Spherical Colloidal Particle in a Salt-Free Medium. *J. Colloid Interface Sci.* **2002**, *248*, 499–503.

28. Muthukumar, M. Communication: Charge, Diffusion, and Mobility of Proteins Through Nanopores. *J. Chem. Phys.* **2014**, *141*, 081104.

29. Rice, S. A.; Nagasawa, M. *Polyelectrolyte Solutions*; Academic Press, 1961.

30. Battistuzzi, G.; Borsari, M.; Cowan, J. A.; Ranieri, A.; Sola, M. Control of Cytochrome c Redox Potential: Axial Ligation and Protein Environment Effects. *J. Am. Chem. Soc.* **2002**, *124*, 5315–5324.

31. Joshi, K.; Bhuyan, A. K. Quasi-Native Transition and Self-Diffusion of Proteins in Water-Glycerol Mixture. *Biophys. Chem.* **2020**, *257*, 106274.

32. Bhuyan, A. K.; Udgaonkar, J. B. Folding of Horse Cytochrome c in the Reduced State. *J. Mol. Biol.* **2001**, *312*, 1135–1160.

33. Tsong, T. Y. The Trp-59 Fluorescence of Ferricytochjrome *c* as a Sensitive Measure of the Overall Protein Conformation. *J. Biol. Chem.* **1974**, *249*, 1988–1990.

34. Barth, A.; Zscherp, C. What Vibrations Tell Us About Proteins. *Q. Rev. Biophys.* **2002**, *35*, 369–430.

35. Bhuyan, A. K.; Udgaonkar, J. B. Observation of Multistate Kinetics During the Slow Folding and Unfolding of Barstar. *Biochemistry* **1999**, *38*, 9158–9168.

36. Sosnick, T. R.; Mayne, L.; Hiller, R.; Englander, S. W. The Barriers in Protein Folding. *Nat. Struct. Biol.* **1994**, *1*, 149–156.

37. Pierce, M. M.; Nall, B. T. Coupled Kinetic Traps in Cytochrome c Folding: His-Heme Misligation and Proline Isomerization. *J. Mol. Biol.* **2000**, *298*, 955–969.

38. Bereau, T.; Bachmann, M.; Deserno, M. Interplay Between Secondary and Tertiary Structure Formation in Protein Folding Cooperativity. *J. Am. Chem. Soc.* **2010**, *132*, 13129–13131.

39. Hol, W. G. J.; Halie, L. M.; Sander, C. Dipoles of the a-Helix and b-Sheet: Their Role in Protein Folding. *Nature* **1981**, *294*, 532–536.

40. Yasin, U. M.; Sashi, P.; Bhuyan, A. K. Free Energy Landscape of Lysozyme: Multiple near-Native Conformational States and Rollover in the Urea Dependence of Folding Energy. *J. Phys. Chem. B* **2014**, *118*, 6662–6669.

41. Elöve, G. A.; Bhuyan, A. K.; Roder, H. Kinetic Mechanism of Cytochrome c Folding: Involvement of the Heme and Its Ligands. *Biochemistry* **1994**, *33*, 6925–6935.

42. Colón, W.; Elöve, G. A.; Wakem, L. P.; Sherman, F.; Roder, H. Side-Chain Packing of the N- and C-Terminal Helices Plays a Critical Role in the Kinetics of Cytochrome c Folding. *Biochemistry* **1996**, *35*, 5538–5549.

43. Roder, H.; Colón, W. Kinetic Role of Early Intermediates in Protein Folding. *Curr. Opin. Struct. Biol.* **1997**, *7*, 15–28.

44. Kumar, R.; Bhuyan, A. K. Two-State Folding of Horse Ferrocytochrome *c*: Analyses of Linear Free Energy Relationship, Chevron Curvature, and Stopped-Flow Burst Relaxation Kinetics. *Biochemistry* **2005**, *44*, 3024–3033.

45. LeVine, H.; Thioflavin, T. Interaction with Amyloid b-Sheets Structure. *Amyloid* **1995**, *2*, 1–6.

46. Naiki, H.; Higuchi, K.; Hosokawa, M.; Takeda, T. Fluorometric Determination of Amyloid Fibrils In Vitro Using the Fluorescent Dye, Thioflavin T1. *Anal. Biochem.* **1989**, *177*, 244–249.

47. Yoshimura, Y.; Lin, Y.; Yagi, H.; Lee, Y. H.; Kitayama, H.; Sakurai, K.; So, M.; Ogi, H.; Naiki, H.; Goto, Y. Distinguishing Crystal-Like Amyloid Fibrils and Glass-Like Amorphous Aggregates from Their Kinetics of Aggregation. *Proc. Natl. Acad. Sci. U. S. A.* **2012**, *109*, 14446–14451.

CHAPTER 5

Protein Crystallization in Very Weak DC Electric Field

Abstract

How electric field (EF) assists in crystal growth has been difficult to describe uniformly. Many factors concerning the amplitude, frequency, and waveform of the field, gating and duration of field application, the requirement of auxiliary physical agents such as high magnetic field and pulsed radiation, and geometric confinement of the protein solution have made the process seemingly complex. This report describes EF-aided crystallization of a batch of five commercially available globular proteins from their respective 7 μM solutions uniformly applying a 1.3 V cm^{-1} DC field for ~90 min. The crystals have been imaged and shown to diffract. The field mechanically unfolds the protein facilitating amorphous aggregation, which is a 'dense' state of unfolded molecules. Upon withdrawal of EF, some molecules undergo slow refolding to the native (N) or quasi-native (QN) 'dense' states still attached to the amorphous substratum. The reduced surface tension of the dense refolded states lowers the Gibbs free energy barrier for nucleation. Nucleation from heterogeneous patches of refolded dense states on the substratum produces size distribution in the crystal population. It is shown that EF-assisted crystallization is an exceedingly easy and enjoyable experiment, requiring nothing special about apparatus and accessories, solution conditions, protein concentration, and experimental methods. Crystals can be grown in very weak DC field. The use of strong field, oscillating field in particular, in conjunction with auxiliary physical agents is redundant.

5.1. Introduction

Stark effect, in which the external electric field **E** exerts torques on a molecular electric dipole $\boldsymbol{\mu}$ to change its rotational motion, is energy perturbation that has played enormous role in the understanding of diatomic and small-molecule spectra.[1–3] The dipole rotation effect is however adverse to the conformation, structure, and functions of proteins and enzymes. Since proteins are investigated in aqueous solutions, the description of continuous EF perturbation must also account for electrochemical effects, including electrophoresis, charge separation and reduction, and entropic and polarization effects on the surrounding water molecules. While persistent efforts are underway to coherently describe the EF effect on structure and activity of proteins and enzymes,[2] the assistance of an external EF in the nucleation and tuned growth of better quality protein crystals has also been increasingly recognized for two decades now.[4–9]

In EF-assisted crystallization, the protein solution is subjected to an electrical potential with the electrodes immersed in the solution (internal EF) or without electrode-solution contact (external EF), and the molecular-level surface changes and crystal growth are visualized by atomic force microscopy or contrast-enhanced laser confocal microscopy.[10] Both static current (DC) ranging from ~0.5 to 6 μA or field strength in the 4.0×10^6 – 2.0×10^7 V m^{-1} range[11] and AC fields as high as 10^4 V cm^{-1} oscillating at ~2–9 MHz have been employed to promote crystallization.[8,12,13]. In advanced methods, hen egg white lysozyme (HEWL) crystal growth was facilitated by employing DC current in conjunction with high magnetic fields of the order of 16.5 T.[14] The approach was made even more sophisticated by combining a low frequency AC field with an external magnetic field and sub-microsecond radiofrequency pulses.[15] The duration of subjecting the protein solution to the EF, from a few to ~10 or more hours or even days, appears to depend on the applied current strength and the protein system studied; for example, cytochrome *c* crystals have been grown by passing 0.8 μA current through the solution for 15 days.[16]

The brief survey above seems to indicate that the extent of EF assistance reachable is dependent on a myriad of factors, including the amplitude and frequency of the field, the time duration of imposing the field, spatial and geometric constraints on the protein solution subjected to the field, temperature and ionic strength of the solution, and the presence of other external agents like magnetic field and radiation pulses. The experimenter still looks for an optimum solution condition, an optimized apparatus, and appropriate field parameters that would deliver most in crystal growth. It appears as though the performance of a 'black magic' trick of crystallization is not dispensed with even if the assistance of EF is sought. This is probably the reason for the lack of a sizable set of proteins crystalized with EF assistance. Most of the EF-promoted crystallization has been described using HEWL, with fewer sporadic reports on insulin, BPTI, thaumatin,[17] cytochrome *c*, and estradiol 17 β-dehydrogenase.[8] Furthermore, because protein concentration used in all of these reported EF-aided crystallization is typically in the 1–4 mM range, which is the standard usage in classical protein crystallization methods, the EF assistance so far has not mitigated the concentration requirement either.

One can then ask questions. Is there a demonstrable principle of EF-assisted crystallization? Is it necessary to subject the protein solution to EF for hours or even days to induce nucleation? If there is a principle, then a prescribed set of EF parameters and solution conditions can be applied uniformly to different proteins for inducing crystal growth. Contemplating on these, we developed a set of common minimal conditions, 1.3 V cm^{-1} DC applied for ~90 min through a 7 μM protein solution, to crystalize five commercially available globular proteins.

5.2. Experimental section

Platinum wire mesh electrodes were attached to the inside surfaces across a 1-cm path length quartz cuvette containing the protein solution. This mode of subjecting the solution to the electric field in which the electrodes are in contact with the solution is called internal EF application. The positioning of the electrodes did not block the light beam in and out of the cuvette. The electrodes were connected to a DC supply regulated at 1.3 V and monitored with an oscilloscope. An online Jasco FP-8300 fluorometer, whose cuvette chamber was slightly modified to accommodate the EF supply accessories and time-gated data acquisition, was used to take fluorescence spectra (excitation 280 nm).

Infrared spectra in the 400–4000 cm^{-1} spectral width were recorded using a Nicolet iS5 attenuated total reflection infrared (ATR-IR) instrument. The protein solution already subjected to offline EF (1.3 V cm^{-1}) was periodically removed in aliquot of ~75 μL to be deposited on the ATR plate for spectral measurement with the assumption that no major structural change occurs during the time (~2 min) of the spectrum measurement. Each sample measurement accompanied the measurement of a background spectrum of the buffer on the ATR plate. The background spectrum was subtracted from the corresponding sample spectrum, and the resultant spectrum was subjected to a running average or median smoother. The number of overlapping (degenerate) frequencies of secondary structure elements were located and assigned by deconvolution of the amide I band by curve fitting and second derivative methods.[18,19]

Gold coated samples were used for FESEM images taken in a ZEISS Ultra 55 instrument with a 3 kV electron beam. For TEM, samples were deposited on copper grids, treated with 2 mM uranyl acetate for ~30 s, washed and dried, and imaged in a JEOL JEM-F200 instrument using a 200 kV electron beam. The same samples were used to develop electron diffractograms by selected area electron diffraction in TEM.

The proteins hen egg white lysozyme (HEWL), α-lactalbumin (α-LA), β-lactoglobulin (β-LG), horse heart myoglobin (Mb), and trypsin were purchased from Sigma and used without further purification. The proteins and rather uniform experimental conditions are conveniently listed in Table 1.

Table 1. Proteins and experimental conditions for EF-assisted crystallization

Protein	Charge	Buffer	Protein concentration	Buffer ionic strength	DC Field	T
HEWL	+16.4	water, pH 3.8	7 μM	0	1.3 V cm^{-1}	25°C
α-LA	−6.8	20 mM phosphate, pH 7	7 μM	21.9 mM	1.3 V cm^{-1}	25°C
β-LG	−7.7	20 mM phosphate, pH 7	7 μM	21.9 mM	1.3 V cm^{-1}	25°C
Mb	+4.8	20 mM phosphate, pH 7	7 μM	21.9 mM	1.3 V cm^{-1}	25°C
Trypsin	−2.0	20 mM phosphate, pH 8	7 μM	21.9 mM	1.3 V cm^{-1}	25°C

5.3. Results and discussion

5.3.1. *IR-probed mechanical unfolding and α-helix → β-sheet transition in electric field.*

The requisite for a general crystallization protocol is supersaturation of the protein, which when precipitated by an agent can support nucleation of protein crystals.[20] Although our choice of 7 μM protein concentration is absurdly low in the face of supersaturation, one can work with the idea that a dense molecular precipitate can be obtained if the protein is mechanically unfolded to allow for aggregation. To show that even a weak non-oscillating electric field can act as a physical unfolding agent, the secondary structures of all five proteins were monitored for ~90 min in the presence of 1.3 V cm^{-1} DC field. We focus in particular on amide I and II bands (Figure 1) which

originate from the normal modes of vibration of α-helix, β-sheet, and random coil structures.[21] The melting of secondary structures can be assessed to a first approximation by plotting the amide I absorption at 1646 cm^{-1}, characteristic of α-helix and/or parallel β-sheet. The time dependence of the 1646 cm^{-1} absorption (column 2, Figure 1) clearly indicates a fair amount of loss of secondary structure in ~90 min of applying the electric field.

To quantify the total loss of different secondary structure elements over the bin of ~ 90 min, we deconvoluted the amide I band at t=0 when there was no electric field and t ~ 90 min after switching the field on. The deconvoluted components assigned to α-helix, β-sheet, and turn are displayed in Figure 1, and the % change of individual structure elements are listed in Table 2, and graphed in Figure 2. For all five proteins, the electric field consistently reduces the amount of α-helix and turns, the increase of the latter for trypsin is exceptional or outlying. The content of β-sheets on the other hand increases for all proteins (Figure 2). The overwhelming increase of β-sheet content for myoglobin, whose native state has ~80% residues in α-helical conformation, is an indication that the electric field generally induces a α-helix → β-sheet deformation transition akin to a mechanical denaturation (unfolding) process. Since α-helix → β-sheet transitions are widely known to lead to protein aggregation,[22,23] the fate of our proteins under EF influence could also be aggregation. The observation that the protein solution becomes progressively turbid after ~30 min of field application and precipitates at times longer suggests that electric field induces aggregation propensity.

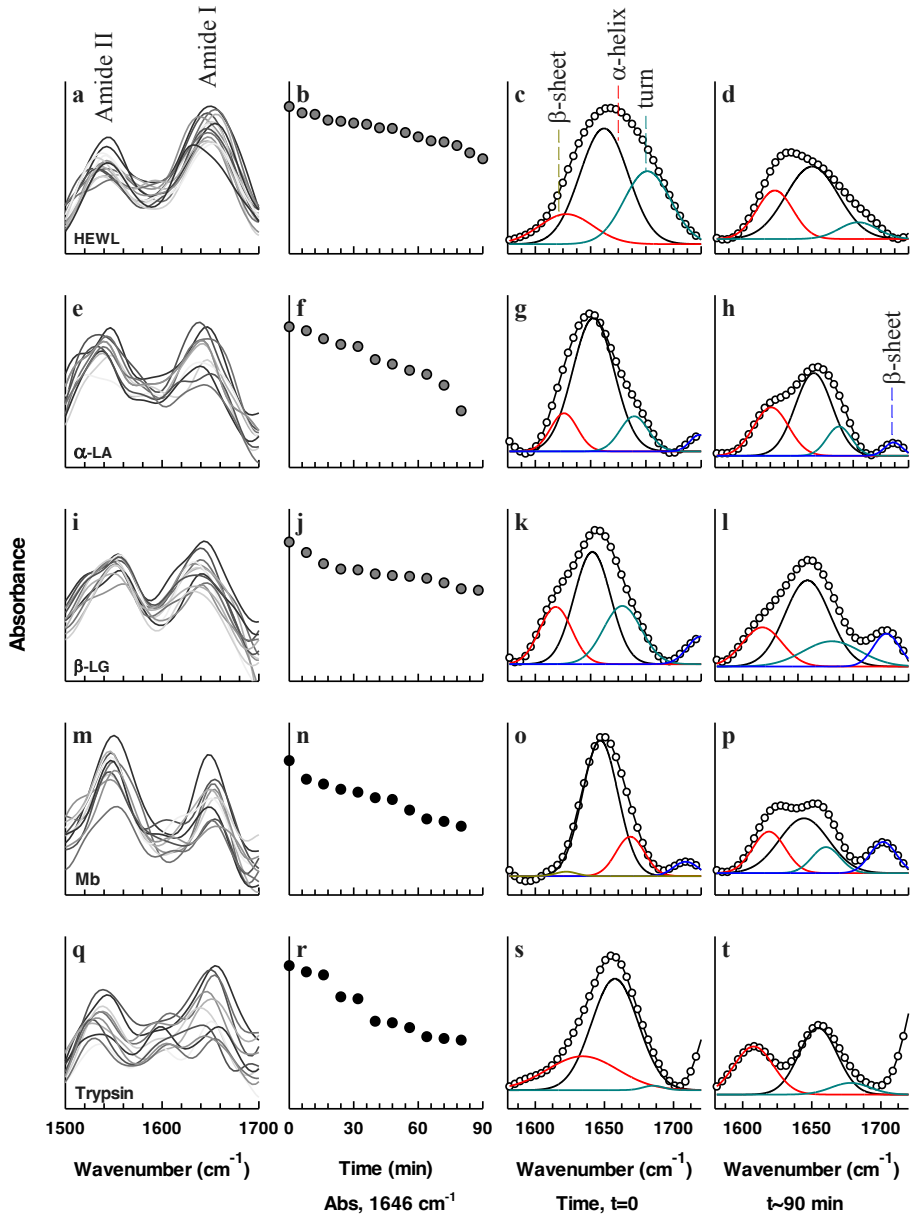

Figure 1. Electric field effect on the IR spectra of proteins. *Column* 1 (a,e,i,m,q) Amide I and II regions of IR spectra of the indicated proteins at different times of electric field application. *Column* 2 (b,f,j,n,r) Time dependence of absorption of the corresponding proteins at 1646 cm^{-1}. *Column* 3 (c,g,k,o,s) Deconvolution of amide I bands of corresponding proteins (connected circles) in the absence of electric field (t=0) to quantify absorptions due to α-helix (black), β-sheets (red), and turns (cyan). *Column* 4 (d,h,l,p,t) Deconvolution of amide I bands of the corresponding proteins (connected circles) after ~90 minutes of application of 1.3 V cm^{-1} DC field. Color codes of absorption bands of structural elements are identical in columns 3 and 4.

Table 2. Changes in band positions, absorbance, and secondary structure content induced by EF (1.3 V cm^{-1}) applied for ~ 90 min.

Protein	Structure types	Band positions in amide I (cm^{-1})*		% change**
		t=0	*t*~90 min	
HEWL	α-helix	1649 (2.46×10^{-3})	1650 (1.62×10^{-3})	34 (–)
	β-sheets	1622 (5.73×10^{-4})	1623 (1.10×10^{-3})	91 (+)
	turn	1681 (1.52×10^{-3})	1682 (3.91×10^{-4})	74 (–)
α-LA	α-helix	1642 (1.45×10^{-3})	1650 (8.62×10^{-4})	40 (–)
	β-sheets	1621 (4.32×10^{-4})	1621 (4.95×10^{-4})	41 (+)
			1709 (1.18×10^{-4})	
	turn	1672 (3.99×10^{-4})	1670 (2.89×10^{-4})	27 (–)
β-LG	α-helix	1641 (1.44×10^{-3})	1647 (1.10×10^{-3})	24 (–)
	β-sheets	1615 (7.20×10^{-4})	1614 (4.53×10^{-4})	14 (+)
			1704 (3.71×10^{-4})	
	turn	1663 (7.32×10^{-4})	1665 (2.72×10^{-4})	62 (–)
Mb	α-helix	1647 (1.58×10^{-3})	1645 (6.34×10^{-4})	60 (–)
	β-sheets	1622 (0.52×10^{-4})	1619 (4.72×10^{-4})	404 (+)
		1709 (1.10×10^{-4})	1701 (3.45×10^{-4})	
	turn	1669 (4.51×10^{-4})	1660 (2.83×10^{-4})	37 (–)
Trypsin	α-helix	1657 (1.23×10^{-3})	1654 (6.70×10^{-4})	45 (–)
	β-sheets	1634 (3.43×10^{-4})	1608 (4.54×10^{-4})	32 (+)
	turn	1685 (0.17×10^{-4})	1678 (0.42×10^{-4})	148 (+)

* Numbers within small brackets are IR absorbance values

** (–) indicates a decrease [{Abs (0) – Abs (90 min)}/ Abs (0)]×100

(+) indicates an increase [{Abs (90 min) – Abs (0)}/ Abs (0)]×100

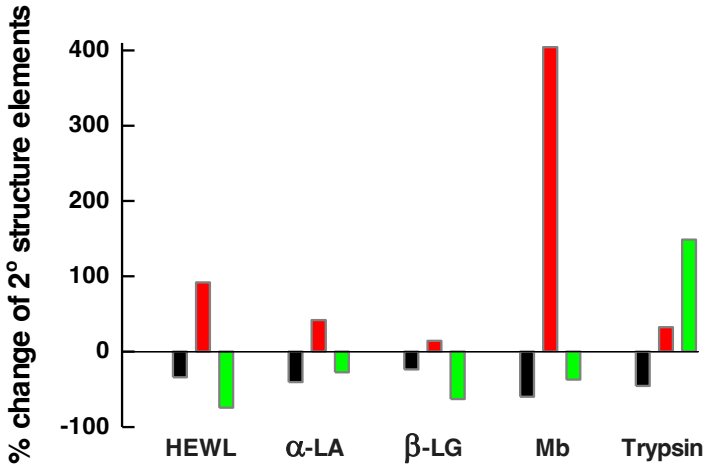

Figure 2. Changes in the content of α-helix (black), β-sheets (red), and turns (green) for the proteins indicated after ~90 minutes of applying 1.3 V cm^{-1} DC field.

5.3.2. *Loss of tertiary structure, amorphous aggregation, and crystal nucleation.*

The loss of α-helical structure and the formation of non-native β-sheets must also be accompanied by disruption of tertiary structure, which is easily checked by monitoring time-base fluorescence emission after switching the electric field on. The two columns from left in Figure 3 show real-time fluorescence-monitored structure unfolding induced by 1.3 V cm^{-1} DC supplied online. But for HEWL whose disulfides are less prone to electrochemical reduction because of lower pH, the fluorescence signals of α-LA, β-LG, Mb, and trypsin start out with an initial baseline extending up to ~ 25 minutes and quench abruptly thereafter, indicated by the vertical dashed line (Column 2, Figure 3). The onset of quenching is presaged by the appearance of solution turbidity. The quenching of fluorescence, which may have complex exponential or power law dependence on time, is the indicator of structure unfolding that leads to amorphous aggregation. Quenching presumably arises from increased rate of resonance energy transfer between the fluorophores and intramolecular quenchers due to their increasing proximity in the aggregated state. The Tyr

fluorescence of myoglobin however increases due to departure of the residues from the heme proximity. At the end of ~90 min, a dense region of insoluble aggregates appears in the bottom of the cuvette.

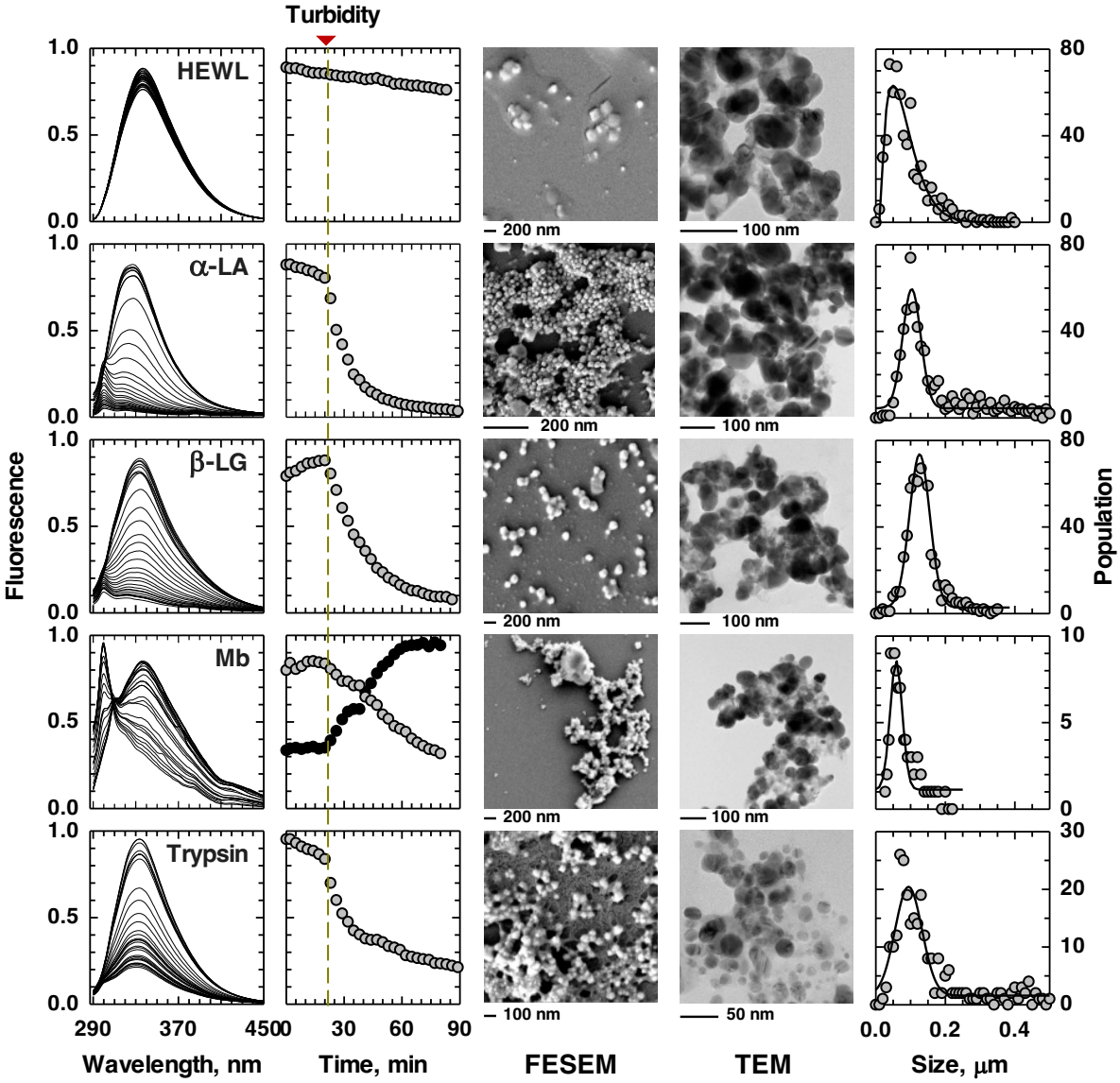

Figure 3. (Column 1) Online tryptophan fluorescence spectra of the indicated proteins (7 μM) gated to uniform time interval after switching on 1.3 V cm^{-1} DC field. (Column 2) Protein-respective unfolding kinetics plotted from the time-dependent fluorescence spectra. The dashed vertical line appearing at ~25 min indicates the onset of aggregation. Black symbols in the kinetics of Mb unfolding represent tyrosine fluorescence. (Column 3) SEM images of respective protein

aggregates developed after ~24 h of the fluorescence experiments. Hexagonal crystals of α-LA are shown by zooming in. (Column 4) Corresponding TEM images developed by uranyl acetate staining. (Column 5) Gaussian distribution of crystal size; the distribution for HEWL crystals is skewed.

We conclude that the force on the protein dipoles by the electric field vector and the intramolecular charge separation lead to mechanical unfolding, leading to α-helix → β-sheet conversion and assembly of the latter to form aggregates.

A day after, the aggregates were imaged by field emission scanning electron microscopy (FESEM) and transmission electron microscopy (TEM). The FESEM and TEM micrographs of all five proteins clearly show crystal growth from the respective amorphous forms (Figure 3). With residual amorphous forms still visible, one can assume that crystals have grown according to the scheme Native protein → Amorphous aggregate → Crystalline form (N→A→C). Although the images do not resolve the crystal forms to a very high degree, the respective forms visually approximated for HEWL, α-LA, β-LG, Mb, and trypsin are rhombohedral, hexagonal, trigonal/rhombohedral, monoclinic, and orthorhombic. The images also show crystals of different sizes for each protein, the continuous distribution of which plotted in the rightmost column of Figure 3 indicates protein specific distribution characterized by the mean size and standard deviation.

5.3.3. *Electron diffraction by the crystals.*

Crystal growth is confirmed by selected area electron diffraction (SAED) in TEM. While polycrystalline diffraction pattern consisting of spots and rings is obtained for all 5 proteins (Figure

4a–e), the area selection was particularly better for the α-LA sample that provides the example of a monocrystalline diffractogram containing regular hexagonal diffraction spots (Figure 4f). In addition to the crystals each sample also contains a population of amorphous aggregates, an example of which is provided by the TEM image (Figure 4g) and the corresponding electron diffractogram (Figure 4h). This result suggests that the A→C transition representing nucleation and crystallization is a slow heterogeneous process, and complete conversion of A to C probably takes longer time.

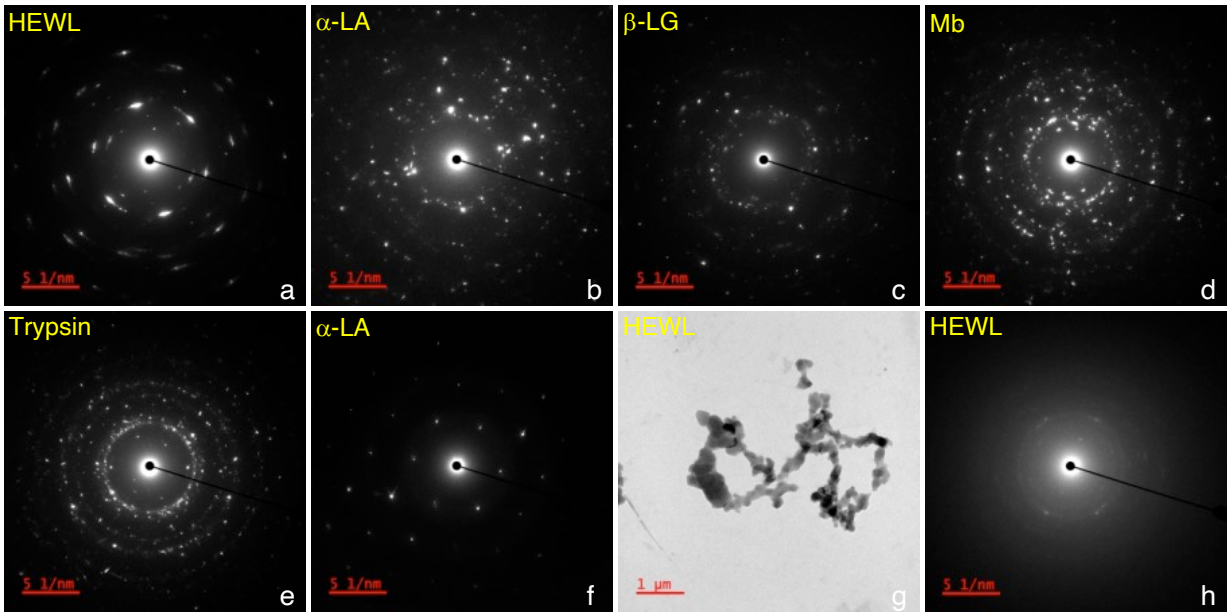

Figure 4. (a–e) 'Spot-and-ring' polycrystalline diffractions obtained by SAED in TEM. (f) α-LA single crystal hexagonal diffraction spots. (g) Amorphous aggregates in the HEWL sample detected by non-diffracting mode TEM. (h) Amorphous diffraction from an area of the HEWL grid, suggesting that complete transformation of the amorphous aggregate to crystals has not yet taken place.

5.3.6. *Gel test of protein crystals.*

To investigate whether the crystals obtained on EF exposure of protein corresponds to the same protein or not, we performed a SDS PAGE test. For this we made two sets of samples containing all the proteins under investigation, viz. lysozyme, α −lactalbumin, β −lactoglobulin, myoglobin and trypsin. First set contains 7 μM protein, freshly prepared under same experimental conditions as mentioned in Table 1. The second set contain solutions obtained after exposing the protein samples (~90 min) to EF. Sample labeling was done using the first letter of the protein followed by set number, such that L1, A1, B1, M1, T1 and L2, A2, B2, M2, T2 corresponds to lysozyme, α −lactalbumin, β −lactoglobulin, myoglobin and trypsin of set 1 and 2 respectively.

A pair of sample containing same protein from set 1 and set 2 were placed adjacent each other in the polyacrylamide gel as shown in Figure 5, against 10-200 kDa marker M. The gel was stained using Coomassie Blue R-250 to obtain the required bands.

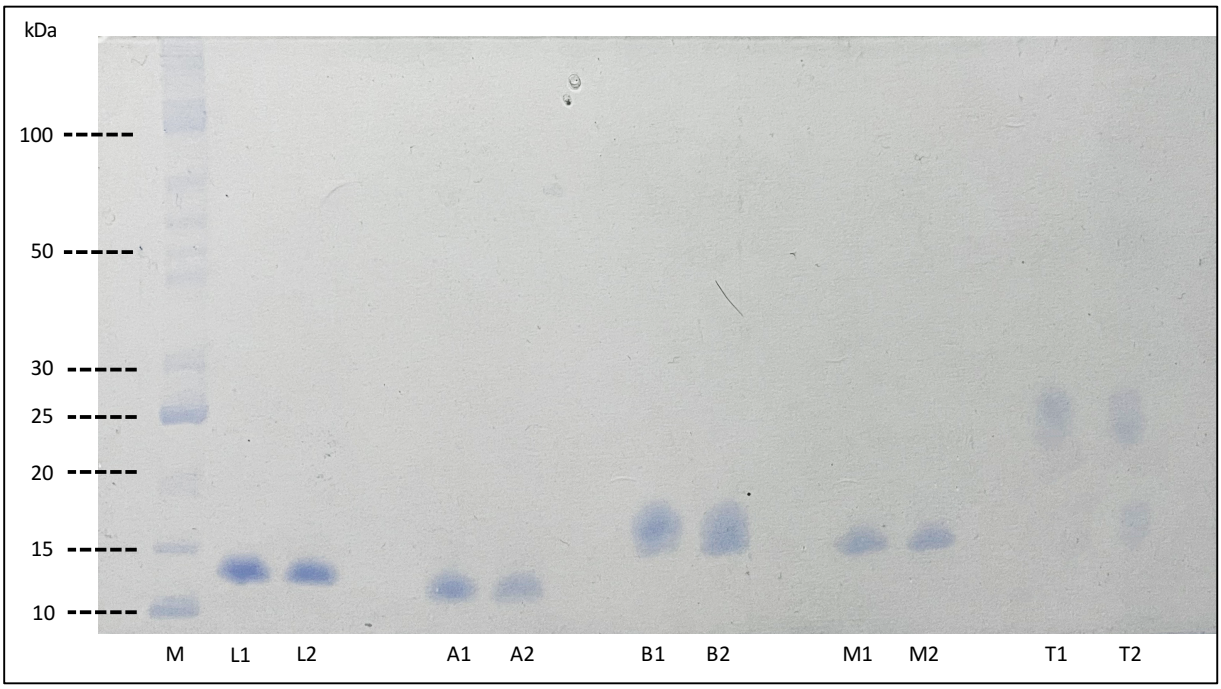

Figure 5. Protein spots obtained from polyacrylamide gel test of both sets of protein. M represents a 10-200 kDa marker.

It was observed that the protein bands are properly visible in the standard samples and the one exposed to EF. The band intensity of samples exposed to EF is slightly less than the standard samples, suggesting loss of some protein in formation of amorphous aggregates. Thus we can clearly say that the crystals obtained are protein crystals.

5.3.4. *Model for EF-assisted protein crystallization.*

The N→A→C mechanism narrated above by interpretation of the present results can be projected onto Vekilov's two-state nucleation (TSN) mechanism.[24] Accordingly, the less dense or dilute native form (N) attains a highly dense aggregated form (A), whose reduced surface tension should lower the Gibbs free energy barrier for transition to the crystalline phase (C). The TSN may be extended to multistep nucleation (MSN) to account for incomplete transformation of the mesophase aggregates to the crystalline phase at times longer.

The apparent difficulty here is to identify the structure of molecules in the mesoscopic phase A after the electric field is withdrawn, whether native (N), quasi-native (QN) or native-like conformations, or highly disordered (D) structure, or fibrillar cross-β structures. Formation of all these types of structures in protein aggregates is possible,[25,26] but the option of fibrillar structures can be eliminated right away because protein crystals will not nucleate from cross-β forms, nor did we observe them in electron micrographs. To account for the presence of crystals and amorphous forms in the electron microscopic images (Figures 3,4), we state that the confined molecules in the aggregated form are thermodynamically unstable and remain unfolded during the whole time that the EF is on. The molecules however tend to refold within the mesoscopic phase when the field is withdrawn. The refolded N or QN population still hangs onto the amorphous solid, maintaining the high population density ('dense liquid') required to serve as nucleation precursors. In this model, the amorphous solid is the substratum onto which crystals of N or QN molecules nucleate,

initially as spherical crystallites that gradually transform into larger crystals. The amorphous population which is slow to nucleate or fails to do so still appears in the mesophase. This mechanism narrated by interpretation of the present results to account for incomplete transformation of the mesophase aggregates to the crystalline phase at longer times is consistent with the MSN model.

5.3.5. *Strong electric field is redundant for crystallization.*

The central idea we convey here is the requirement to mechanically unfold the protein in order to generate the obligate amorphous aggregates, which will at least partly refold to N or QN states after the removal of the EF. The 'dense N/QN state' undergoes nucleation over a period of time. We also underscore that the task of mechanical unfolding in order to create the amorphous aggregates can be achieved using a static field as weak as ~1 V cm^{-1} where the first-order interaction energy of the dipole of a protein molecule the size of Mb (μ~240 D) is μE~8×10^{-26} J, which is sufficient to unfold the molecule. The unfolded molecules and the resultant aggregates largely stay in the solution because the mean electrophoretic velocity calculated by the Hückel solution of the Navier-Stokes equation is ~1 mm h^{-1}, allowing nucleation to occur in the solution. Very strong field, oscillating field in particular, introduces anomalous symmetry and electrophoretic effects because of a large increase in Wien conductance, in which case crystals may occasionally be observed attached to the electrode.[15] High-frequency AC field may actually decrease the crystal growth rate.[7] We find redundancy of strong field for protein crystallization, even though theoretical and experimental evidences suggest that large-magnitude DC field can induce nucleation of small molecules.[27,28]

5.4. References

1. Townes, C. H.; Schawlow, A. L. *Microwave Spectroscopy*; Dover Publications Inc., 1975.

2. Pierce, D. W.; Boxer, S. G. Stark Effect Spectroscopy of Tryptophan. *Biophys. J.* **1995**, *68*, 1583–1591.

3. Bhuyan, A. K. *Fundamental Concepts of Molecular Spectroscopy*; CRC Press, Taylor & Francis Group, 2023.

4. Taleb, M.; Didierjean, C.; Jelsch, C.; Mangeot, J. P.; Capelle, B.; Aubry, A. J. Crystallization of Proteins Under an External Electric Field. *J. Cryst. Growth* **1999**, *200*, 575–582.

5. Taleb, M.; Didierjean, C.; Jelsch, C.; Mangeot, J. P.; Aubry, A. Equilibrium Kinetics of Lysozyme Crystallization Under an External Electric Field. *J. Cryst. Growth* **2001**, *232*, 250–255.

6. Nanev, C. N. Recent Insights into the Crystallization Process; Protein Crystal Nucleation and Growth Peculiarities; Processes in the Presence of Electric Fields. *Crystals* **2017**, *7*, 310.

7. Koizumi, H.; Uda, S.; Fujiwara, K.; Okada, J.; Nozawa, J. Effect of an External Electric Field on the Kinetics of Dislocation-Free Growth of Tetragonal Hen Egg White Lysozyme Crystals. *Crystals* **2017**, *7*, 170.

8. Alexander, L. F.; Radacsi, N. Application of Electric Fields for Controlling Crystallization. *CrystEngComm* **2019**, *21*, 5014–5031.

9. Yuan, Z.; Wu, M.; Meng, Y.; Niu, Y.; Xiao, W.; Ruan, X.; He, G.; Jiang, X. Protein Crystal Regulation and Harvest via Electric Field-Based Method. *Curr. Opin. Chem. Eng.* **2022**, *36*, 100744.

10. Sleutel, M.; Maes, D.; Van Driessche, A. Kinetics and Thermodynamics of Multistep Nucleation and Self-Assembly in Nanoscale Materials. In *Advances in Chemical Physics*; Vol. 151; Nicolis, G., Maes, D., Eds.; Wiley-Blackwell, 2015, pp 223–276.

11. Adrjanowicz, K.; Paluch, M.; Richert, R. Formation of New Polymorphs and Control of Crystallization in Molecular Glass-Formers by Electric Field. *Phys. Chem. Chem. Phys.* **2018**, *20*, 925–931.

12. Koizumi, H.; Fujiwara, K.; Uda, S. Role of the Electric Double Layer in Controlling the Nucleation Rate for Tetragonal Hen Egg White Lysozyme Crystals by Application of an External Electric Field. *Cryst. Growth Des.* **2010**, *1*, *2595*, 1591.

13. Koizumi, H.; Uda, S.; Fujiwara, K.; Tachibana, M.; Kojima, K.; Nozawa, J. Improvement of Crystal Quality for Tetragonal Hen Egg White Lysozyme Crystals Under Application of an External Alternating Current Electric Field. *J. Appl. Crystallogr.* **2013**, *46*, 25–29.

14. Pareja-Rivera, C.; Cuéllar-Cruz, M.; Esturau-Escofet, N.; Demitri, N.; Polentarutti, M.; Stojanoff, V.; Moreno, A. Recent Advances in the Understanding of the Influence of Electric and Magnetic Fields on Protein Crystal Growth. *Cryst. Growth Des.* **2017**, *17*, 135–145.

15. Rodríguez-Romero, A.; Esturau-Escofet, N.; Pareja-Rivera, C.; Moreno, A. Crystal Growth of High-Quality Protein Crystals Under the Presence of an Alternant Electric Field in Pulse-Wave Mode, and a Strong Magnetic Field with Radio Frequency Pulses Characterized by X-ray Diffraction. *Crystals* **2017**, *7*, 179.

16. Mirkin, N.; Jaconcic, J.; Stojanoff, V.; Moreno, A. High Resolution X-ray Crystallographic Structure of Bovine Heart Cytochrome c and Its Application to the Design of an Electron Transfer Biosensor. *Proteins* **2008**, *70*, 83–92.

17. Wakamatsu, T. Low Applied Voltage Effects on Thaumatin Protein Crystallization. *Trans. Mater. Res. Soc. Jpn.* **2016**, *41*, 13–15.

18. Dong, A.; Huang, P.; Caughey, W. S. Protein Secondary Structure in Water from Second Derivative Amide I Infrared Spectra. *Biochemistry* **1990**, *29*, 3303–3308.

19. Jackson, M.; Mantsch, H. H. The Use and Misuse of FTIR Spectroscopy in the Determination of Protein Structure. *Crit. Rev. Biochem. Mol. Biol.* **1995**, *30*, 95–120.

20. Dessau, M. A.; Modis, Y. Protein Crystallization for X-ray Crystallography. *J. Vis. Exp.* **2011**, 47, 2285.

21. Miyazawa, T. Perturbation Treatment of the Characteristic Vibrations of Polypeptide Chains in Various Configurations. *J. Chem. Phys.* **1960**, *32*, 1647–1652.

22. Ding, F.; Borreguero, J. M.; Buldyrey, S. V.; Stanley, H. E.; Dokholyan, N. V. Mechanism for the a-Helix to b-Hairpin Transition. *Proteins* **2003**, *53*, 220–228.

23. Qin, Z.; Buehler, M. J. Molecular Dynamics Simulation of the a-Helix to b-Sheet Transition in Coiled Protein Filaments: Evidence for a Critical Filament Length Scale. *Phys. Rev. Lett.* **2010**, *104*, 198304.

24. Vekilov, P. G. The Two-Step Mechanism of Nucleation of Crystals in Solution. *Nanoscale* **2010**, *2*, 2346–2357.

25. Chiti, F.; Dobson, C. M. Protein Misfolding, Amyloid Formation, and Human Disease: A Summary of Progress over the Last Decade. *Annu. Rev. Biochem.* **2017**, *86*, 27–68.

26. Almeida, Z. L.; Brito, R. M. M. Structure and Aggregation Mechanisms in Amyloids. *Molecules* **2020**, *25*, 1195.

27. Svishchev, I. M.; Kusalik, P. G. Crystallization of Liquid Water in a Molecular Dynamics Simulation. *Phys. Rev. Lett.* **1994**, *73*, 975–978.

28. Aber, J. E.; Arnold, S.; Garetz, B. A. Strong dc Electric Field Applied to Supersaturated Glycine Solution Induces Nucleation of the g Polymorph. *Phys. Rev. Lett.* **2005**, *94*, 145503.

CHAPTER 6

Conclusion and Future Prospects

6.1. Overview of the present work and future prospects

Here, the findings of the thesis study along with future prospects are summarized. The thesis is mainly divided in two parts that discusses about the effects of surfactants, particularly SDS and the effect of weak electric field on protein structure, conformation and function. These conformational and structural changes occur via transitions through mesophases, which is the central idea of the thesis.

It was crucial to look at the process by which SDS self-associates to form a micelle in order to better comprehend protein-SDS interaction. Interestingly we found the existence of small premicellar aggregates of SDS below CMC. The step-wise self-association process of micellization consistently showed linear variation of weight average molecular weights of micelles having aggregation number in the limit of ~60. As a result, we looked at how SDS affected protein structure and conformation below CMC. The study found that all generic structural changes of proteins occur completely within submicellar limit of SDS. Additionally, a connection between protein charge and protein fibrillation has been found.

The second part discusses how weak EF affects the structure, conformation, and function of proteins. EF can mechanically unfold the protein, causing a partial loss of secondary and tertiary structures. Charge separation upon unfolding produces electrostatic interaction within the protein molecules, leading to their aggregation. The majority of these aggregates stay suspended in the solutions where they gradually crystallize. This electric field-induced crystallization was observed for half a dozen proteins and is expected to be a generic property. The weak EF-induced

crystallization of micromolar concentrations of substances in the absence of any auxiliary chemical or physical agents holds great promise in the crystallization of a variety of molecules spanning the sizes of CdS to proteins through amino acids.

Publications

1. **Huda, N.**; Hossain, M.; Bhuyan, A. K. Complete Observation of All Structural, Conformational, and Fibrillation Transitions of Monomeric Globular Proteins at Submicellar Sodium Dodecyl Sulfate Concentrations. *Biopolymers* **2019**, *110*, e23255.

2. **Huda, N.**; Bhuyan, A. K. Mechanical Unfolding and Amorphous Aggregation of Protein in Very Low DC Field. *J. Phys. Chem. B* **2023**, *127*, 4386–4395.

3. **Huda, N.**; Bhuyan, A. K. Protein Crystallization in Very Weak DC Electric Field. *Cryst. Growth Des.* **2023**. (accepted for publication)

4. Ramesh, H.; **Huda, N.**; Hossain, M.; Bhuyan, A. K. Food Additives Benzoic Acid and Its Methyl and Propyl Parahydroxy Derivatives Aggregate Proteins. *ACS Food Sci. Technol.* **2021**, *1*, 2162–2173.

5. Hossain, M.; **Huda, N.**; Bhuyan, A. K. A Surprisingly Simple Three-State Generic Process for Reversible Protein Denaturation by Trifluoroethanol. *Biophys. Chem.* **2022**, *291*, 106895.

6. Hossain, M.; **Huda, N.**; Bhuyan, A. K. A Three-State Mechanism for Trifluoroethanol Denaturation of an Intrinsically Disordered Protein (IDP). *J. Biochem.* **2023**. (accepted for publication)

Presentations

1. **Poster:** "**Conformational Analysis of Protein in Electric Field**" in Chemfest 2020 (In-house symposium) at University of Hyderabad.

2. **Oral and Poster:** "**Effect of Electric Field on Protein Conformation**" in Chemfest 2022 (In-house symposium) at University of Hyderabad

3. **Poster:** "**Obligate amorphous aggregate in electric field-promoted protein crystallization**" in Chemfest 2023 at University of Hyderabad. (**Best Poster presentation**)

Protein Transformation by Mesophases: Studies with Sodium Dodecyl Sulfate and Electric Field

by Noorul Huda

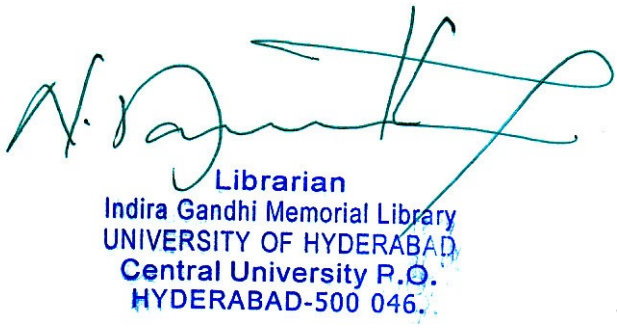

Submission date: 27-Jun-2023 10:29AM (UTC+0530)
Submission ID: 2123318007
File name: Noorul_Huda.pdf (534.85K)
Word count: 20450
Character count: 110844

Protein Transformation by Mesophases: Studies with Sodium Dodecyl Sulfate and Electric Field

ORIGINALITY REPORT

40%	2%	39%	1%
SIMILARITY INDEX	INTERNET SOURCES	PUBLICATIONS	STUDENT PAPERS

PRIMARY SOURCES

1	Noorul Huda, Abani K. Bhuyan. "Mechanical Unfolding and Amorphous Aggregation of Protein in a Very Low DC Field", The Journal of Physical Chemistry B, 2023 Publication	20%
2	Noorul Huda, Mujahid Hossain, Abani K. Bhuyan. "Complete observation of all structural, conformational, and fibrillation transitions of monomeric globular proteins at submicellar sodium dodecyl sulfate concentrations", Biopolymers, 2019 Publication	17%
3	D. Demus, J. Goodby, G. W. Gray, H. - W. Spiess, V. Vill. "Handbook of Liquid Crystals Set", Wiley, 1998 Publication	1%
4	www.pubfacts.com Internet Source	<1%
5	Abani K. Bhuyan. " Off-Pathway Status for the Alkali Molten Globule of Horse	<1%

ABANI K. BHUYAN, Ph.D.
Professor
University of Hyderabad
School of Chemistry
Hyderabad - 500 046.

ABANI K. BHUYAN, Ph.D.
Professor
University of Hyderabad
School of Chemistry
Hyderabad - 500 046.

	Ferricytochrome ", Biochemistry, 2010 Publication	
6	Abani K. Bhuyan. "On the mechanism of SDS-induced protein denaturation", Biopolymers, 2009 Publication	<1 %
7	Submitted to University of Hyderabad, Hyderabad Student Paper	<1 %
8	www.researchgate.net Internet Source	<1 %
9	Kumar, . "Introduction", Liquid Crystals Book Series, 2010. Publication	<1 %
10	Mujahid Hossain, Noorul Huda, Abani K. Bhuyan. "A surprisingly simple three-state generic process for reversible protein denaturation by trifluoroethanol", Biophysical Chemistry, 2022 Publication	<1 %
11	brochurexpress.com Internet Source	<1 %
12	David J.R. Cristaldi, Salvatore Pennisi, Francesco Pulvirenti. "Chapter 1 Liquid Crystals", Springer Science and Business Media LLC, 2009 Publication	<1 %

13	Halavath Ramesh, Noorul Huda, Mujahid Hossain, Abani K. Bhuyan. "Food Additives Benzoic Acid and its Methyl and Propyl Parahydroxy Derivatives Aggregate Proteins", ACS Food Science & Technology, 2021 Publication	<1 %
14	Submitted to University of Huddersfield Student Paper	<1 %
15	etheses.dur.ac.uk Internet Source	<1 %
16	Bisoyi, Hari Krishna, and Quan Li. "Liquid Crystals", Kirk-Othmer Encyclopedia of Chemical Technology, 2014. Publication	<1 %
17	www.science.org Internet Source	<1 %
18	Nataša Poklar, Jens Völker, Gregor Anderluh, Peter Maček, Tigran V Chalikian. "Acid- and base-induced conformational transitions of equinatoxin II", Biophysical Chemistry, 2001 Publication	<1 %
19	Submitted to University of Nottingham Student Paper	<1 %
20	Goldblatt, Greg, Jason O. Matos, Jeremy Gornto, and Suren A. Tatulian. "Isotope-edited FTIR reveals distinct aggregation and	<1 %

structural behaviors of unmodified and pyroglutamylated amyloid β peptides", Physical Chemistry Chemical Physics, 2015.
Publication

21	Submitted to University of Oklahoma Student Paper	<1 %
22	scholarsmine.mst.edu Internet Source	<1 %

Exclude quotes	On	Exclude matches	< 14 words
Exclude bibliography	On		